ASME V&V 20-2009

Standard for Verification and Validation in Computational Fluid Dynamics and Heat Transfer

ASMENORMDOC.COM : Click to view the full PDF of ASME V&V 20-2009

AN AMERICAN NATIONAL STANDARD

The American Society of Mechanical Engineers

ASME
SETTING THE STANDARD

Intentionally left blank

ASMENORMDOC.COM : Click to view the full PDF of ASME V V 20 2009

ASME V&V 20-2009

Standard for Verification and Validation in Computational Fluid Dynamics and Heat Transfer

ASMENORMDOC.COM : Click to view the full PDF of ASME V&V 20 2009

AN AMERICAN NATIONAL STANDARD

The American Society of Mechanical Engineers

ASME SETTING THE STANDARD

Date of Issuance: November 30, 2009

This Standard will be revised when the Society approves the issuance of a new edition. There will be no addenda issued to this edition.

ASME issues written replies to inquiries concerning interpretations of technical aspects of this Standard. Periodically certain actions of the ASME V&V 20 Committee may be published as Cases. Cases and interpretations are published on the ASME Web site under the Committee Pages at http://cstools.asme.org as they are issued.

ASMENORM.COM : Click to view the full PDF of ASME V V 20 2009

ASME is the registered trademark of The American Society of Mechanical Engineers.

This code or standard was developed under procedures accredited as meeting the criteria for American National Standards. The Standards Committee that approved the code or standard was balanced to assure that individuals from competent and concerned interests have had an opportunity to participate. The proposed code or standard was made available for public review and comment that provides an opportunity for additional public input from industry, academia, regulatory agencies, and the public-at-large.

ASME does not approve, rate, or endorse any item, construction, proprietary device, or activity.

ASME does not take any position with respect to the validity of any patent rights asserted in connection with any items mentioned in this document, and does not undertake to insure anyone utilizing a standard against liability for infringement of any applicable letters patent, nor assumes any such liability. Users of a code or standard are expressly advised that determination of the validity of any such patent rights, and the risk of infringement of such rights, is entirely their own responsibility.

Participation by federal agency representative(s) or person(s) affiliated with industry is not to be interpreted as government or industry endorsement of this code or standard.

ASME accepts responsibility for only those interpretations of this document issued in accordance with the established ASME procedures and policies, which precludes the issuance of interpretations by individuals.

No part of this document may be reproduced in any form,
in an electronic retrieval system or otherwise,
without the prior written permission of the publisher.

The American Society of Mechanical Engineers
Three Park Avenue, New York, NY 10016-5990

Copyright © 2009 by
THE AMERICAN SOCIETY OF MECHANICAL ENGINEERS
All rights reserved
Printed in U.S.A.

CONTENTS

ASMENORMDOC.COM : Click to view the full PDF of ASME V V 20 2009

Figures

ASMENORMDOC.COM : Click to view the full PDF of ASME V V 20 2009

Tables

Mandatory Appendices

Nonmandatory Appendices

ASMENORMDOC.COM : Click to view the full PDF of ASME V V 20 2009

FOREWORD

This Standard addresses verification and validation (V&V) in computational fluid dynamics (CFD) and computational heat transfer (CHT). The concern of V&V is to assess the accuracy of a computational simulation. The V&V procedures presented in this Standard can be applied to engineering and scientific modeling problems ranging in complexity from simple lumped masses, to 1-D steady laminar flows, to 3-D unsteady turbulent chemically reacting flows. In V&V, the ultimate goal of engineering and scientific interest is validation, which is defined as the process of determining the degree to which a model is an accurate representation of the real world from the perspective of the intended uses of the model. However, validation must be preceded by code verification and solution verification. Code verification establishes that the code accurately solves the mathematical model incorporated in the code, i.e. that the code is free of mistakes for the simulations of interest. Solution verification estimates the numerical accuracy of a particular calculation.

The estimation of a range within which the simulation modeling error lies is a primary objective of the validation process and is accomplished by comparing a simulation result (solution) with an appropriate experimental result (data) for specified validation variables at a specified set of conditions. *There can be no validation without experimental data with which to compare the result of the simulation.*[*] Usually a validation effort will cover a range of conditions within a domain of interest.

Both the American Institute of Aeronautics and Astronautics (AIAA) and the American Society of Mechanical Engineers (ASME) have published V&V Guides that present the philosophy and procedures for establishing a comprehensive validation program, but both use definitions of error and uncertainty that are not demonstrated within the guides to provide quantitative evaluations of the comparison of the validation variables predicted by simulation and determined by experiment. ASME V&V 10-2006, for instance, defines error as "a recognizable deficiency in any phase or activity of modeling or experimentation that is not due to lack of knowledge" and defines uncertainty as "a potential deficiency in any phase or activity of the modeling, computation, or experimentation process that is due to inherent variability or lack of knowledge."

In contrast, this Standard presents a V&V approach that is based on the concepts and definitions of error and uncertainty that have been internationally codified by the experimental community over several decades. In 1993, the Guide to the Expression of Uncertainty in Measurement was published by the International Organization for Standardization (ISO) in its name and those of six other international organizations.[†] According to the Foreword in the ISO Guide, "In 1977, recognizing the lack of international consensus on the expression of uncertainty in measurement, the world's highest authority in metrology, the Comite International des Poids et Mesures (CIPM), requested the Bureau International des Poids et Mesures (BIPM) to address the problem in conjunction with the national standards laboratories and to make a recommendation." After several years of effort, this led to the assignment of responsibility to the ISO Technical Advisory Group on Metrology, Working Group 3, to develop a guidance document. This ultimately culminated in the publication of the ISO Guide, which has been accepted as the de facto international standard for the expression of uncertainty in measurement.

The V&V approach presented in this Standard applies these concepts to the errors and uncertainties in the experimental result and also to the errors and uncertainties in the result from the simulation. Thus, the uncertainties in the experimental value and in the simulation value are treated using the same process. Using the approach of the ISO Guide, for each error source (other than the simulation modeling error) a standard uncertainty, u, is estimated such that u is the standard deviation of the parent population of possible errors from which the current error is a single realization. This allows estimation of a range within which the simulation modeling error lies.

The objective of this Standard is the specification of a verification and validation approach that quantifies the degree of accuracy inferred from the comparison of solution and data for a specified variable at a specified validation point. The scope of this Standard is the quantification of the degree of accuracy for cases in which the conditions of the actual experiment are simulated. Consideration of the accuracy of simulation results at points within a domain other than the validation points (e.g., interpolation/extrapolation in a domain of validation) is a matter of engineering judgment specific to each family of problems and is beyond the scope of this Standard.

ASMENORMDOC.COM : Click to view the full PDF of ASME V&V 20-2009

[*]This is implicit in the phrase "real world" used in the definition of validation.

[†]Bureau International des Poids et Mesures (BIPM), International Electrotechnical Commission (IEC), International Federation of Clinical Chemistry (IFCC), International Union of Pure and Applied Chemistry (IUPAC), International Union of Pure and Applied Physics (IUPAP), and International Organization of Legal Metrology (OIML)

ASME PTC 19.1-2005 "Test Uncertainty" is considered a companion document to this Standard, and it is assumed the user has both so many of the details of estimating the uncertainty in an experimental result are not repeated herein. ASME PTC 19.1-2005 illustrates the application of the ISO Guide methodology in straightforward and also in complex experiments.

Ideally, as a V&V program is initiated, those responsible for the simulations and those responsible for the experiments should be involved cooperatively in designing the V&V effort. The validation variables should be chosen and defined with care. Each measured variable has an inherent temporal and spatial resolution, and the experimental result that is determined from these measured variables should be compared with a predicted result that possesses the same spatial and temporal resolution. If this is not done, such conceptual errors must be identified and corrected or estimated in the initial stages of a V&V effort, or substantial resources can be wasted and the entire effort may be compromised.

Finally, as an aid to the reader of this Standard, the following guide to the topics and discussions of each section are presented. It is recommended that the reader proceed through the Standard beginning in Section 1 and successively read each subsequent section. The presentation in this Standard follows a procedure starting with verification (code and solution), proceeding to parameter uncertainty assessment, experimental uncertainty assessment, simulation validation, and concluding with a comprehensive example problem. As stated, this Standard follows an overall procedure; however, each section of this Standard may also be viewed as a standalone presentation on each of the relevant topics. The intent of this document is validation in which uncertainty is determined for both the experimental data and the simulation of the experiment. However, the material in Sections 2, 3, and 4 can be studied independently of the remainder of the document as they are important in their own right. A reader's guide follows:

Section 1 presents an introduction to the concepts of verification and validation, the definitions of error and uncertainty, and the introduction of the overall validation methodology and approach as defined in this Standard. The key concepts of this Section are the validation comparison error and the validation standard uncertainty. It is shown that validation standard uncertainty is a function of three standard uncertainties associated with errors due to numerical solution of the equations, due to simulation inputs, and due to experimental data.

Section 2 presents two key topics:

(a) the details of a method for code verification based on the technique of the method of manufactured solutions

(b) the details of a method for solution verification based on the technique of the Grid Convergence Index (an extension of Richardson Extrapolation).

The outcome of Section 2 is a method for estimating the standard uncertainty associated with numerical errors.

Section 3 presents two different approaches for estimating the standard uncertainty associated with errors in simulation input parameters. One approach evaluates response of the simulation or system in a local neighborhood of the input vector, while the other approach evaluates response in a larger global neighborhood. The first approach is commonly referred to, for example, as the sensitivity coefficient method, and the second approach is generally referred to as the sampling or Monte Carlo method.

Section 4 presents a brief overview of the method presented in the ASME PTC 19.1-2005 Test Uncertainty standard for estimating uncertainty in an experimental result. At the conclusion of this Section, the reader will have methods for estimating the key uncertainties required to complete a validation assessment.

Section 5 presents two approaches for estimating the validation standard uncertainty given the estimates of uncertainty associated with numerical, input, and experimental data errors as developed in the three previous sections. At the conclusion of this Section, the reader will have the necessary tools to estimate validation standard uncertainty and the error associated with the mathematical model.

Section 6 presents a discussion of the interpretation of the key validation metrics of validation comparison error and validation uncertainty. It is shown that the validation comparison error is an estimate of the mathematical model error and that the validation uncertainty is the standard uncertainty of the estimate of the model error.

Section 7 summarizes the methods presented in the previous sections by implementing them in a comprehensive example problem working through each element of the overall procedure and results in a complete validation assessment of a candidate mathematical model.

Finally, several appendices are included in this Standard. Some are considered as part of the Standard and are identified as mandatory appendices. Other included appendices are considered as nonmandatory or supplementary and are identified as such.

ASME V&V 20-2009 was approved by the V&V 20 (previously PTC 61) Committee on January 9, 2009 and approved by the American National Standards Institute (ANSI) on June 3, 2009.

ASMENORMDOC.COM : Click to view the full PDF of ASME V V 20 2009

ASME PTC COMMITTEE
Performance Test Codes

(The following is the roster of the Committee at the time of approval of this Standard.)

STANDARDS COMMITTEE OFFICERS

M. P. McHale, *Chair*
J. R. Friedman, *Vice Chair*
J. H. Karian, *Secretary*

STANDARDS COMMITTEE PERSONNEL

P. G. Albert
R. P. Allen
J. M. Burns
W. C. Campbell
M. J. Dooley
J. R. Friedman
G. J. Gerber
P. M. Gerhart
T. C. Heil
R. E. Henry
J. H. Karian
D. R. Keyser
T. K. Kirkpatrick
S. J. Korellis
M. P. McHale
P. M. McHale
J. W. Milton
S. P. Nuspl
R. R. Priestley
J. A. Rabensteine
J. A. Silvaggio, Jr.
W. G. Steele, Jr.
J. C. Westcott
W. C. Wood

HONORARY MEMBERS

R. L. Bannister
W. O. Hays
R. Jorgensen
F. H. Light
G. H. Mittendorf, Jr.
J. W. Siegmund
R. E. Sommerlad

V&V 20 COMMITTEE — VERIFICATION AND VALIDATION IN COMPUTATIONAL FLUID DYNAMICS AND HEAT TRANSFER

H. W. Coleman, *Chair*, University of Alabama, Huntsville
C. J. Freitas, *Vice Chair*, Southwest Research Institute
R. L. Crane, *Secretary*, The American Society of Mechanical Engineers
B. F. Blackwell, Consultant
K. J. Dowding, Sandia National Laboratories
U. Ghia, University of Cincinnati
R. G. Hills, Sandia National Laboratories
R. W. Logan, Consultant
P. J. Roache, Consultant
W. G. Steele, Jr., Mississippi State University

ASMENORMDOC.COM : Click to view the full PDF of ASME V V 20 2009

CORRESPONDENCE WITH THE V&V 20 COMMITTEE

General. ASME Codes are developed and maintained with the intent to represent the consensus of concerned interests. As such, users of this Code may interact with the Committee by requesting interpretations, proposing revisions, and attending Committee meetings. Correspondence should be addressed to

Secretary, V&V 20 Committee
The American Society of Mechanical Engineers
Three Park Avenue
New York, NY 10016-5990

Proposing Revisions. Revisions are made periodically to the Code to incorporate changes that appear necessary or desirable, as demonstrated by the experience gained from the application of the Code. Approved revisions will be published periodically. The Committee welcomes proposals for revisions to this Code. Such proposals should be as specific as possible, citing the paragraph number(s), the proposed wording, and a detailed description of the reasons for the proposal, including any pertinent documentation.

Proposing a Case. Cases may be issued for the purpose of providing alternative rules when justified, to permit early implementation of an approved revision when the need is urgent, or to provide rules not covered by existing provisions. Cases are effective immediately upon ASME approval and shall be posted on the ASME Committee Web page.

Requests for Cases shall provide a Statement of Need and Background Information. The request should identify the Code, the paragraph, figure or table number(s), and be written as a Question and Reply in the same format as existing Cases. Requests for Cases should also indicate the applicable edition(s) of the Code to which the proposed Case applies.

Interpretations. Upon request, the V&V 20 Committee will render an interpretation of any requirement of the Code. Interpretations can only be rendered in response to a written request sent to the Secretary of the V&V 20 Committee. The request for interpretation should be clear and unambiguous. It is further recommended that the inquirer submit his/her request in the following format:

Subject:	Cite the applicable paragraph number(s) and the topic of the inquiry.
Edition:	Cite the applicable edition of the Code for which the interpretation is being requested.
Question:	Phrase the question as a request for an interpretation of a specific requirement suitable for general understanding and use, not as a request for an approval of a proprietary design or situation. The inquirer may also include any plans or drawings that are necessary to explain the question; however, they should not contain proprietary names or information.

Requests that are not in this format will be rewritten in this format by the Committee prior to being answered, which may inadvertently change the intent of the original request.

ASME procedures provide for reconsideration of any interpretation when or if additional information that might affect an interpretation is available. Further, persons aggrieved by an interpretation may appeal to the cognizant ASME Committee or Subcommittee. ASME does not approve, certify, rate, or endorse any item, construction, proprietary device, or activity.

Attending Committee Meetings. The V&V 20 Committee regularly holds meetings, which are open to the public. Persons wishing to attend any meeting should contact the Secretary of the V&V 20 Committee.

ASMENORMDOC.COM : Click to view the full PDF of ASME V V 20 2009

Intentionally left blank

ASMENORMDOC.COM : Click to view the full PDF of ASME V V 20 2009

STANDARD FOR VERIFICATION AND VALIDATION IN COMPUTATIONAL FLUID DYNAMICS AND HEAT TRANSFER

Section 1
Introduction to Validation Methodology

ASMENORM.COM : Click to view the full PDF of ASME V&V 20 2009

1-1 GENERAL

This Standard addresses verification and validation (V&V) in computational fluid dynamics (CFD) and computational heat transfer (CHT). The concern of V&V is to assess the accuracy of a computational simulation. The V&V procedures presented in this Standard can be applied to engineering and scientific modeling problems ranging in complexity from simple lumped masses to 1-D steady laminar flows to 3-D unsteady turbulent chemically reacting flows. In V&V, the ultimate goal of engineering and scientific interest is validation, which is defined as the process of determining the degree to which a model is an accurate representation of the real world from the perspective of the intended uses of the model. However, validation must be preceded by code verification and solution verification. Code verification establishes that the code accurately solves the mathematical model incorporated in the code (i.e., that the code is free of mistakes for the simulations of interest). Solution verification estimates the numerical accuracy of a particular calculation. Both code and solution verification are discussed in detail in Section 2.

The estimation of a range within which the simulation modeling error lies is a primary objective of the validation process and is accomplished by comparing a simulation result (solution) with an appropriate experimental result (data) for specified validation variables at a specified set of conditions. *There can be no validation without experimental data with which to compare the result of the simulation.*[1] Usually a validation effort will cover a range of conditions within a domain of interest.

1-2 OBJECTIVE AND SCOPE

The objective of this Standard is the specification of a verification and validation approach that quantifies the degree of accuracy inferred from the comparison of solution and data for a specified variable at a specified validation point. The approach, proposed by Coleman and Stern [1], uses the concepts from experimental uncertainty analysis [2–4] to consider the errors and uncertainties in both the solution and the data.

The scope of this Standard is the quantification of the degree of accuracy of simulation of specified validation variables at a specified validation point for cases in which the conditions of the actual experiment are simulated. Consideration of solution accuracy at points within a domain other than the validation points (e.g., interpolation/extrapolation in a domain of validation) is a matter of engineering judgment specific to each family of problems and is beyond the scope of this Standard.

Fluid dynamics and heat transfer are the areas of engineering and science that are specifically addressed, but the validation approach discussed is applicable in other areas as well. Discussion and examples are centered on models using partial differential equations, but simpler models also fall within the purview of the validation approach.

1-3 ERRORS AND UNCERTAINTIES

Pertinent definitions from metrology are as follows:

(a) error (of measurement), δ: "result of a measurement minus a true value of the measurand" [5]

(b) uncertainty (of measurement), u: "parameter, associated with the result of a measurement, that characterizes the dispersion of the values that could reasonably be attributed to the measurand" [5]

These concepts were extended in reference [1] to apply to the value of a solution variable from a simulation as well as a measured value of the variable from an experiment.

In that context, then, an error, δ, is a quantity that has a particular sign and magnitude, and a specific error, δ_i, is the difference caused by error source i between a quantity (measured or simulated) and its true value. In the approach outlined in this Standard, it is assumed

[1] This is implicit in the phrase "real world" used in the definition of validation.

Fig. 1-4-1 Schematic of Finned-Tube Assembly for Heat Transfer Example

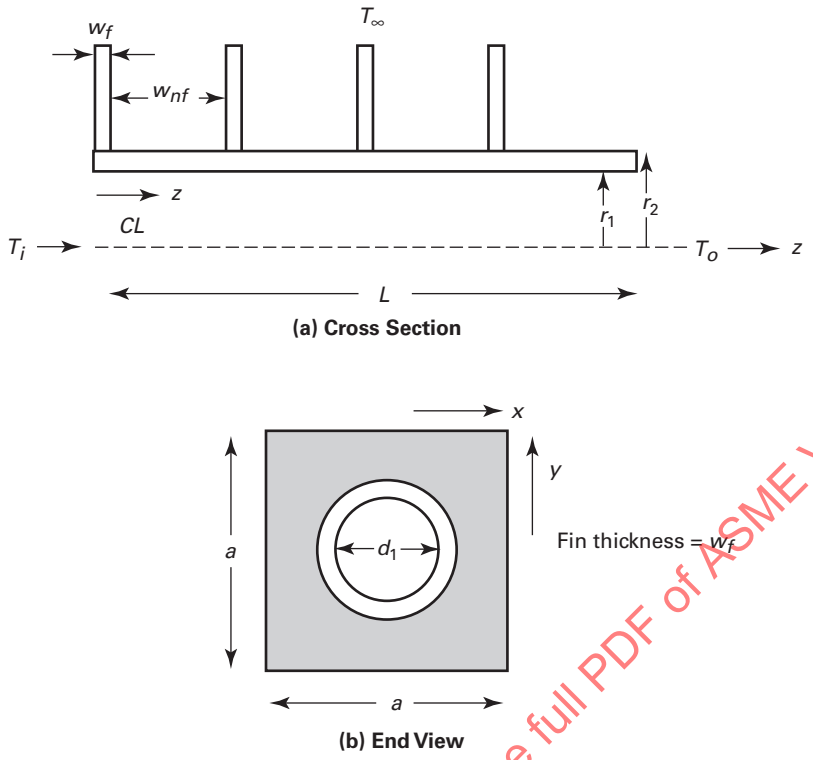

ASMENORMDOC.COM : Click to view the full PDF of ASME V V 20 2009

that each error whose sign and magnitude is known has been removed by correction. Any remaining error is thus of unknown sign and magnitude,[2] and an uncertainty u is estimated with the idea that $\pm u$ characterizes the range containing δ. In experimental uncertainty analysis [2], u is the *standard uncertainty* and corresponds conceptually to an estimate of the standard deviation, σ, of the parent distribution from which δ is a single realization. It is significant to note that no assumption about the form of the parent distribution is associated with the definition of u.

The concepts of verification and validation used in this Standard are consistent with the definitions used in previously published guides and texts on V&V [6–8]. The concepts and definitions for error and uncertainty used herein differ from those in the previously published guides, however. Both the American Institute of Aeronautics and Astronautics (AIAA) and the American Society of Mechanical Engineers (ASME) have published V&V Guides [6, 7] that present the philosophy and procedures for establishing a comprehensive validation program, but both use definitions of error and uncertainty that are not demonstrated within the guides to provide quantitative evaluations of the comparison of the validation variables predicted by simulation and determined by experiment. ASME V&V 10-2006, for instance, defines error as "a recognizable deficiency in any phase or activity of modeling or experimentation that is not due to lack of knowledge" and defines uncertainty as "a potential deficiency in any phase or activity of the modeling, computation, or experimentation process that is due to inherent variability or lack of knowledge."

1-4 EXAMPLE FOR VALIDATION NOMENCLATURE AND APPROACH

In the validation process, a simulation result (solution) is compared with an experimental result (data) for specified validation variables at a specified set of conditions (validation point). As an example (shown schematically in Fig. 1-4-1), consider the case of fully developed flow of a hot fluid inside a round tube. Square fins are attached to the outside tube wall to enhance the heat transfer. Validation variables of interest are the downstream bulk fluid temperature, T_o, and the rate of heat loss, q, over the tube length, L. A description of the problem, the corresponding simulation model, and nomenclature are presented in detail in Mandatory Appendix I.

This example is discussed in the context of validation in Section 5 for cases in which the following occur.

[2] There are asymmetric errors that are more likely to (or are certain to) have one sign rather than the other. Treatment of these by either "zero-centering" or by estimating asymmetric uncertainties is discussed in references [3] and [4].

Fig. 1-5-1 Schematic Showing Nomenclature for Validation Approach

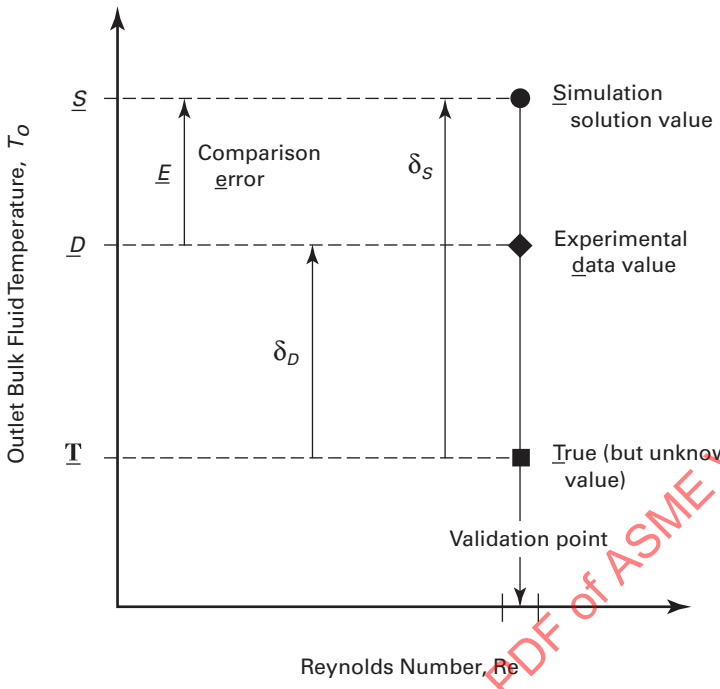

ASMENORMDOC.COM : Click to view the full PDF of ASME V V 20 2009

1-4.1 Case 1

The validation variable, T_o, is directly measured.

1-4.2 Case 2

The validation variable, q, is determined using a data reduction equation that combines multiple variables from the experiment as

$$q = \rho Q C_p (T_i - T_o) \quad (1\text{-}4\text{-}1)$$

and T_i and T_o are separately measured and have no shared error sources.

1-4.3 Case 3

The validation is the same as Case 2 in para. 1-4.2 above, except the T_i and T_o measurements have shared error sources.

The validation set point is at the Reynolds number defined as

$$\mathrm{Re} = \frac{4\rho Q}{\pi \mu d_1} \quad (1\text{-}4\text{-}2)$$

Consider Case 1 in para. 1-4.1 above as an example to describe the validation approach nomenclature. In the experiment, the validation variable, T_o, is directly measured. In the simulation, the experimentally determined values of T_i, T_∞, Q, d_1, d_2, L and the reference quantities ρ, μ, C_p, h_1, h_2, h_f, h_c, k_f, k_t, w_f, and w_{nf} are inputs to the model and the value of T_o is predicted. The specific validation point Re is calculated from eq. (1-4-2).

1-5 VALIDATION APPROACH

The nomenclature used in the validation approach presented in this Standard is shown in Fig. 1-5-1 using the heat transfer example discussed in the preceding paragraph.

Denote the predicted value of T_o from the simulation solution as S, the value determined from experimental data as D, and the true (but unknown) value as T. (Obviously, the relative magnitudes of S, D, and T will differ among cases and will not necessarily be in the order shown in the figure.) The validation comparison error[3] E is defined as

$$E = S - D \quad (1\text{-}5\text{-}1)$$

The error in the solution value, S, is the difference between S and the true value $\mathbf{T}$

$$\delta_S = S - \mathbf{T} \quad (1\text{-}5\text{-}2)$$

and similarly the error in the experimental value D is

$$\delta_D = D - \mathbf{T} \quad (1\text{-}5\text{-}3)$$

Using eqs. (1-5-1) through (1-5-3), E can be expressed as

$$E = S - D = (\mathbf{T} + \delta_S) = (\mathbf{T} + \delta_D) = \delta_S - \delta_D \quad (1\text{-}5\text{-}4)$$

The validation comparison error E is thus the combination of all of the errors in the simulation result and the experimental result, and its sign and magnitude are known once the validation comparison is made.

NOTE: The "truth" is the value of a quantity of interest defined by the observer and is an abstraction. However, incomplete definition of the quantity gives rise to an additional

[3] Equation (1-5-1) actually defines E as a discrepancy rather than an error at this point in the development, but E is shown to be an error by eq. (1-5-6).

uncertainty [2]. In this Standard, the experiment "as run" is defined as the reality of interest (truth), and thus the conditions of the actual experiment are the "validation point" that is simulated.

All errors in S can be assigned to one of three categories [1]:

(a) the error δ_{model} due to modeling assumptions and approximations

(b) the error δ_{num} due to the numerical solution of the equations

(c) the error δ_{input} in the simulation result due to errors in the simulation input parameters (T_i, T_∞, Q, d_1, d_2, L, ρ, μ, C_p, h_1, h_2, h_f, h_c, k_f, k_t, w_f, and w_{nf} in the heat transfer example)

These δ's will be defined further in later sections.

Thus

$$\delta_S = \delta_{model} + \delta_{num} + \delta_{input} \qquad (1\text{-}5\text{-}5)$$

The objective of a validation exercise is to estimate δ_{model} to within an uncertainty range.

The comparison error can then be written as

$$E = \delta_{model} + \delta_{num} + \delta_{input} - \delta_D \qquad (1\text{-}5\text{-}6)$$

This approach is shown schematically in Fig. 1-5-2, where the sources of error are shown in the ovals.

Rearranging eq. (1-5-6) to isolate δ_{model} gives

$$\delta_{model} = E - \left(\delta_{num} + \delta_{input} - \delta_D\right) \qquad (1\text{-}5\text{-}7)$$

Consider the terms on the right hand side of the equation. Once S and D are determined, the sign and magnitude of E are known from eq. (1-5-1). However, the signs and magnitudes of δ_{num}, δ_{input}, and δ_D are unknown. The standard uncertainties corresponding to these errors are u_{num}, u_{input}, and u_D (where u_D, for instance, is the estimate of the standard deviation of the parent distribution from which δ_D is a single realization).

NOTE: Once D and S have been determined, their values always differ by the same fixed amount from the true value. That is, all errors affecting D and S have become "fossilized" [4] and δ_D, δ_{input}, δ_{num}, and δ_{model} are all systematic errors. This means that the uncertainties to be estimated (u_{input}, u_{num}, and u_D) are systematic standard uncertainties. In the conceptual approach of the ISO Guide [2], there is no distinction made in the mathematical treatment of uncertainties that are "random" and those that are "systematic." A systematic error is a single realization from some parent population of possible values from a systematic error source, and the corresponding systematic standard uncertainty, u, is the estimate of the standard deviation, σ, of that parent population.

Following reference [1], a *validation standard uncertainty*, u_{val}, can be defined as an estimate of the standard deviation of the parent population of the combination of errors ($\delta_{num} + \delta_{input} - \delta_D$). Considering the relationship shown in eq. (1-5-7),

$$(E \pm u_{val}) \qquad (1\text{-}5\text{-}8)$$

then characterizes an interval within which δ_{model} falls, or

$$\delta_{model} \in [E - u_{val}, E + u_{val}] \qquad (1\text{-}5\text{-}9)$$

ASMENORMDOC.COM : Click to view the full PDF of ASME V&V 20-2009

Fig. 1-5-2 Overview of the Validation Process With Sources of Error in Ovals

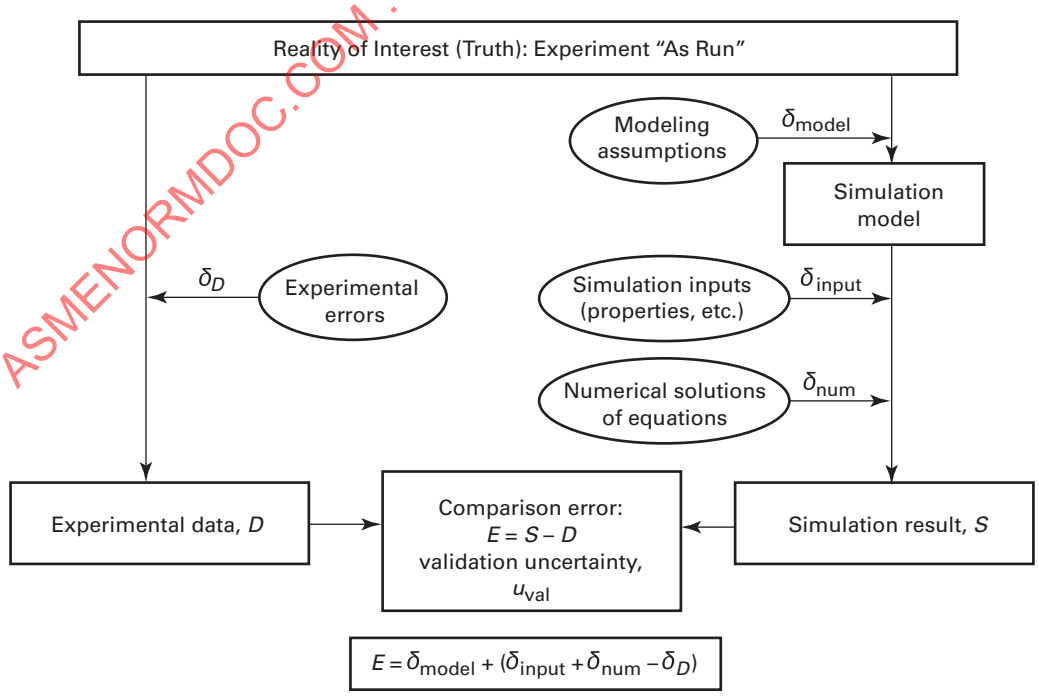

The estimation of u_{val} is thus at the core of the methodology presented in this Standard, and E and u_{val} are the validation metrics.

If the three errors on the RHS of eq. (1-5-7) are effectively independent, then

$$u_{val} = \sqrt{u_{num}^2 + u_{input}^2 + u_D^2} \qquad (1\text{-}5\text{-}10)$$

As will be discussed in detail in Section 5, when the validation variable is directly measured — as is T_o in the Case 1 (para. 1-4.1) example — the assumption of effectively independent errors is generally reasonable. However, when the validation variable is determined using a data reduction equation — as is q in Cases 2 and 3 (paras. 1-4.2 and 1-4.3) — the experimental q_D and predicted q_S values can be functions of shared variables and δ_{input} and δ_D are not independent. The equivalent to eq. (1-5-10) is shown for these cases in Section 5.

If, as demonstrated in the basic methodology in this Standard, uncertainty contributions to u_{val} are considered that take into account all of the error sources in δ_{num}, δ_{input}, and δ_D, then δ_{model} includes only errors arising from modeling assumptions and approximations ("model form" errors). In practice, there are numerous gradations that can exist in the choices of which error sources are accounted for in δ_{input} and which error sources are defined as an inherent part of δ_{model}.

The code used will often have more adjustable parameters or data inputs than the analyst may decide to use (e.g., for a commercial code). The decision of which parameters to include in the definition of the computational *simulation* (conceptually separate from the *code*) is somewhat arbitrary. Some (even all[4]) of the parameters available may be considered fixed for the simulation. For example, an analyst may decide to treat parameters in a chemistry package as fixed ("hard-wired") and therefore not to be considered in estimating u_{input}, even though these parameters could have been accessed and had associated uncertainties. The point here is that the computational simulation that is being assessed consists of the code and a selected number of simulation inputs that are considered part of the simulation, while other simulation inputs have uncertainties that are accounted for in u_{input} and thus do not contribute to δ_{model}. See Nonmandatory Appendix C for related discussion of specific and general senses of *model*, and parametric uncertainties vs. model form uncertainties.

It is crucial in interpreting the results of a validation effort that those error sources that are included in δ_{model} and those that are accounted for in the estimation of u_{val} be defined precisely and unambiguously.

[4] If all parameter values are considered fixed in the model, this is the limit of what has been termed a strong-model approach. See Roache [8] for further discussion, history, and implications to the philosophy of scientific validation.

1-6 OVERVIEW OF SUBSEQUENT SECTIONS

Considering the relationship shown in eq. (1-5-10), an estimate of u_{num} must be made to obtain an estimate of u_{val}; estimates must be made of the standard uncertainties in all input parameters that contribute to u_{input} and of the standard uncertainties in the experiment that contribute to u_D.

Code verification and solution verification processes, discussed in Section 2, result in estimation of u_{num}. Code verification is the process of determining that a code is mathematically correct for the simulations of interest (i.e., it can converge to a correct continuum solution as the discretization is refined). Code verification involves error evaluation from a known benchmark solution. Solution verification is the process of estimating numerical uncertainty for a particular solution of a problem of interest. Solution verification involves error *estimation* rather than *evaluation* from a known benchmark solution.

Techniques for estimation of u_{input}, the standard uncertainty in the solution S due to the standard uncertainties in the simulation input parameters, are presented in Section 3. Obviously, estimates of the standard uncertainties of all of the input parameters are required. Then u_{input} is determined from propagation by either of the following:

(a) using a sensitivity coefficient (local) method that requires estimates of simulation solution sensitivity coefficients

(b) using a Monte Carlo (sampling, global) method that makes direct use of the input parameter standard uncertainties as standard deviations in assumed parent population error distributions

The standard uncertainty in the experimental result u_D is determined using well-accepted techniques [2–4, 9] developed by the international community over a period of decades and is discussed in Section 4 of this document. The estimate u_D is the standard uncertainty appropriate for D. It includes all effects of averaging, includes all random and systematic uncertainty components, and includes effects of any correlated experimental errors and any other factors that influence D and u_D. As explained previously, when D and u_D are used in the validation comparison any random uncertainty components have been fossilized and u_D is a systematic standard uncertainty.

The estimation of u_{val} for a range of practical V&V situations is demonstrated in Section 5, and a discussion of the interpretation of the results of a validation effort is presented in Section 6.

A comprehensive end-to-end example of the application of the techniques covered in Sections 1 through 6 is presented and discussed in Section 7.

1-7 REFERENCES

[1] Coleman, H. W. and Stern, F., "Uncertainties in CFD Code Validation," *ASME J. Fluids Engineering*, Vol. 119, pp. 795–803, Dec. 1997.

ASMENORMDOC.COM : Click to view the full PDF of ASME V&V 20-2009

[2] *Guide to the Expression of Uncertainty in Measurement* (corrected and reprinted, 1995), International Organization for Standardization, Geneva, Switzerland, 1995.

[3] ASME PTC 19.1-2005, Test Uncertainty, 2006.

[4] Coleman, H. W. and Steele, W. G., *Experimentation, Validation, and Uncertainty Analysis for Engineers*, 3rd ed., John Wiley & Sons, New York, 2009.

[5] *International Vocabulary of Basic and General Terms in Metrology*, 2nd ed., International Organization for Standardization, Geneva, Switzerland, 1993.

[6] AIAA G-077-1998, *Guide for the Verification and Validation of Computational Fluid Dynamics Simulations*.

[7] ASME V&V 10-2006, *Guide for Verification and Validation in Computational Solid Mechanics*.

[8] Roache, P. J., *Verification and Validation in Computational Science and Engineering*, Hermosa Publishers, Albuquerque,1998.

[9] Joint Committee for Guides in Metrology, "Evaluation of Measurement Data — Supplement 1 to the 'Guide to the Expression of Uncertainty in Measurement' — Propagation of Distributions using a Monte Carlo Method," JCGM 101:2008, France, 2008.

ASMENORMDOC.COM : Click to view the full PDF of ASME V V 20 2009

Section 2
Code Verification and Solution Verification

2-1 GENERAL

This Section is ultimately concerned with the evaluation of the uncertainty of a numerical solution due to numerical error, denoted by u_{num} in eq. (1-5-10), Section 1. Prior to estimating u_{num} it is necessary to verify the code itself [i.e., to determine that the code is free of mistakes (code verification)]. Solution verification is then the process to estimate u_{num}.

2-2 INTRODUCTION

The objective of verification is to establish numerical accuracy, independent of the physical (modeling) accuracy that is the subject of validation. The necessity for requiring quantitative assessment of numerical accuracy was first formally asserted in the editorial policy statement of the ASME Journal of Fluids Engineering [1] and subsequently updated in two revised policy statements [2, 3]. As described in Section 1, code verification is distinct from solution verification and must precede it, even though both procedures utilize grid convergence studies. In general, code verification assesses code correctness and specifically involves error *evaluation* for a known solution. By contrast, solution verification[5] involves error *estimation*, since the exact solution to the specific problem is unknown. Code and solution verification are mathematical activities, with no concern whatsoever for the agreement of the simulation model results with physical data from experiments; that is the concern of validation. Note, however, that the solution and its error estimation from a solution verification will be used in the validation process. In this way, code verification, solution verification, and validation are coupled into an overall process for assessing the accuracy of the computed solution.

The verification methods discussed in this Section are specific to grid-based simulations. These include primarily finite difference, finite volume, and finite element methods in which discrete grid intervals are defined between computational nodes. The grids may be unstructured or structured (including nonorthogonal boundary-fitted grids), two-dimensional or three-dimensional, quadrilateral (or hexahedral) or triangular (or tetrahedral), and static or dynamic.[6]

The remainder of this Section 2 provides a recommended approach to successfully completing a code and solution verification effort. Code verification is treated throughout subsection 2-3. Solution verification is treated throughout subsection 2-4.

2-3 CODE VERIFICATION

Code verification, establishing the correctness of the code itself, can only be done by systematic discretization convergence tests and monitoring the convergence of the solutions towards a known "benchmark" solution (i.e., a standard of comparison). The best benchmark solution is an exact analytical solution (i.e., a solution expressed in simple primitive functions like sin, exp, tanh, etc.). Further, it is not sufficient that the analytical solution be exact; it is also necessary that the solution structure be sufficiently complex that all terms in the governing equation(s) of the code being tested are exercised.

A perception may exist, and has often been stated in research journal articles, that general accuracy verification of codes for difficult problems (e.g., the full Navier-Stokes equations of fluid dynamics) is not possible because exact solutions exist only for relatively simple problems that do not fully exercise a code. This perception has resulted in a haphazard and often piecemeal approach to code verification. In actuality, there exists a systematic approach based on grid convergence tests that is both tractable and effective (subsection 2-3.3). Some modeling approaches such as large eddy simulation (LES) and direct numerical simulation (DNS) may pose some challenges to the use of grid convergence for assessing code accuracy, but fundamentally the approach discussed in this standard may be applied (see subsection 2-5 for an additional discussion).

[5] The term "solution verification" is used in this Standard; in other references the term "calculation verification" is also used interchangeably with "solution verification" and is the equivalent term used by Freitas [2] and in the ASME V&V 10-2006 Guide.

[6] Dynamic grid methods include adaptive, Lagrangian, or arbitrary Lagrangian Eulerian. Free Lagrangian methods such as discrete vortex and discrete element methods may also use the approach defined in this Section, where the Lagrangian markers and initial distribution can be viewed as analogous to a grid distribution. Based on the initial distribution of Lagrangian markers, a refinement strategy may be deployed to determine "grid" convergence order and an assessment of uncertainty.

ASMENORMDOC.COM : Click to view the full PDF of ASME V&V 20-2009

2-3.1 Requirements of Code Verification

The process of developing a computer code for nonlinear partial differential equations (PDEs) necessarily involves much testing and evaluation of algorithms and coding. Mostly, this is performed for sets of simplified problems with analytical solutions. For example, a 3-D time-dependent fully nonlinear Navier-Stokes code will probably have been tested on a simple 1-D linear advection-diffusion equation, a 2-D or 3-D Burgers equation, and other such problems. These tests are helpful in ascertaining code performance, and classical analytical solutions for restricted problems (e.g., heat conduction) can sometimes provide convincing evidence for code verification. For more general problems (e.g., Reynolds-Averaged Navier-Stokes codes), while these piecemeal analytical solutions taken all together can constitute a partial or informal code verification, they are often inadequate to convincingly demonstrate that the code is correct for the targeted problems.

To achieve convincing code verification, one needs an exact analytical solution or family of solutions that exercises all the relevant features of a code (e.g., variable properties, nonlinearities, turbulence model, etc.). It is well known that even the laminar Navier-Stokes equations do not have known analytical solutions for any but the most trivial boundary and initial conditions. Fortunately, a very general procedure does exist for generating exact analytical solutions required for accuracy verification of codes. This procedure, the method of manufactured solutions (MMS), is described in subsection 2-3.3.

In today's simulation community, many engineers are using commercial tools provided by a vendor. In general, the vendor community has attempted to address code verification, and many follow software quality control protocols to address coding accuracy. However, the CFD/CHT (computational fluid dynamics/computational heat transfer) research community has found that the documentation of code verification provided to users by vendors is often inadequate. Therefore the commercial code user is cautioned not to rely on vendor verification of a code. The user should recognize that, even though a commercial code may have enjoyed widespread use and even verification for some problems, the code may not have been verified for the specific problems that the user intends to solve. It is always useful to obtain from the vendors the available documentation on their code verification, but it is also recommended that the user perform a code verification independently.

2-3.2 Code Option Combinations

The practical difficulties arising from the large numbers of user input options and combinations are widely recognized, but are often exaggerated, as discussed by Roache [4]. Briefly, option combinations are countable, and pessimistic computer science conclusions about complex codes being unverifiable are based on unrealistic conditions like "arbitrary complexity." Furthermore, the number of option combinations required often can be greatly reduced by "partitioning the option matrix" [4] based on common sense and knowledge of code structure (a "glass box" philosophy [5] as opposed to the more demanding "black box" philosophy). Failing this, codes can be verified only for a subset of option combinations. In fact, this is the most practical approach to take for a commercial code user. The generality of the MMS approach described next will reduce these difficulties arising from option complexity because less testing will be required for each option combination compared to a less formal approach to code verification.

2-3.3 Method of Manufactured Solutions (MMS)

The method of manufactured solutions (MMS) [4–8] provides a methodology for code verification that has been successfully demonstrated in a variety of codes. It is applicable to codes based on the solution of partial differential or integro-differential equations (usually, nonlinear systems of equations) — the subject of this document and of much of computational science and engineering. For some mathematical models, the method can be set up with no special code requirements, but this subsection will outline the most general and easy-to-apply approach, which requires code features that may not be already built into the computer code (i.e., the ability to incorporate user-written subroutines and the ability to handle source terms and nonhomogeneous boundary conditions). The following discussion of MMS is given to provide a general sense of the method; detailed examples of the implementation of the method are given in Nonmandatory Appendix A for a heat conduction problem.

As noted previously, Code Verification requires an *exact*, *analytical* solution to a nontrivial problem that covers the same options as the problem to be eventually addressed with the verified code. The formulation of an exact, analytical solution may seem difficult for nonlinear systems of PDEs, but in fact it is relatively easy. MMS starts at the end, with a sufficiently complex solution form (e.g., hyperbolic tangents or other transcendental functions). A linear solution, however, would not exercise the terms in our PDEs. Also, tanh is easily evaluated and differentiated, and contains all orders of derivatives (other functional forms also possess this attribute). One can use tanh, or another nonphysical analytical solution, or a physically realistic solution (an approximate solution to a physical problem) in the MMS method as long as sufficient complexity is embedded in the functional form.

2-3.3.1 Simple 1-D Example of MMS. To emphasize the generality of the MMS concept, as in references [4, 6, 7] the example solution is selected *before the governing equations are specified*. Then the same solution may be used for different problems, where the problem consists of a set of

ASMENORMDOC.COM : Click to view the full PDF of ASME V V 20 2009

governing PDEs and boundary conditions. The chosen solution $V(t,x)$ in this example is the following:

$$V(t, x) = A + \sin(B), \quad B = x + Ct \tag{2-3-1}$$

This 1-D transient solution is applied to the nonlinear Burgers equation, often taken as a model problem for CFD algorithm development [4].

$$\partial v/\partial t = -v\partial v/\partial x + \alpha\partial^2 v/\partial x^2 \tag{2-3-2}$$

or, using the more compact subscript notation to indicate partial derivatives,

$$v_t = -vv_x + \alpha v_{xx} \tag{2-3-3}$$

Incidentally, this specified solution $V(t,x)$ is the exact solution for the constant velocity advection equation with boundary condition of $v(t,0) = A + \sin(Ct)$. However, the physical realism of the solution selected for MMS is irrelevant to the code verification process. All that is required of the solution is that it be nontrivial, and that it exercise the computational algorithm appropriately.

The source term $Q(t,x)$ is determined that, when added to the Burgers equation for $v(t,x)$, produces the solution $v(t,x) = V(t,x)$. The Burgers equation is written as an operator (nonlinear) of v,

$$L(v) \equiv v_t + vv_x - \alpha v_{xx} = 0 \tag{2-3-4}$$

Then the source function Q that produces V by operating on V with L is evaluated.

$$Q(t, x) = L[V(t, x)] = \partial V/\partial t + V\partial V/\partial x - \alpha\partial^2 V/\partial x^2 \tag{2-3-5}$$

By elementary operations on the manufactured solution $V(t,x)$ stated in eq. (2-3-1),

$$Q(t, x) = C\cos(B) + [A + \sin(B)]\cos(B) + \alpha\sin(B) \tag{2-3-6}$$

If the modified equation is now solved

$$L(v) \equiv v_t + vv_x - \alpha v_{xx} = Q(t, x) \tag{2-3-7}$$

or

$$v_t = -vv_x + \alpha v_{xx} + Q(t, x) \tag{2-3-8}$$

with compatible initial and boundary conditions, the exact solution of the modified problem will be $V(t,x)$ given by eq. (2-3-1).

The initial conditions are obviously just $v(0,x) = V(0,x)$ everywhere. The boundary conditions are determined from the manufactured solution $V(t,x)$ given by eq. (2-3-1). Note that the domain of the solution is not even specified as yet. To consider the usual model $0 \le x \le 1$ or something like $-10 \le x \le 100$, the same solution eq. (2-3-1) applies, but of course, the boundary values are determined at the corresponding locations in x. Note also that the *type* of boundary condition as yet has not been specified. This aspect of the methodology has often caused confusion. It is widely known that different boundary conditions on a PDE produce different answers, but not everyone recognizes immediately that the same solution $V(t,x)$ can be produced by more than one set of boundary condition types. The following combinations of inflow (left boundary, e.g., $x = 0$) or outflow (e.g., $x = 1$) boundary conditions will produce the same solution $V(t,x)$ over the domain $0 \le x \le 1$.

Dirichlet–Dirichlet:

$$v(t, 0) = V(t, 0) = A + \sin(Ct) \tag{2-3-9}$$

$$v(t, 1) = A + \sin(1 + Ct) \tag{2-3-10}$$

Dirichlet–Outflow Gradient (Neumann):

$$v(t, 0) = V(t, 0) = A + \sin(Ct) \tag{2-3-11}$$

$$\partial v/\partial x|(t, 1) = \cos(1 + Ct) \tag{2-3-12}$$

Robin (Mixed)–Outflow Gradient (Neumann):

$$av + b\partial v/\partial x = c \quad at \quad (t, 0). \text{ Given } a \text{ and } b, \text{ select}$$
$$c = a[A + \sin(Ct)] + b\cos(Ct) \tag{2-3-13}$$

$$\partial v/\partial x|(t, \pi) = \cos(\pi + Ct) \tag{2-3-14}$$

For this time-dependent solution, the boundary values are time-dependent as well. It also will be possible to manufacture time-dependent solutions with steady boundary values, if required by the code. In reference [7], the same solution is applied to a new and more complicated Burgers-like PDE that might be a candidate for a 1-D turbulence formulation based on the mixing length concept. A third example in reference [7] uses a physically unrealistic manufactured solution; other examples are given in references [4, 8].

2-3.3.2 General Operator Formulation of MMS. In the general MMS approach, the problem is written symbolically as a nonlinear (system) operator L.

$$L[f(x, y, z, t)] = 0 \tag{2-3-15}$$

Choose a manufactured solution and denote it by M.

$$f = M(x, y, z, t) \tag{2-3-16}$$

The problem is now changed to a new operator, L', such that the solution to

$$L'[f(x, y, z, t)] = 0 \tag{2-3-17}$$

is exactly the manufactured solution M. The most general and straightforward approach is to determine L' by adding a source term to the original problem.

$$L'[f] = L[f] - Q \tag{2-3-18}$$

The required source term is evaluated by passing the manufactured solution M through the operator, L.

$$Q = L[M] \tag{2-3-19}$$

So instead of solving the original problem $L(f) = 0$ with an unknown solution, $L(f) = Q$ [or equivalently, $L'(f) = 0$], which has the known solution, M, is solved. Boundary values, for any boundary condition to be tested, are

ASMENORMDOC.COM : Click to view the full PDF of ASME V&V 20 2009

determined from the manufactured solution, M, as are the initial conditions.

Armed with a nontrivial exact analytical solution, M, one may perform grid convergence tests on the code and verify not only that it converges, but also at what rate it converges. Further, the magnitude (and sign) of the error is directly computed from the difference between the numerical solution and the analytical solution.

For complex models involving much chain-rule differentiation, computer Symbolic Manipulation is recommended for evaluating the source term, Q. It is not even necessary to look at the complex continuum equations and then encode them. Rather, one can just use the code-writing capability of a commercial Symbolic Manipulation code to produce a source code segment (in Fortran, C, etc.) for the source term.

For conciseness of presentation, no further examples are presented in this Section on the basic concept of MMS. However, a detailed example on an easily replicated problem is given in Nonmandatory Appendix A. Even this brief description of MMS will be sufficient for many readers to get started using it, but a potential user may not see all the ramifications at first glance. Many details and issues are addressed in references [4, Chapter 3; 6–8].

2-3.3.3 Application of MMS to Verification of Codes. Once a nontrivial exact analytic solution has been generated, by this method of manufactured solutions or perhaps another method, the solution is now used to verify a code by performing systematic discretization convergence tests (usually, grid convergence tests) and monitoring the convergence as $h \to 0$, where h is a measure of discretization [e.g., Δx (in space), Δt (in time) in a finite difference or finite volume code, and element size in a finite element code, number of vortices in a discrete vortex method, number of surface facets in a radiation problem, etc.].

The principal definition of "order of convergence" is based on the behavior of the error of the discrete solution. There are various measures of discretization error E_h, but in some sense this discussion is always referring to the difference between the discrete solution $f(h)$ (or a functional of the solution, such as lift coefficient) and the exact (continuum) solution,

$$E_h = f(h) - f^{\text{exact}} \tag{2-3-20}$$

For an order p method and a well-behaved problem, the error in the solution E_h asymptotically will be proportional to h^p. This terminology applies to the "consistent" methodologies of finite difference methods (FDM), finite volume methods (FVM), finite element methods (FEM), vortex-in-cell, etc., regardless of solution smoothness.[7] Thus,

$$E_h = f(h) - f^{\text{exact}} = C\,h^p + H.O.T \tag{2-3-21}$$

where $H.O.T.$ are higher order terms. (For smooth problems, it may be possible in principle to evaluate the coefficient C and the $H.O.T.$ from the continuum solution, but as a practical matter, this is not done in the accuracy verification procedure.) The discretization error is then monitored as the grid is systematically refined. Only refinement — not successive grid halving — is required. It should be noted, however, that for a meaningful assessment of p, grid refinement should not be trivial (a minimum value of 1.3 is recommended in subsection 2-4). In addition, thorough iterative convergence is required. Theoretically [from eq. (2-3-21)], values of $C = E_h / h^p$ should become constant as the grid is refined for a uniformly p-th order method, "uniformly" implying at all points for all derivatives. Graphical presentation is also common; the slope of E_h vs. h^p should become constant. Examples will be given in Section 7; details and many other examples are given in reference [4].

2-3.3.3.1 Differences Between Observed *p* and Theoretical *p*. The value of the observed p versus a theoretically expected value of p provides valuable insights to the numerical error in the computer code. If the values of the observed p and the theoretical p vary greatly from each other, then this indicates one of several possible issues:

(a) the grid convergence study has not been carried out to a sufficient level of refinement

(b) there are more significant errors being generated in the code than those due to discretization and thus a detailed review of the code is required

(c) boundary conditions may not be appropriate (e.g., some convective outflow boundary conditions set by simple vortex models are not ordered in h, or the implementation of the boundary condition is flawed such that the global order is affected, or the boundary conditions over-constrain the problem and propagate into the interior, thus reducing the observed order)

(d) initial conditions may not be appropriate (e.g., exact continuum initial conditions may not be compatible with solutions to the discretized equations, or are incompatible with the boundary conditions)

(e) incomplete iterative convergence and round-off errors

2-3.3.3.2 Verification of a Systematic Grid Convergence Test. Finally, when a systematic grid convergence test is verified (for all point-by-point values), then the following have been verified:

(a) any equation transformations used (e.g., nonorthogonal boundary fitted coordinates)

(b) the order of the discretization

(c) the encoding of the discretization

(d) the matrix solution procedure

As with any nontrivial technique, there are always additional details and subtleties in the application that a

[7] This order of convergence description will not apply to global spectral methods or to p-refinement FEM, but the exact solutions of MMS will still be useful for code verification.

ASMENORMDOC.COM : Click to view the full PDF of ASME V&V 20 2009

serious user should be aware of. This is true for MMS. The reader is directed to Nonmandatory Appendix C for additional details and summary points relevant to the advanced use of MMS.

2-3.3.4 Code-to-Code Comparisons. Verification of codes is sometimes approached by code-to-code comparisons. The idea is to take the solution(s) of a previously verified code as the benchmark. This can be done at two levels of applications:

(a) solutions on a specific grid

(b) "grid-free" solutions (i.e., high resolution solutions that are taken as good approximations to the exact solutions, such as with Direct Numerical Simulations)

The first approach can be useful and economical, but it requires that both codes have identical discretizations: not only at interior points, but also at all boundary points. It also requires tight iterative convergence tolerance (in essence, close to machine-zero convergence). In practice, it is effective when the new code to be verified is a new version of the previously verified code, and the new version does not change any of the discretizations. For example, the new version might contain a new linear solver, or simply use a new compiler or hardware platform (an important and practical situation). Such comparisons can be done advantageously even on very coarse grids. However, beyond this limited though important application, this approach will not give very convincing results because of the tolerances involved. It can be used economically to develop confidence during a code development program (even if the benchmark code does not use identical discretizations) but the tolerances involved will usually be too crude or large to enable truly convincing verification [4].

The same follows for the second approach. In principle, this would work if the benchmark code were itself thoroughly verified and if the solutions were indeed "grid-free" or have resolved all the pertinent length scales of the problem (possibly down to viscous dissipation) as is the requirement for Direct Numerical Simulations (DNS). In general, however, small coding errors can be masked by the lack of complete agreement due to the fuzziness of the benchmark. As with the first approach, it can be used economically to develop confidence during a code development program, but a more convincing and credible (final) code verification will always be attained by the preferred approach of MMS. Note that DNS results are often used as being equivalent to "whole-field experimental data," which then are used to assess predictive performance of Large Eddy Simulation subgrid scale models. However, this should not be confused with a formal verification and validation effort as discussed in this Standard, but rather is a strategy for developing new subgrid scale models.

Similar evaluation applies to the common approach of validation by code-to-code comparisons. In principle, one could view a previously validated code as a benchmark repository of experimental data including interpolation algorithms (by solving nonlinear PDEs). The benchmark code must be accurate to be worthwhile; there is nothing to be gained by comparison with another code that is merely *old*. In historical practice, code-to-code comparisons for code verification and validation have been notoriously unsatisfying. It is more convincing to perform validation by direct comparison with experimental data. For further discussion see reference [4].

The methods discussed above do provide valuable support in the development of computer codes and models. And these are approaches that should be routinely used to support development and enhancement of codes. However, these are not appropriate methods for a formal, convincing, and documented verification and validation effort.

2-4 SOLUTION VERIFICATION

Prior to performing solution verification, it is assumed that code verification has been completed and documented.

Systematic grid refinement is the cornerstone of verification processes for either codes or solutions [4–9]. Whereas grid-refinement studies in the context of code verification provide an *evaluation* of error, grid-refinement studies used in solution verification provide only an *estimate* of error. The most widely used method to obtain an error estimate is classical Richardson Extrapolation (RE) [10, 11]. Since its first elegant application by its originator, L. F. Richardson, in 1910 and later in 1927, this method has been studied by many authors. Its intricacies, pitfalls, and generalizations have been exhaustively investigated and cataloged [4, 9–12]. A generalized RE and a Least Squares version [13] are more widely applicable to difficult problems. There are also single grid error estimators (notably Zhu-Zienkiewicz estimators) of more specialized application [4, 14].

Error estimates and uncertainty estimates are related but are not equivalent, and confusion is common. An *error* estimate is intended to provide an improvement to the result of a calculation. For example, if the result of a calculation for heat transfer coefficient using a particular grid is f and the error estimate is ε, then an improved value (closer to the true value f_t) is $f - \varepsilon$. On the other hand, an (expanded)[8] *uncertainty* estimate $U_{x\%}$ is intended to provide a statement that the interval $f \pm U_{x\%}$ characterizes a range within which the true (mathematical) value of f_t probably falls, with probability of x%.

Quantifying that probability is the goal of uncertainty estimation. A common uncertainty target (for both

[8] By contrast, the *standard* uncertainty u has no level of probability inherently associated with it until a distribution of errors is assigned; this will be discussed more in Section 6.

ASMENORMDOC.COM : Click to view the full PDF of ASME V&V 20 2009

experiments and computations) is ~95% (i.e., ~20:1 odds that the true value f_t is in fact in the interval $f \pm U_{95\%}$), where $U_{95\%}$ is the estimate of the (expanded) uncertainty at the 95% confidence level. Note that this target confidence level is compatible with the 2σ range for a Gaussian distribution, but the concept and the semi-empirical methods presented here do not depend on the assumption of Gaussian distribution or any other distribution.

Uncertainty estimates ($U_{95\%}$) can be calculated by Roache's [4, 14–16] Grid Convergence Index (GCI). The GCI is an estimated 95% uncertainty obtained by multiplying the absolute value of the (generalized) RE error estimate (or any other ordered error estimator) by an empirically determined factor of safety, *Fs*. The *Fs* is intended to convert an ordered *error* estimate into a 95% *uncertainty* estimate. (Since all ordered error estimators for the same quantity will asymptotically produce the same error estimate, the GCI factor of safety *Fs* could be applied to any of these, at least asymptotically; the empirical value of *Fs* has been determined from RE estimates.)

Richardson Extrapolation is based on the assumption that discrete solutions, *f*, have a power series representation in the grid spacing, *h*. If the formal order of accuracy of an algorithm is known, then the method provides an estimate of the error when using solutions from two different grids. If the formal order of accuracy is not known, then three different grid solutions are required to determine the observed order of convergence and the error estimate. Although grid doubling (or halving) is often used with RE, it is not required [4], and the ratio of grid spacing, *r*, may be any real number. Integer grid refinement is not required; it has an advantage of simplicity (especially for local values that can be co-located in the grid family) but can cause difficulty. For example, when the finer grid is just sufficient to resolve scales of interest (e.g., boundary layer resolution) then a coarse grid with half the resolution may be insufficient for the problem being simulated.

Before any discretization error estimation is calculated, it must be ensured that iterative convergence is achieved. (Iterative methods are always required for nonlinear problems solved by implicit formulations and may be used as part of an explicit formulation as well.) Otherwise, the incomplete iteration error will pollute the uncertainty estimation. (RE amplifies incomplete iteration errors [4].) A commonly used but unjustifiable rule of thumb is to require at least three orders of magnitude decrease in properly normalized residuals for each equation solved over the entire computational domain. This criterion is used as a default in some commercial codes, but is demonstrably inadequate for many problems even for basic accuracy, without considering the added requirements of uncertainty estimation. Results in references [17, 18] belie the casualness of this rule. For time-dependent simulations, iterative convergence at every time step should be checked, and example convergence trends should be documented for selected, critically important, variables. The preferred approach is to reduce the iterative error to a level negligible compared to the discretization error. This does not necessarily require iteration to (nearly) machine zero.

Iteration error and its interaction with discretization error has been thoroughly studied in reference [18] for one class of problems; there is no reason to assume that other problems are more benign. A method for estimation of iteration error based on extrapolating by geometric progressions was developed and justified, and applied to realistic turbulent flows. These results show that the iteration error needs to be 2 to 3 orders of magnitude smaller than the discretization error to guarantee a negligible influence. This is often assumed, although seldom demonstrated convincingly. If the uncertainty u_i contributed by the (estimated) iteration error is much less than u_h contributed by the (ordered) discretization error, then we take the numerical uncertainty u_{num} to be

$$u_{\text{num}} = u_h \tag{2-4-1}$$

If more care is taken and u_i is to be added, it is *not* adequate (conservative) to use RMS addition, because the iteration error affects the results for discretization error (i.e., u_i and u_h are not uncorrelated), violating the underlying assumption of RMS addition. Rather, the two must be combined by less optimistic simple addition [18].

$$u_{\text{num}} = u_h + u_i \tag{2-4-2}$$

Application of RE and GCI often encounter some difficulties in practical problems. Local values of predicted variables may not exhibit a smooth, monotonic dependence on grid resolution, and in a time-dependent calculation, this nonsmooth response will also be a function of both time and space. However, integral quantities like overall heat transfer coefficient, lift coefficient, etc. are usually better behaved (i.e., are more likely to converge monotonically). The GCI, especially the Least Squares versions pioneered by Eça and Hoekstra [13; see also 14, 19, 20 in Nonmandatory Appendix C], is currently the most robust and tested method available for the prediction of numerical uncertainty.

The influence of the outflow boundary position on the interior solution will depend on the outflow condition used and on the distance to the outflow boundary. The errors of these approximations do not vanish as $h \to 0$, and hence are "nonordered approximations" or modeling errors rather than discretization errors. (See also Nonmandatory Appendix C.) The same can be stated for other far-field boundaries. The adequacy of these approximations should be assessed by sensitivity tests [4] at least on similar problems, but unfortunately in practice these tests are not often addressed convincingly.

ASMENORMDOC.COM : Click to view the full PDF of ASME V V 20 2009

2-4.1 Five-Step Procedure for Uncertainty Estimation

A five-step procedure is defined below for the application of the Grid Convergence Index (GCI) method [3].

Step 1: Define a representative cell, mesh, or grid size, h. For example, for three-dimensional, structured, geometrically similar grids (not necessarily Cartesian),

$$h = \left[(\Delta x_{\max})(\Delta y_{\max})(\Delta z_{\max})\right]^{1/3} \tag{2-4-3}$$

For nonstructured grids one can define

$$h = \left[\left(\sum_{i=1}^{N} \Delta V_i\right)/N\right]^{1/3} \tag{2-4-4}$$

where

N = total number of cells used for the computations

ΔV_i = volume of the i^{th} cell [4]

Step 2: Select three significantly different sets of grid resolutions and run simulations to determine the values of key variables important to the objective of the simulation study (e.g., a variable φ). There are some advantages to using integer grid refinement but it is not necessary. It is desirable that the grid refinement factor, $r = h_{\text{coarse}}/h_{\text{fine}}$, should be greater than 1.3 for most practical problems. This value of 1.3 is again based on experience and not on some formal derivation. The grid refinement should, however, be made systematically; that is, the refinement itself should be structured even if the grid is unstructured. Geometrically similar cells in the grid sequence are required to avoid noisy and erroneous observed p. It is highly recommended not to use different grid refinement factors in different directions (e.g., $r_x = 1.3$ and $r_y = 1.6$), because erroneous observed p values are produced, as shown in [21]. (The computational solutions still converge to the correct answers with $r_x \neq r_y$, but the observed rate of convergence p is affected.)

Step 3: Let $h_1 < h_2 < h_3$ and $r_{21} = h_2/h_1$, $r_{32} = h_3/h_2$ and calculate the apparent (or observed) order, p, of the method from reference [4]

$$p = \left[1/\ln(r_{21})\right]\left[\ln\left|\varepsilon_{32}/\varepsilon_{21}\right| + q(p)\right] \tag{2-4-5}$$

$$q(p) = \ln\left(\frac{r_{21}^{p} - s}{r_{32}^{p} - s}\right) \tag{2-4-6}$$

$$s = 1 \cdot \text{sign}(\varepsilon_{32}/\varepsilon_{21}) \tag{2-4-7}$$

where $\varepsilon_{32} = \varphi_3 - \varphi_2$, $\varepsilon_{21} = \varphi_2 - \varphi_1$, and φ_k denotes the simulation value of the variable on the k^{th} grid. Note that $q(p) = 0$ for $r = constant$. This set of three equations can be solved using fixed point iteration with the initial guess equal to the first term (i.e., $q = 0$).

A minimum of four grids is required to demonstrate that the observed order p is constant for a simulation series. A three-grid solution for the observed order p may be adequate if some of the values of the variable φ predicted on the three grids are in the asymptotic region for the simulation series. In fact, it may require more than four grids to convincingly demonstrate asymptotic response in difficult problems, possibly five or six grid resolutions in cases where the convergence is noisy [13, 19, 20]. It is all dependent on the initial grid resolution used and where the predicted value of φ lies as a function of grid resolution. However, to provide a balance between providing both a tractable method and ensuring a level of accuracy in the predicted observed order p, at least a three-grid study should be performed. If the solution verification error and uncertainty terms δ_{SN} and u_{SN}, respectively, are then found to be small compared to the other δ_i and u_i terms in this Standard, three grids may then be sufficient. If not, then more grids will be required.

Step 4: Calculate the extrapolated values from the equation

$$\varphi_{\text{ext}}^{21} = \left(r_{21}^{p}\varphi_1 - \varphi_2\right)/\left|r_{21}^{p} - 1\right) \tag{2-4-8}$$

Step 5: Calculate and report the following error estimates along with the observed order of the method p. Approximate relative error may be cast as a dimensionless form [eq. (2-4-9)] or in a dimensioned form [eq. (2-4-10)]:

$$e_a^{21} = \left|\frac{\varphi_1 - \varphi_2}{\varphi_1}\right| \tag{2-4-9}$$

$$e_a^{21} = \left|\varphi_1 - \varphi_2\right| \tag{2-4-10}$$

If φ_1 is zero or the user wishes to calculate u_{num} (see eqs. 2-4-13 and 2-4-14) then one should use eq. (2-4-10).

Estimated extrapolated relative error:

$$e_{\text{ext}}^{21} = \left|\frac{\varphi_{\text{ext}}^{21} - \varphi_1}{\varphi_{\text{ext}}^{21}}\right| \tag{2-4-11}$$

The fine Grid Convergence Index:

$$\text{GCI}_{\text{fine}}^{21} = \frac{Fs \cdot e_a^{21}}{r_{21}^{p} - 1} \tag{2-4-12}$$

The relative error estimates and the GCI may use normalizing based on values other than local values; in fact, this is often advantageous for avoiding indeterminacies. Also, the error estimates and the GCI may use dimensional values instead of relative or normalized values [4, pp. 113, 115]. This is often the more natural choice for use with experimental results and will be used in the examples in Section 7.

The Factor of Safety, Fs, originally was assigned a value of 3 for two-grid studies [16], but Roache [4] has subsequently recommended a less conservative value for $Fs = 1.25$, but only when using at least three grid

ASMENORM.COM : Click to view the full PDF of ASME V&V 20 2009

solutions and the observed p. He arrived at this value through empirical studies, and this value roughly correlates with the definition of uncertainty U used in references [22, 23] and suggests that using a value of 1.25 results in a GCI with a 95% confidence interval. Further experience in hundreds of CFD cases (more than 500 demonstrated cases) by dozens of groups has supported this empiricism [4, 13, 14, 15, 19, 20, 24]. Based on this current evidence, we recommend that a value of $Fs = 1.25$ be used with three-grid studies involving structured grid refinement. (Note that a base grid may be unstructured, but the grid sequence may be generated by structured refinement of an unstructured grid [4].)

The value of $Fs = 1.25$ has not been thoroughly evaluated for unstructured refinement. Scatter in observed p is to be expected because the grid refinement factor r is well defined only for geometrically similar grids. The accuracy of the GCI will obviously depend on the quality of the unstructured grid refinement algorithm. Until a sufficient data set is collected and studies are completed for unstructured refinement, it is generally recommended that the more conservative value of $Fs = 3$ be used to obtain a GCI for unstructured grid refinement. (The results to be presented in Section 7 are well behaved, and $Fs = 1.25$ is sufficient.)

If the calculated order of the method p is less than 1.0, an uncertainty band may also be given by assuming $p = 1.0$. This is done not to ignore the observed p, but simply to give two calculations, one with the observed p and one with $p = 1.0$, as an indicator of the sensitivity of the error band to the observed value of p. However, the GCI computed with the observed $p < 1$ is the more conservative approach. It should also be noted that if the observed value of p is significantly different from the expected order of the method (for example, the method might be expected to be third-order for the primary variables but it is observed to be less than 1), then one should delve into the root cause of this difference. It may suggest a possible error in the method or its implementation, or that the grid resolutions are not in the asymptotic region, or that a singularity is present. (See references [25, 26] for methods to detect and distinguish singularities during grid convergence studies.)

The form of the GCI is based on theory, but the use of absolute values for estimated errors and the factor Fs are based on empiricism involving the examination of several hundred CFD case studies. The empirical tests involved the determination of conservatism in 95% of the cases, corresponding to (dimensional) GCI = U_{num} at 95% confidence. No assumptions on the form of the error distributions were made nor were necessary for these empirical studies, since actual data was examined with a simple pass/fail criterion. Specifically, the common statistical assumption of a Gaussian distribution was not used. To agree with the new international standard use of one standard deviation σ, eq. (1-5-10) was developed using 1σ, and the corresponding uncertainty is u_{num}. If the procedure adopted for the other uncertainty components is to base everything on the commonly used expanded uncertainty level $U_{95\%}$, then U_{num} = GCI and no assumption of a distribution is required. Otherwise, to convert this (partially) empirical GCI from U_{num} to the u_{num} needed in eq. (1-5-10) it is now necessary to make an assumption. If the distribution were Gaussian about the fine grid solution, the value of u_{num} would be obtained using an expansion factor $k = 2$, and the required term for eq. (1-5-10) would be

$$u_{num} = U_{num}/k = \text{GCI}/2 \qquad (2\text{-}4\text{-}13)$$

However, the error distribution about the fine grid solution is roughly Gaussian only for poorly behaved problems (oscillatory convergence). For well behaved and highly resolved problems, the error distribution is roughly Gaussian not about the fine grid solution φ_1 but rather about the extrapolated solution φ_{ext}^{21} of eq. (2-4-8) [i.e., the fine grid solution φ_1 plus the estimated signed error e_{ext}^{21} of eq. (2-4-11)]. Thus the error distribution about the fine grid solution is roughly a shifted Gaussian. Analyses of this situation indicate an expansion factor $k = 1.1$ to 1.15 to obtain a conservative value for u_{num}.

$$u_{num} = U_{num}/k = \text{GCI}/1.15 \qquad (2\text{-}4\text{-}14)$$

If the overall u_{val} is later expanded to $U_{95\%}$ using $k = 2$, the numerical contribution will then be more conservative than 95% (see Section 6).

The five-step procedure presented in this section makes no distinction between steady state computations or time-dependent computations. The method is independent of temporal resolution in the sense that Δt does not appear in any of the equations. So, for time-dependent computations, the five-step procedure should be applied at each relevant time step in the computation at a given node. However, it should be noted that as the spatial grid is refined during the convergence study, the size of Δt is likely decreasing as well due to numerical stability issues and thus Δt is implicitly accounted for in the convergence study. Although not discussed here, it has been shown that the above procedure may be applied accounting for both spatial and temporal grid convergence explicitly. The Δt is treated just like Δx is treated. However, some minor complications arise in the typical case where the numerical methods have different orders of accuracy in space and time, or even different orders in different spatial directions, as may occur in boundary layer codes [4].

Paragraphs 2-4.2 and 2-4.3 present example Solution Verifications for two realistic and difficult problems in CFD. This Standard will also present examples for heat conduction problems that are less demanding numerically and exhibit close to theoretical performance. But the following two CFD problems are not so ideal, and the convergence behaviors are representative of many real and practical problems that the reader will likely need to deal with.

ASMENORMDOC.COM : Click to view the full PDF of ASME V&V 20 2009

2-4.2 Example 1: Turbulent Flow Over a Backstep

To demonstrate the results of the GCI calculation following this five-step procedure, data of Table 2-4-1 are used from Celik and Karatekin [12], where steady, turbulent flow over a backward facing step was simulated on nonuniform structured grids with the total number of cells defined by three grid resolutions, N_1, N_2, and N_3. Two variables were used in the evaluation of uncertainies: the dimensionless reattachment length, L, and the axial velocity, V, at a specific location. In this particular study, two different sets of grid refinements were used for the two variables of interest. For the dimensionless reattachment length, L, the three grid resolutions used were 4,500, 8,000, and 18,000 cells; while for the axial velocity, V, three grid resolutions of 980, 4,500, and 8,000 cells were used. Since the order of the method in terms of axial velocity is less than 1 in this example, column four displays results where the value of p is assumed to be 1. Based on this analysis with $Fs = 1.25$, the value of the reattachment length would be reported as 6.06 ± 0.09 (±1.46%), and the axial V velocity at a point as 10.8 ± 0.12 (±1.06%).

The calculated values of observed p being noninteger and less than the theoretical value ($p = 2$ in this case) are not at all unusual in difficult applications, even for thoroughly verified codes (often not the case for commercial software). Real problems involving local high gradients in the solution, and especially shock waves or other singularities, reduce the observed p (or even the actual asymptotic p [4]) because the locally large values of higher-order solution derivatives cause higher-order terms to be significant in the power-series expansion of the discretization errors [4]. This example (and the second, following) illustrates the importance of evaluating the GCI using values of p observed for the actual case under study, rather than theoretical values or code verification studies based on well-behaved problems.

Table 2-4-1 Sample Uncertainty Analysis: Backward Facing Step

	L	V	$V(p = 1)$
N_1	18,000	8,000	8,000
N_2	8,000	4,500	4,500
N_3	4,500	980	980
r_{21}	1.5	2.0	2.0
r_{32}	1.33	2.14	2.14
φ_1	6.06	10.8	10.8
φ_2	5.97	10.7	10.7
φ_3	5.86	10.6	10.6
p	1.53	0.75	1.00
φ_{ext}^{21}	6.17	10.9	10.9
e_a^{21}	1.50%	0.58%	0.58%
e_{ext}^{21}	1.71%	0.85%	0.58%
GCI_{fine}^{21}	1.46%	1.06%	0.73%

In many practical cases, the observed p's calculated over more than one grid triplet will be noisy, indicating erratic or even nonmonotonic convergence; in such cases, a least-squares approach developed in references [13, 14, 19, 20] is recommended (Nonmandatory Appendix C). Alternative techniques with a choice of GCI or other methods for oscillatory or nonmonotonic convergence are discussed in references [25, 26]. Note, however, that observed p values that approximate the theoretical p can be obtained with good algorithms, good grid generation, high resolution, and careful work, even for time-dependent turbulent flows [4], or problems with shock fronts. For heat conduction problems, it is common for observed p to be well-behaved, as demonstrated in Section 7.

2-4.3 Example 2: Confined Detonation

Figure 2-4-1 provides another example of the five-step procedure of the GCI calculation for a TNT charge detonated in a rigid, fluid-filled box. The quantity of interest

Fig. 2-4-1 Sample Uncertainty Analysis: Explosive Detonation in a Fluid Filled Box

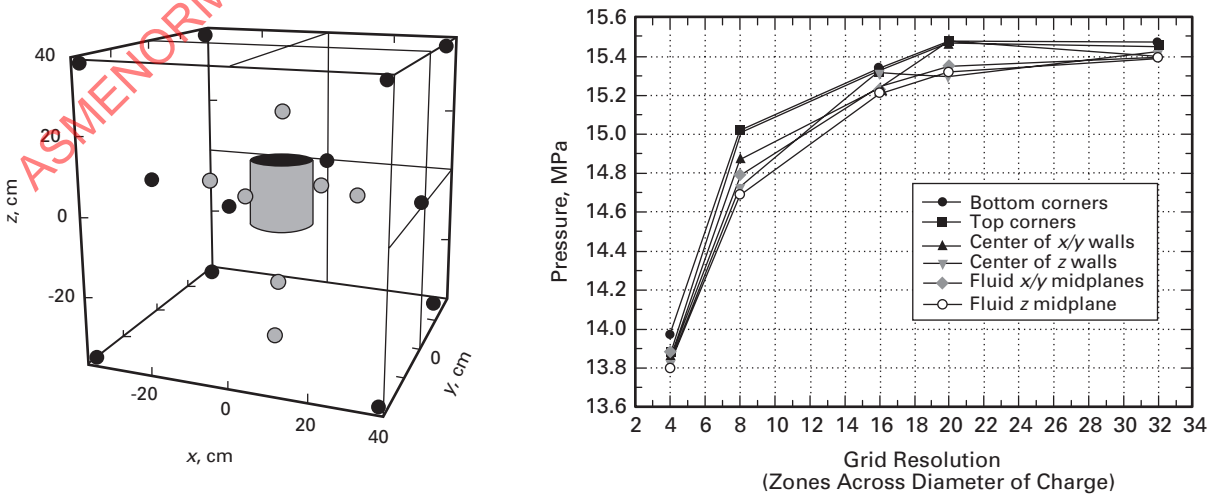

ASMENORMDOC.COM : Click to view the full PDF of ASME V V 20 2009

Table 2-4-2 Sample Uncertainty Analysis: Explosive Detonation

Location of Variable	Corner	Wall	Fluid
Observed order p	1.7	1.5	1.02
GCI value (%)	1.2	1.6	3.6
Value $\pm U_{num}$	15.34 $\pm$ 0.18 MPa	15.23 $\pm$ 0.24 MPa	15.24 $\pm$ 0.55 MPa
Value $\pm u_{num}$	15.34 $\pm$ 0.16 MPa	15.23 $\pm$ 0.21 MPa	15.24 $\pm$ 0.48 MPa
Fine grid prediction	15.47 MPa	15.40 MPa	15.39 MPa

is the quasi-static pressure at various locations in the box (shaded dots in left image) after a finite elapsed time in the time-dependent simulation. The right image in this figure displays the predicted value of pressure as a function of grid resolution at various measurement locations predicted by the set of simulations. In this example, the magnitude of pressure has a smooth dependence on grid resolution. The basis for the grid resolution used is the number of zones across the diameter of the charge.

Table 2-4-2 summarizes the results of the application of the GCI to the explosive detonation problem. Here pressures at three different locations are used [i.e., a node in the corner of the box (corner), a node near the center of a box side (wall), and a node at mid-distance between the charge centerline and a box side (fluid)]. The second row of the table provides the computed (observed) order of the method, and the third row provides the computed GCI using $Fs = 1.25$. To compute these values, the first four grid resolutions (4, 8, 16, and 20 zones across the diameter of the charge) were used. Rows four and five provide the range in pressure as predicted by the GCI, but presented with the uncertainty estimates of U_{num} and u_{num}. The range of value $\pm U_{num}$ is intended to bound the exact mathematical solution with a 95% confidence or a 2σ uncertainty estimate, while value $\pm u_{num}$ (fifth row of Table 2-4-2) is a σ uncertainty estimate. The sixth row in the table displays the predicted value of pressure on the finest grid (resolution of 32 zones across the diameter of the charge). The ranges displayed in row four of the table should then bound the values here, and they do, again, demonstrating both the validity of this approach and the appropriateness of the magnitude of $Fs = 1.25$ in the GCI method.

2-5 SPECIAL CONSIDERATIONS

The simulation variable, φ, that is evaluated by the five-step procedure of para. 2-4.1 can be any result of the simulation: local values of the dependent variables like u, v, p; volume-weighted RMS values; or integrated functionals of the solution like lift coefficient or heat flux. The same principles of solution verification apply in all cases, but the following should be noted. First, integrated functionals typically are better behaved (more smooth) than local values and thus the observed p tends to be less noisy. Second, different simulation variables can converge at different rates. Third, the same techniques for solution verification can be applied to derivatives of integrated functionals with respect to input parameters, as will be required in the following Section.

Care must be taken in determining the appropriate grid resolution requirements for both the grid convergence exercise and the grid resolution required to minimally resolve the physics of the problem. For example, if the problem to be solved has a specific range of length scales that characterize the flow physics such as boundary layers or thermal gradients, then the grid resolution for the coarsest grid used in the grid convergence study must still adequately resolve these length scales. This is particularly important in the context of large eddy simulation (LES). The LES filter width is usually related to a measure of the grid resolution, and thus as the grid resolution is changed during the grid convergence study, the filter width also is changed. This means that the partitioning of energy between the resolved and unresolved scales is changing. Thus, if the users are not careful and as the grid convergence study is executed, they may be solving a different problem for some of the coarse-grid resolutions if the boundary between resolved and unresolved scales changes significantly from grid to grid. The same logic applies to direct numerical simulation (DNS) as well, in that coarser grid resolutions may not resolve the same set of appropriate flow scales adequately to qualify the simulation as DNS. A DNS simulation by definition resolves all pertinent flow scales (in frequency domain) up to viscous dissipation.

Finally, the following is suggested as an approach to effectively and efficiently perform and use a solution verification exercise in applications. For the given problem to be simulated, the first step is to define a set of simulation objectives (i.e., why the problem is being simulated, what quantities are of interest for prediction, and what level of accuracy is required). Given the simulation objectives, a nominal simulation problem is defined, including boundary and initial conditions. This nominal problem should be representative of the problem set to be studied (where typically many simulations are performed to achieve the problem solution). This nominal problem will then serve as the basis for the solution verification grid convergence study. A detailed grid convergence study of this specific, nominal problem is executed with 3 to 6 levels of grid refinement (similar to the confined detonation example problem of para. 2-4.3). Based on the results of the solution verification for the nominal problem, a base grid resolution is defined that achieves

ASMENORMDOC.COM : Click to view the full PDF of ASME V V 20 2009

the simulation objectives for estimated accuracy. This base grid resolution is then used in all subsequent simulations for the particular problem. If, during the course of the subsequent simulations, the problem definition changes significantly such that the nominal problem no longer is representative of the study, then a new nominal problem should be defined and a new solution verification performed.

2-6 FINAL COMMENT

At the conclusion of a *code verification* activity following the procedures defined in this section, the analyst will have determined potential code errors. It is assumed then that these errors have resulted in modifications and enhancements to the computer code to eliminate or fix them. Once a verified code is achieved for the application of interest, then a *solution verification* effort following the procedures defined in this section will result in an estimate of the uncertainty (u_{num}) associated with a simulation result. In many applications in engineering and scientific practice, these two procedures, *code verification* and *solution verification*, may be all that is required for the application of interest as dictated by project requirements or may be all that is possible due to a lack of appropriate experimental data for validation. If that is the case, then successfully completing a *solution verification* effort (which assumes that it was preceded by a *code verification* effort) for the application of interest will result in a significant step forward in understanding the accuracy of a given simulation study in that now it may be reported that the solution is a value X with a numerical uncertainty of Y. However, at this point in this Standard, the user can only state the estimated magnitude of u_{num}. One can not at this point assess overall model accuracy. That can only be done through *validation*, which requires the material presented in Sections 3 through 7 of this Standard.

2-7 REFERENCES

[1] Roache, P. J., Ghia, K. and White, F. (1986), "Editorial Policy Statement on the Control of Numerical Accuracy," *ASME Journal of Fluids Engineering*, Vol. 108, No. 1, March 1986, pg. 2.

[2] Freitas, C. J. (1993), "Editorial Policy Statement on the Control of Numerical Accuracy," *Journal of Fluids Engineering*, Vol. 115, September, pp. 339–340, 1993.

[3] Celik, I. B., Ghia, U., Roache, P. J., Freitas, C. J., Coleman, H. W., and Raad, P. E. (2008), "Procedure for Estimation and Reporting of Uncertainty due to Discretization in CFD Applications," *ASME Journal of Fluids Engineering*, Editorial, Vol. 130, No. 7, July 2008, pp. 078001-1– 078001-4, 4 pages.

[4] Roache, P. J. (1998), *Verification and Validation in Computational Science and Engineering*, Hermosa Publishers, Albuquerque.

[5] Oberkampf, W. L. and Trucano, T. G., "Verification and Validation in Computational Fluid Dynamics," *Progress in Aerospace Sciences*, Vol. 38, No. 3, 2002, pp. 209–272.

[6] Roache, P. J. (2004), "Building PDE Codes to be Verifiable and Validatable," *Computing in Science and Engineering*, Special Issue on Verification and Validation, September/October 2004, pp. 30–38.

[7] Roache, P. J. (2002), "Code Verification by the Method of Manufactured Solutions," *ASME Journal of Fluids Engineering*, Vol. 114, No. 1, March 2002, pp. 4–10.

[8] Knupp, P. and Salari, K. (2002), *Verification of Computer Codes in Computational Science and Engineering*, CRC Press, Boca Raton.

[9] Celik, I., Chen, C. J., Roache, P. J., and Scheuerer, G, eds. (1993), *Proceedings: Symposium on Quantification of Uncertainty in Computational Fluid Dynamics*, ASME Fluids Engineering Division Summer Conference, June 20–24, Washington, D.C., Vol. 158.

[10] Richardson, L. F. (1910) "The Approximate Arithmetical Solution by Finite Differences of Physical Problems Involving Differential Equations, with an Application to the Stresses In a Masonry Dam," *Transactions of the Royal Society of London, Ser. A*, Vol. 210, pp. 307–357.

[11] Richardson, L. F. and Gaunt, J. A. (1927), "The Deferred Approach to the Limit," *Philos. Trans. R. Soc. London, Ser. A*, Vol. 226, pp. 299–361.

[12] Celik, I., and Karatekin, O. (1997), "Numerical Experiments on Application of Richardson Extrapolation With Nonuniform Grids," *J. Fluids Engineering*, Vol. 119, pp. 584–590.

[13] Eça, L. and Hoekstra, M. (2002), "An Evaluation of Verification Procedures for CFD Applications," 24th Symposium on Naval Hydrodynamics, Fukuoka, Japan, 8–13 July 2002.

[14] Pelletier, D. and Roache, P. J. (2006), "Verification and Validation of Computational Heat Transfer", Chapter 13 of *Handbook of Numerical Heat Transfer*, Second Edition, W. J. Minkowycz, E. M. Sparrow, and J. Y. Murthy, eds., Wiley, New York.

[15] Roache, P. J. (2003), "Error Bars for CFD," AIAA Paper 2003-0408, AIAA 41st Aerospace Sciences Meeting, January 2003, Reno, Nevada.

[16] Roache, P. J. (1993), "A Method for Uniform Reporting of Grid Refinement Studies," *Proceedings of Quantification of Uncertainty in Computation Fluid Dynamics*, Edited by Celik, et al., ASME Fluids Engineering Division Spring Meeting, Washington D.C., June 23–24, ASME Publ. No. FED-Vol. 158.

[17] Eça, L. and M. Hoekstra, M. (2006), "On the Influence of the Iterative Error in the Numerical Uncertainty of Ship Viscous Flow Calculations," Proc. 26th Symposium on Naval Hydrodynamics, Rome, Italy, 17–22 Sept. 2006.

ASMENORMDOC.COM : Click to view the full PDF of ASME V&V 20-2009

[18] Eça, L. and M. Hoekstra, M. (2007), Evaluation of Numerical Error Estimation Based on Grid Refinement Studies with the Method of Manufactured Solutions," Report D72-42, Instituto Superior Tecnico, Lisbon.

[19] Eça, L., Hoekstra, M., and Roache, P. J. (2005), "Verification of Calculations: an Overview of the Lisbon Workshop," AIAA Paper No. 4728, AIAA Computational Fluid Dynamics Conference, Toronto, June 2005.

[20] Eça, L., Hoekstra, M., and Roache, P. J. (2007), "Verification of Calculations: an Overview of the Second Lisbon Workshop," AIAA Paper 2007-4089, AIAA Computational Fluid Dynamics Conference, Miami, June 2007.

[21] Salas, M. D. (2006), "Some Observations on Grid Convergence," *Computers and Fluids*, Vol. 75, No. 7, Aug. 2006, pp. 688–692 .

[22] Coleman, H. W. and Stern, F. (1997), "Uncertainties and CFD Code Validation," *ASME Journal of Fluids Engineering*, Vol. 119, December 1997, pp. 795–803.

[23] Stern, F., Wilson, R. V., Coleman, H. W., and Paterson, E. G. (2001), "Comprehensive Approach to Verification and Validation of CFD Simulations — Part 1: Methodology and Procedures," ASME Journal of Fluids Engineering, Vol. 123, pp. 793–802, December.

[24] Roache, P. J. (2003), "Conservatism of the GCI in Finite Volume Computations on Steady State Fluid Flow and Heat Transfer," *ASME Journal of Fluids Engineering*, Vol. 125, No. 4, July 2003, pp. 731–732.

[25] Sinclair, G. B., Anaya-Dufresne, M., Meda, G, and Okajima, M. (1997), "Tuned Test Problems for Numerical Methods in Engineering," *International Journal for Numerical Methods in Engineering*, Vol. 40, pp. 4183–4209.

[26] Sinclair, G. B., Beisheim, J. R., and Sezer, S. (2006), "Practical Convergence-Divergence Checks for Stresses from FEA," Proc. 2006 International ANSYS Users Conference and Exposition, 2–4 May 2006, Pittsburgh, PA, U.S.A. See also Report ME-MS1-08, Department of Mechanical Engineering, Louisiana State University.

ASMENORMDOC.COM : Click to view the full PDF of ASME V&V 20-2009

Section 3
Effect of Input Parameter Uncertainty on Simulation Uncertainty

3-1 INTRODUCTION

This Section is concerned with the estimation of simulation uncertainty due to uncertainty of the simulation input parameters, denoted by u_{input} in eq. (1-5-10), Section 1.

The validation uncertainty has been previously defined in Section 1 as being composed of uncertainty in the numerical simulations u_{num}, input parameters u_{input} and data u_D and is given by

$$u_{\text{val}}^2 = u_{\text{num}}^2 + u_{\text{input}}^2 + u_D^2 \qquad (3\text{-}1\text{-}1)$$

Section 2 presented techniques for estimating u_{num} and Section 4 discusses techniques for estimating u_D. The focus of Section 3 is to estimate u_{input}, the simulation uncertainty due to uncertainty in simulation input parameters.

Computational simulations usually contain experimentally determined parameters that have uncertainty associated with them. The model of the system may range from an algebraic equation to a system of partial differential equations. For a heat transfer example, it might be desired to estimate the uncertainty in the model temperature predictions, given the uncertainty in thermal conductivity(s), volumetric heat capacity(s), and convective heat transfer coefficient(s). For a fluid flow example, it might be desired to estimate the uncertainty in the drag coefficient, given uncertainty in fluid properties.

Two different approaches for estimating u_{input} will be presented. The two approaches depend on whether one takes a *local* or *global* view of the uncertainty estimation process. The *local* view is concerned with the response of the system in a small (*local*) neighborhood of the nominal parameter vector. In the literature, the local view is known by a variety of names: sensitivity coefficient method, perturbation method, mean value method, first order method, and possibly others. The *global* view is concerned with the response of the system in a large (*global*) neighborhood of the nominal parameter vector. In the literature, the global view is known by a variety of names: sampling method, Monte Carlo method, and possibly others. In the sections that follow, a description of the local and global uncertainty estimation procedures will be presented along with an example of each.

3-2 SENSITIVITY COEFFICIENT (LOCAL) METHOD FOR PARAMETER UNCERTAINTY PROPAGATION

Using a linear Taylor series expansion in parameter space, the input uncertainty propagation equation for a simulation result S with n uncorrelated random input parameters is

$$u_{\text{input}}^2 = \sum_{i=1}^{n} \left(\frac{\partial S}{\partial X_i} u_{X_i} \right)^2 \qquad (3\text{-}2\text{-}1)$$

where

S = simulation result

u_{X_i} = corresponding standard uncertainty in input parameter X_i

X_i = input parameter

For situations in which parameters are obtained from a database, the assumption of uncorrelated errors is a good one.

Simulation result S in eq. (3-2-1) could be a point value of a simulation variable or an integral quantity such as total drag or heat transfer. The partial derivatives, $\partial S/\partial X_i$, are termed sensitivity coefficients of the result S with respect to input parameter, X_i. The term inside the parentheses in eq. (3-2-1) is often written as $\overline{X}_i \frac{\partial S}{\partial X_i} \frac{u_{X_i}}{\overline{X}_i}$ where $\overline{X}_i$ is the nominal parameter value. This approach makes it convenient to specify the relative standard uncertainty $u_{X_i}/\overline{X}_i$ instead of the absolute standard uncertainty u_{X_i}. The remaining sensitivity coefficient $\overline{X}_i \frac{\partial S}{\partial X_i}$ is termed a scaled sensitivity coefficient and has the units of S. Equation (3-2-1) indicates the following two ingredients are required for the uncertainty propagation equation:

(a) the sensitivity coefficient

(b) input parameter uncertainty

In the material that follows, a discussion of how to obtain these two quantities in eq. (3-2-1) will be presented.

3-2.1 Estimation of Input Parameter Uncertainty

Ideally, the input standard uncertainty values, u_{X_i}, come from prior experiments. For example, suppose one has a transient thermal model of a multi-material system with convective boundary conditions. Laboratory scale experiments would have been performed to determine the thermal conductivity and volumetric

ASMENORMDOC.COM : Click to view the full PDF of ASME V&V 20 2009

heat capacity of each of the materials. If property measurements are performed, the techniques of Section 4 should be used to estimate the experimental uncertainty. A more likely scenario is that one will use "database (handbook) property values" and may have to resort to expert opinion for the uncertainty in property values. Experimentally determined correlations for the convective heat transfer coefficient may be used. Again, it is assumed that the experimenter reported the experimental uncertainty; if not, expert opinion will have to be used for the uncertainty.

3-2.2 Local Techniques for Computing Sensitivity Coefficients

Many techniques available for computing local sensitivity coefficients $(\partial S/\partial X_i)$ include the following:

(a) finite difference (FD) in parameter space
(b) analytical differentiation of analytical solutions
(c) complex step (CS)
(d) software differentiation (e.g. ADIFOR/ADIC)
(e) sensitivity equation method (SEM)
(f) adjoint method

Of the sensitivity methods listed, all generally require access to source code with the exception of FD. The access to source code requirement likely excludes their use with commercial software. Consequently, our focus will be on the finite difference (in parameter space) method, which will allow the code to be used in a "black box" approach. The remaining sensitivity methods are topics of current research and the reader is referred to [1–3].

3-2.3 Computation of Sensitivity Coefficients by Finite Differences

A measure of the sensitivity of the simulation result $S(z, t, \boldsymbol{X})$ to changes in a parameter $\boldsymbol{X}_i$ is termed the sensitivity coefficient and is defined as

$$\text{Sensitivity Coefficient} = \frac{\partial S(z, t, \boldsymbol{X})}{\partial X_i} \qquad (3\text{-}2\text{-}2)$$

where
t = time
X_i = one element of $\boldsymbol{X}$ (the vector of all problem parameters)
z = position vector

In this section, it is implicit that the sensitivity coefficient is evaluated at the nominal value of the parameter vector. The simulation result S could be temperature, velocity, heat flux, shear stress, drag, heat transfer, etc. For a single material heat transfer problem involving thermal conductivity, volumetric specific heat, viscosity, and emittance, the nominal parameter vector would be $\boldsymbol{X} = \{k\ \rho c_p\ \mu\ \varepsilon\}$. Many materials will be present for industrial heat conduction or conjugate heat transfer problems. In this case, the thermal properties of all the materials present will be part of the parameter vector; consequently, the parameter vector can contain tens to hundreds of elements.

In the simple case of an algebraic model, sensitivity coefficients $\partial S/\partial X_i$ may be computed analytically. However, a more likely scenario is that the model is a complex numerical simulation for which a finite difference differentiation is the most practical approach. The term "finite difference" as used here refers to the parameter space and not the finite difference in space/time discretization algorithm for numerically solving partial differential equations. The procedure is to run the simulation with nominal values of the parameter vector $\overline{\boldsymbol{X}}$. A second run is made with a perturbed value $(X_i + \Delta X_i)$ for input parameter X_i. A finite difference approximation in parameter space is then used to compute the sensitivity coefficient from

$$\frac{\partial S}{\partial X_i} = \frac{S(X_1, X_2, \ldots, X_i + \Delta X, \ldots, X_n) - S(X_1, X_2, \ldots, X_i, \ldots, X_n)}{\Delta X_i} + O(\Delta X_i) \qquad (3\text{-}2\text{-}3)$$

The above process is repeated for each input parameter. If there are n parameters, then $n + 1$ runs of the simulation code will be required to compute the n first-order sensitivity coefficients. A second-order accurate finite difference is

$$\frac{\partial S}{\partial X_i} = \frac{S(X_1, X_2, \ldots, X_i + \Delta X_i, \ldots, X_n) - S(X_1, X_2, \ldots, X_i - \Delta X_i, \ldots, X_n)}{2\Delta X_i} + O(\Delta X_i^2) \qquad (3\text{-}2\text{-}4)$$

If a second-order central difference is used, then the number of simulations goes to $2n$ +1. The computational load for the finite difference in parameter space method scales linearly with the number of input parameters for which uncertainty is considered. The primary difficulty with the finite difference method is choosing an appropriate perturbation size ΔX_i. If ΔX_i is too large, the truncation error in eqs. (3-2-3) or (3-2-4) will be too large. If ΔX_i is too small, machine round off becomes significant because of subtractive cancellation in the numerator of eqs. (3-2-3) or (3-2-4). Finite difference sensitivity coefficients can be problematic for incomplete nonlinear iteration; see reference [4] for a discussion of this issue. Some numerical experimentation is recommended. An example problem will help solidify some of the issues associated with the finite difference (in parameter space) method.

3-2.4 Local Uncertainty Propagation Example

Consider a planar 1-D slab exposed to a constant heat flux (q) on one face, adiabatic on the other face, and uniform initial temperature (T_i). The analytical solution for the temperature field $T(z,t)$ is given in reference [5] as

ASMENORMDOC.COM : Click to view the full PDF of ASME V V 20 2009

$$\phi = \frac{T - T_i}{qL/k} =$$

$$\frac{\alpha t}{L^2} + \frac{1}{3} - \frac{z}{L} + \frac{1}{2}\left(\frac{z}{L}\right)^2 - \frac{2}{\pi^2}\sum_{n=1}^{\infty}\frac{1}{n^2}\exp\left(-n^2\pi^2\frac{\alpha t}{L^2}\right)\cos\left(n\pi\frac{z}{L}\right) \quad (3\text{-}2\text{-}5)$$

where
k = thermal conductivity
L = slab thickness
q = heat flux
z = distance from the heated surface
$\alpha\left(=k/\rho c_p\right)$ = thermal diffusivity

The sensitivity of the temperature field to the thermal conductivity can be computed by analytically differentiating eq. (3-2-5) with respect to k, resulting in

$$k\frac{\partial T}{\partial k} = \frac{qL}{k}\left(\alpha\frac{\partial\phi}{\partial\alpha} - \phi\right) \quad (3\text{-}2\text{-}6)$$

where

$$\alpha\frac{\partial\phi}{\partial\alpha} = \frac{\alpha t}{L^2}\left[1 + 2\sum_{n=1}^{\infty}\exp\left(-n^2\pi^2\frac{\alpha t}{L^2}\right)\cos n\pi\frac{z}{L}\right] \quad (3\text{-}2\text{-}7)$$

Note that eq. (3-2-6) is the scaled sensitivity coefficient for the thermal conductivity k and has the units of temperature.

While analytical techniques can be used for this example problem, numerical techniques will likely have to be used for most practical problems. A significant use for analytical differentiation is to provide verification problems for other techniques for computing sensitivity coefficients. Even if analytical sensitivity coefficients are available, finite difference methods are often used to verify the correct implementation of analytical expressions.

This example problem was solved numerically using a second order in space finite difference method and a first-order fully implicit time integrator. The sensitivity coefficient was then calculated using the first-order finite difference in parameter space given by eq. (3-2-3). The example problem parameters, which are representative of a stainless steel, are as follows:

$$q = 4\times10^5\,\mathrm{W\,m^{-2}},\quad k = 10\,\mathrm{W\,m^{-1}K^{-1}},\quad L = 0.01\,\mathrm{m}$$
$$\rho = 8\,000\,\mathrm{kg\,m^{-3}},\ c_p = 500\,\mathrm{J\,kg^{-1}\,K^{-1}},\ T_i = 300\,\mathrm{K}$$
$$t_f = 20\,s,\ \alpha t_f/L^2 = 0.5,\ \alpha\,\Delta t/\Delta z^2 = 2.5 \quad (3\text{-}2\text{-}8)$$

Fig. 3-2-1 Relative Error in Finite Difference Computation of $k\partial T/\partial k$ Using a Backwards Difference

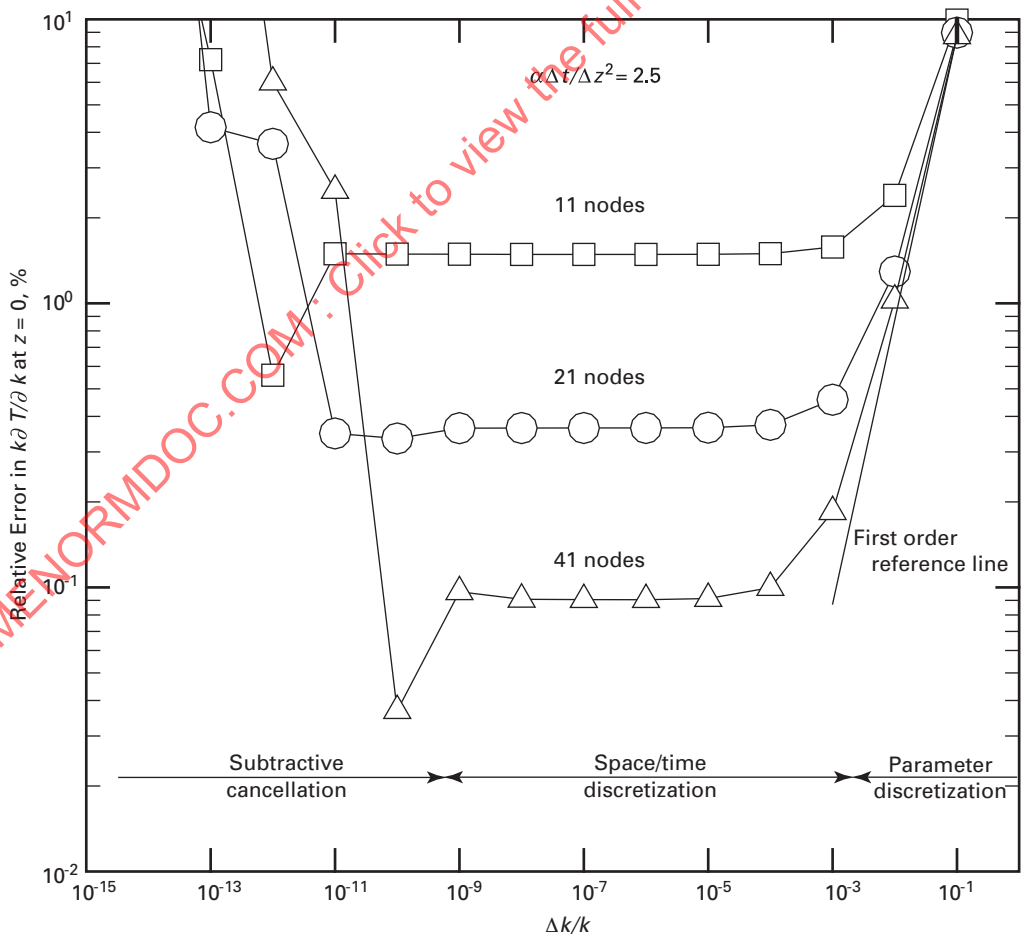

GENERAL NOTE: Numerical discretization algorithm was second order spatial finite difference with a first order implicit time integrator and the space/time grid refinement maintained $\alpha\Delta t/\Delta z^2 = 2.5$.

ASMENORMDOC.COM : Click to view the full PDF of ASME V 20 2009

The relative error in this numerical solution for the scaled sensitivity coefficient $k\partial T/\partial k$ was computed with the analytical solution from eq. (3-2-6) taken as the exact answer. The computational domain was spatially discretized into uniformly spaced nodes. Figure 3-2-1 presents the computational results for the error in thermal conductivity sensitivity coefficient for grids of 11, 21, and 41 nodes. During the space/time grid refinement, $\alpha\Delta t/\Delta z^2$ was kept fixed; if Δz was reduced by a factor of 2, then Δt was reduced by a factor of 4. For a given spatial discretization (number of nodes or elements), the results can be divided into approximate regimes in which different effects dominate the relative error in the sensitivity coefficient:

$$\begin{aligned} &\text{parameter discretization} && \Delta k/k > 10^{-3} \\ &\text{space/time discretization} && 10^{-9} < \Delta k/k < 10^{-3} \\ &\text{subtractive cancellation} && \Delta k/k < 10^{-9} \end{aligned} \qquad (3\text{-}2\text{-}9)$$

The above boundaries were determined using double precision arithmetic on a 32 bit computer and should be viewed as fuzzy. If either the precision or word length is changed, these boundaries are likely to change. For $\Delta k/k > 10^{-3}$, the parameter discretization errors dominate. For the relatively flat portion of the error curve in Fig. 3-2-1, the space/time discretization dominates. In this region, the results are relatively independent of $\Delta k/k$; this is the region in which one wants to be operating. For $\Delta k/k < 10^{-9}$, subtractive cancellation dominates and the errors can actually increase as $\Delta k/k$ is made smaller.

The range of $\Delta k/k$ for which the error in $k\partial T/\partial k$ reaches a stable minimum depends on the number of nodes. This range is broader for a coarse grid than for a fine grid. Hopefully this example will provide some impetus to perform numerical experiments when using the finite difference method in parameter space.

If the second order finite difference (in parameter space) given by eq. (3-2-4) is used, then similar results will be obtained with the exception that the results will follow a second order reference line instead of a first order line. The decision of first order versus second order will likely be made based on whether the computational budget can afford $2n+1$ simulations as opposed to $n+1$ simulations.

ASMENORMDOC.COM : Click to view the full PDF of ASME V V 20 2009

Fig. 3-2-2 Estimated Uncertainty in Model Temperature Due to Uncertainty in q, k, and ρc_p

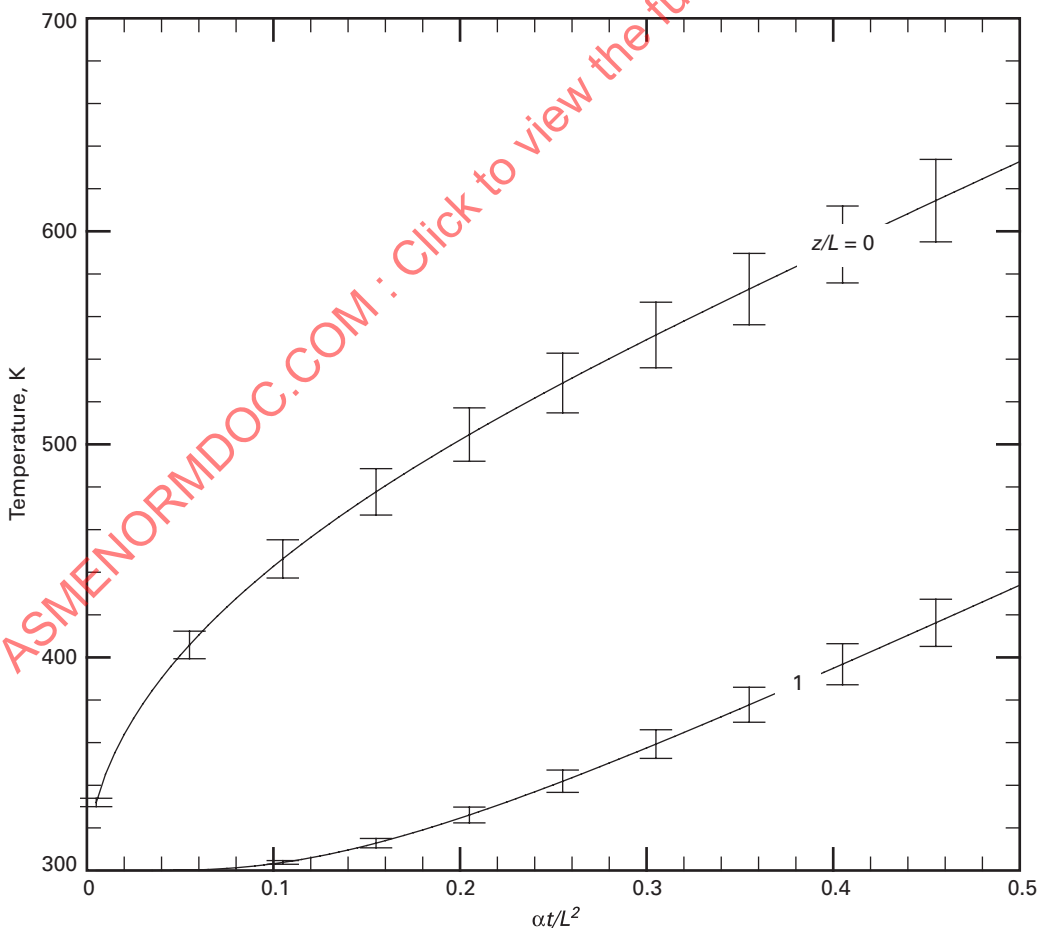

GENERAL NOTE: All relative standard uncertainties were 0.05. The mean value method, eq. (3-2-1), was used.

Using eq. (3-2-1), the uncertainty in the computed temperature due to input parameter uncertainty was computed for the above constant heat flux example. The parameter vector for this example is

$$\boldsymbol{X} = \{q\ k\ \rho c_p\} \tag{3-2-10}$$

The relative standard uncertainty values were all taken to be $u_{X_i}/X_i = 0.05$. The property values were those given in eq. (3-2-8). The nominal temperature response and the corresponding uncertainty is given in Fig. 3-2-2. From the (estimated) input parameter uncertainty, the standard uncertainty in the front face temperature may be as much as ±20 K. This ±20 K range characterizes standard uncertainty of the model output due to uncertainty in the model input parameters.

3-3 SAMPLING (GLOBAL) METHODS FOR PARAMETER UNCERTAINTY PROPAGATION

The sensitivity coefficient method presented in the preceding section has been termed *local* sensitivity and uncertainty propagation because the function evaluations are in a small (local) neighborhood of the mean parameter value. This approach will not capture highly nonlinear behavior in the parameter space; sampling based methods (Monte Carlo) will address this deficiency.

The most reliable sampling technique for uncertainty analysis is to sample the parameter space using the full Monte Carlo method. This technique requires the distribution functions to represent the uncertainties in each parameter. A representative probability distribution function for the thermal conductivity is shown in Fig. 3-3-1; the mean and standard deviation of the distribution of are 10 W/m-K and 0.5 W/m-K, respectively. A random sample is drawn from each parameter's distribution function, and standard statistical techniques are used to compute the mean and variance of the simulations. If parameters are correlated, joint probability distributions are required; in this case, sampling methods should properly account for correlation between input parameters.

ASMENORMDOC.COM : Click to view the full PDF of ASME V V 20 2009

Fig. 3-3-1 Representative Probability Distribution Function for Thermal Conductivity

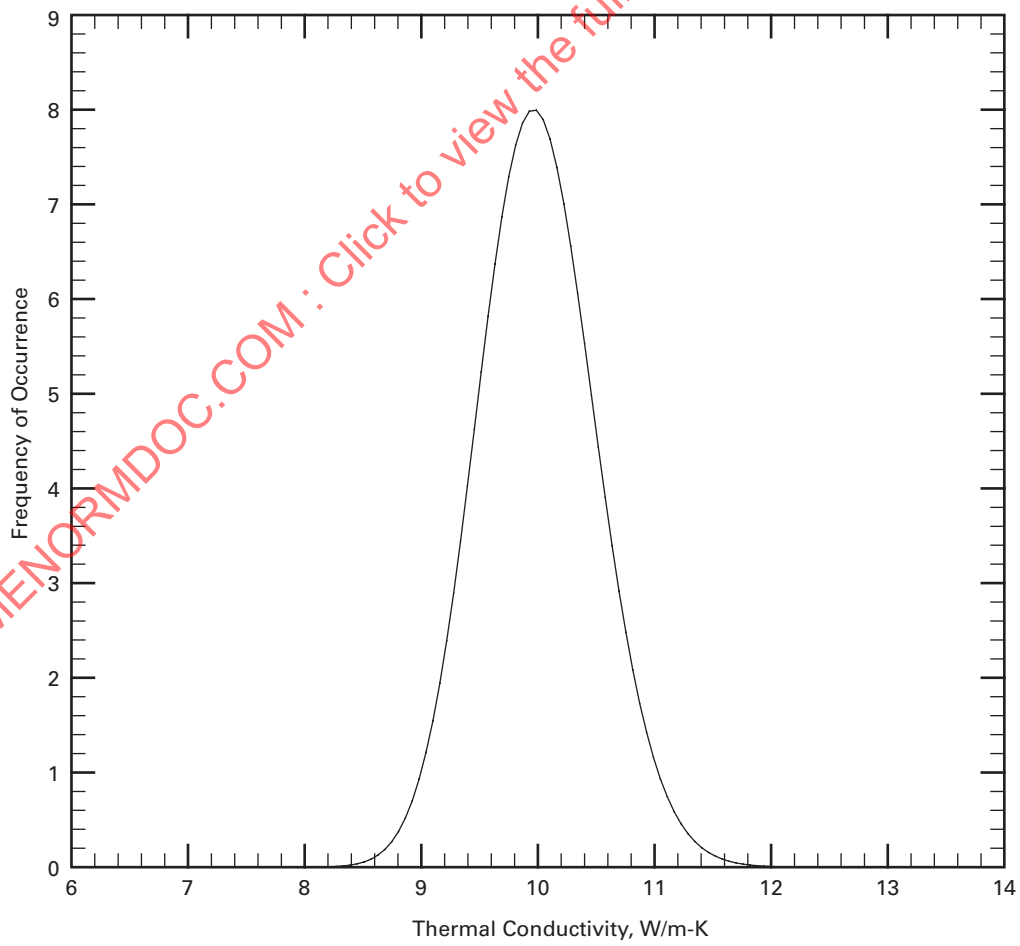

GENERAL NOTE: The mean and standard uncertainty are 10 W/m-K and 0.5 W/m-K, respectively.

The term "function evaluation" is applied to running the simulation for one value of the parameter vector. The number of function evaluations required for statistical convergence (results independent of number of function evaluations) may lie in the range of tens to thousands, depending on the degree of convergence required. The full Monte Carlo approach is cpu intensive. An alternative to the full Monte Carlo method is the latin hypercube sampling (LHS) method presented in reference [6]. In the LHS method, the cumulative probability distribution of a given variable is divided into n_{LHS} ($\geq n_p + 1$, generally when sensitivity is desired) bands of equal probability. Within each band, a random sample is drawn from the probability distribution of the band. This process is repeated for each of the n_p model parameters (or variables) such as thermal conductivity, heat capacity, volumetric source, etc. The matrix of $n_{\text{LHS}} \times n_p$ values is represented in Table 3-3-1. The columns in Table 3-3-1 represent the LHS samples for a given variable while the rows represent the model parameter vector for a given probability band. To ensure full coverage, the model parameters are combined in a random fashion in a process described by references [7] and [8] as follows: "The n_{LHS} values thus obtained for X_1 are paired at random and without replacement with the n_{LHS} values obtained for X_2. These n_{LHS} pairs are combined in a random manner without replacement with the n_{LHS} values of X_3 to form n_{LHS} triples. This process is continued until a set of n_{LHS} n_p-tuples is formed." The above methodology has been documented in references [9] and [10] and is implemented in reference [11]. Section 1 of reference [10] contains a very readable description of LHS. The LHS method will capture nonlinear behavior over the sampled parameter space provided the number of samples is adequate for statistical convergence, and the distribution functions are known with sufficient accuracy.

Once the simulation has been run for the n_{LHS} parameter vectors, standard statistical techniques can be used to process the results. Estimates of the expected value (mean) and variance of response S are given by

$$\bar{S} = \frac{1}{n_{LHS}} \sum_{i=1}^{n_{LHS}} S_i \qquad \text{(3-3-1)}$$

$$u^2_{input} = \frac{1}{n_{LHS} - 1} \sum_{i=1}^{n_{LHS}} \left(S_i - \bar{S}\right)^2 \qquad \text{(3-3-2)}$$

Table 3-3-1 Matrix Representation of Number of LHS Samples (n_{LHS}) and Number of Parameters (n_p)

↓ Probability Band\Parameters →	X_1	X_2	...	X_{n_p}
1	X_{11}	X_{12}	...	X_{1n_p}
2	X_{21}	X_{22}	...	X_{2n_p}
⋮	⋮	⋮	⋱	⋮
n_{LHS}	X_{nLHS1}	X_{nLHS2}	...	X_{nLHSn_p}

Table 3-3-2 LHS Samples for the Three Parameters *q*, *k*, and *C*

Sample	q, W/m²	k, W/m-K	$\rho c_p = C$, J/m³-K
1	378378	9.6984	3828080
2	407452	9.4573	4271520
3	438268	9.8618	4092520
4	368497	10.5484	4196800
5	399413	10.3684	4021160
6	386260	9.8795	3948668
7	403336	8.8858	3898340
8	391985	9.9936	3850160
9	412212	11.1242	4138320
10	417844	10.2519	3634980

GENERAL NOTE: The parent distributions were log-normal with relative standard uncertainty of 0.05.

If the mean response and its uncertainty are the only things of interest, then the computational process is complete. From the LHS results, the distribution function of S can be estimated. Since the distribution function of the input variables is often assumed, the sensitivity of u^2_{input} to this assumption can be explored.

With sampling-based methods, there may be some question if the number of samples was adequate. One way of answering this question is to perform replicates. With the LHS procedure, this is accomplished by starting the random number generator with a different seed. The entire analysis is then repeated and the results are compared for the different replicates. The replicates can be processed individually or as a group.

The above LHS methodology has been applied to the constant heat flux problem used throughout this section. Ten LHS runs were made with the finite difference numerical code; the model contained 11 equally spaced nodes. The three variables $\{q\ k\ \rho c_p\}$ were assumed to have independent log-normal distributions, each with a relative standard uncertainty of 0.05; the corresponding LHS parameter vectors are given in Table 3-3-2. Equations (3-3-1) and (3-3-2) were used to compute the average and standard deviation of the nodal temperatures; the results for $z/L = 0$ and 1 are shown in Fig. 3-3-2. For comparison purposes, the sensitivity coefficient (mean value) results are also presented. The two methods are in agreement for $z/L = 1$ but there is some disagreement for $z/L = 0$. Since both the LHS and mean value methods are approximate, further investigation is required to ascertain which method is the most accurate for this problem. The mean value method assumes a linear dependence in the parameters model; for this example, the model is nonlinear in k and ρc_p. The LHS method is a small sample approximation to the full Monte Carlo method; an adequate number of samples for statistical convergence is required. Conclusions drawn as to the "best" method for a particular problem may not be valid for all problems.

ASMENORMDOC.COM : Click to view the full PDF of ASME V 20 2009

Fig. 3-3-2 Standard Deviation in Temperature at $z/L = 0$ and 1 for Constant Heat Flux Example Using 10 LHS Runs and Mean Value Method (With $u_x/X = 0.05$)

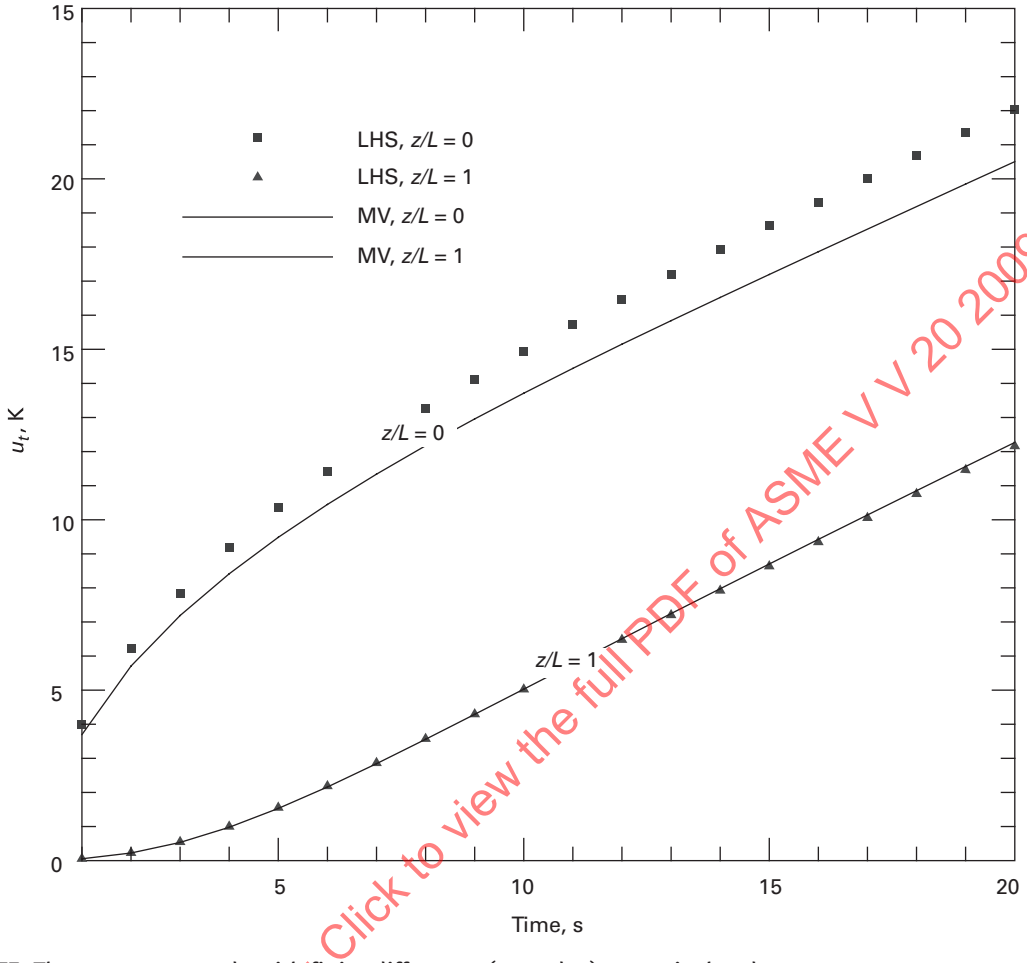

GENERAL NOTE: The runs were made with finite difference (11 nodes) numerical code.

ASMENORMDOC.COM : Click to view the full PDF of ASME V V 20 2009

3-4 IMPORTANCE FACTORS

Importance factors are quantities that allow one to assess the relative importance of the input parameters on the model uncertainty u_{input}. While importance factors are not necessary for the formal validation process, they are extremely important in that they help the experimentalist/analyst in deciding how to best spend resources if it is desired to reduce u_{input}. Nonmandatory Appendix B presents techniques for computing importance factors for both sensitivity coefficient and sampling methods.

3-5 SPECIAL CONSIDERATIONS

All the calculations presented in this section were performed on a 32 bit computer using double precision arithmetic. Computer precision will have an impact on how small one can make the finite difference step size without encountering subtractive cancellation problems.

For those problems with a large (>> 10) number of parameters, it is recommended that expert opinion be used to reduce the number of parameters for which sensitivity coefficients are computed.

In managing the large number of simulations that must be performed in a computational uncertainty analysis, some kind of scripting language is very helpful. Some software exists that was designed specifically to aid this process; in the literature, this is termed "putting a wrapper around the analysis code" [11].

The input parameters (u_{input}) uncertainty is treated as independent of the numerical uncertainty (u_{num}). This is a good assumption for small parameter perturbations and finite difference sensitivity coefficients. One can demonstrate that grid errors approximately cancel when computing finite difference sensitivity coefficients. For sampling methods, u_{input} could have dependence on u_{num} for the case of using a coarse grid for the individual samples. To avoid this dependency, it is recommended that u_{input} be computed on the finest grid used to estimate u_{num} if both u_{input} and u_{num} are comparable in size. For those

problems in which $u_{num} << u_{input}$, then the calculations for u_{input} can be computed on a coarser grid.

If the parameter variation causes a movement from one flow regime to another, then the methods presented here for computing u_{input} will not work. An example is the movement from laminar to turbulent flow or vice versa. This effect is less likely to happen with small perturbation methods than with sampling methods.

It is reasonable to expect a certain amount of subjectivity in estimating u_{X_i} (and its associated distribution function for the LHS).

3-6 FINAL COMMENT ON PARAMETER UNCERTAINTY

At the conclusion of Section 3, one will have determined the contribution of each parameter to u_{input}. At this time, it is appropriate to compare u_{input} to S and ask if u_{input} is larger than is programmatically acceptable. This is an important question to ask, independent of the validation process. If the answer to the above question is yes, then the individual contributors to u_{input} must be studied to determine which parameter uncertainties should be reduced. Further work may be required to reduce the uncertainties in the dominant parameters, which in turn will reduce u_{input}. If the answer is no, then one can proceed with the remainder of the validation process given in Sections 4 through 7.

3-7 REFERENCES

[1] Blackwell, B. F. and Dowding, K. J., "Sensitivity Analysis and Uncertainty Propagation of Computational Models," in Minkowycz, W. J., Sparrow, E. M., and Murthy, J. Y., *Handbook of Numerical Heat Transfer*, 2nd ed., Wiley, New York, 2006, pp. 443–469.

[2] Anon, "ADIFOR 2.0 Automatic Differentiation of Fortran," World Wide Web page, http://www-unix.mcs.anl.gov/autodiff/ADIFOR.

[3] Martins, J. R. R. A., "A Guide to the Complex-Step Derivative Approximation," World Wide Web page, http://mdolab.utias.utoronto.ca/resources/complex-step.

[4] Eca, L. and Hoekstra, M., "On the Influence of the Iterative Error in the Numerical Uncertainty of Ship Viscous Flow Calculations," *Proceedings of 26th Symposium on Naval Hydrodynamics*, Rome, Italy, September 2006.

[5] Beck, J. V., Blackwell, B. F., and St. Clair, C. R., *Inverse Heat Conduction*, Wiley, New York, 1985.

[6] McKay, M. D., Conover, W. J., and Beckman, R. J., "A Comparison of Three Methods for Selecting Values of Input Variables in the Analysis of Output from a Computer Code," *Technometrics*, Vol. 21, 1979, pp. 239–245.

[7] Helton, J. C. and Davis, F. J., "Latin Hypercube Sampling and the Propagation of Uncertainty in Analyses of Complex Systems," *Reliability Engineering and System Safety*, Vol. 81, 2003, pp. 23–69.

[8] Helton, Jon C. and Davis, Freddie J., "Sampling Based Methods," in Saltelli, A., Chan, K., and Scott, E. M., editors, *Sensitivity Analysis*, Wiley, New York, 2000, pp. 101–153.

[9] Iman, R. L. and Shortencarier, M. J., "A FORTRAN 77 Program and User's Guide for the Generation of Latin Hypercube and Random Samples for Use With Computer Models," Tech. Rep. SAND83-2356, Sandia National Laboratories, March 1984.

[10] Wyss, G. D. and Jorgensen, K. H., "A User's Guide to LHS: Sandia's Latin Hypercube Sampling Software," Tech. Rep. SAND98-0210, Sandia National Laboratories, February 1998.

[11] Eldred, M. S., Adams, B. M., Haskell, K., Bohnhoff, W. J., Eddy, J. P., Gay, D. M., Griffin, J. D., Hart, W. E., Hough, P. D., Kolda, T. G., Martinez-Canales, M. L., Swiler, L. P., Watson, J. P., and Williams, P. J., 2007. "DAKOTA: A Multilevel Parallel Object-Oriented Framework for Design Optimization, Parameter Estimation, Uncertainty Quantification, and Sensitivity Analysis. Version 4.1 Users Manual," Sandia Technical Report SAND2006-6337, Updated September 2007.

ASMENORMDOC.COM : Click to view the full PDF of ASME V&V 20 2009

Section 4
Uncertainty of an Experimental Result

4-1 OVERVIEW

This Section presents the basic concepts from experimental uncertainty analysis that are used in the determination of the uncertainty of the experimental result, u_D, in eq. (1-5-10). The ASME standard [1] on this subject, PTC 19.1-2005, *Test Uncertainty*, is considered to be a companion document for V&V 20. This Section provides an overview of the basic methodology in PTC 19.1.

The validation process is dependent upon having an appropriate experimental result that has a quantified uncertainty estimate, u_D. In addition, the experiment will provide many of the simulation inputs and their associated uncertainties. It is critical for the modeler and the experimentalist to work together in the design of the validation experiment. The experiment will be the reality of interest that the modeler is trying to simulate. Preliminary simulation results can help in the design of the experiment and in the proper specification and placement of instrumentation.

4-2 EXPERIMENTAL UNCERTAINTY ANALYSIS

The accepted standards for experimental uncertainty analysis are references [1] and [2]. The process used in experimental uncertainty analysis is to calculate the uncertainties of individual measured variables and then to use these to estimate the uncertainty of the result(s) determined from these variables. For a measured variable X, the total error is caused by multiple error sources. The sum of all of these errors for a measurement is the difference between the value of the measurement determined in the experiment and the true value of the measured variable. In experimental programs, corrections to the measurements are made for those errors that are known, as in the calibration process. For those errors where the magnitude and sign are unknown, uncertainty estimates are made to represent the dispersion of possible values for the errors. Both references [1] and [2] use the standard deviation for each error source to calculate the uncertainty in the measured variable. This standard deviation quantity is called the standard uncertainty u.

In reference [2], these uncertainties are grouped by the method used to evaluate them. Those that are calculated by statistical means are classified as Type A and those that are estimated by other means are classified as Type B. Reference [1] uses this classification but also includes a grouping of the uncertainties by their effect on the measured variable. Those uncertainties from error sources that contribute to the variability of the measurement are classified as random and those uncertainties from error sources that remain fixed during the measurement process are classified as systematic. The discussion below uses the random and systematic classifications to discuss the uncertainty of a measurement and the uncertainty of the test result.

4-2.1 Uncertainty of a Measurement

The systematic standard uncertainty of the measurement of a variable is obtained from the square root of the sum of the squares of the systematic standard uncertainties for all independent error sources. For each systematic error source, the experimenter must estimate a systematic standard uncertainty, b_{i_k}. Systematic standard uncertainties are estimated from previous experience, calibration data, analytical models, and the application of sound engineering judgment [3]. The systematic standard uncertainty for variable X_i is then

$$b_i = \sqrt{b_{i_1}^2 + b_{i_2}^2 + \ldots + b_{i_k}^2} \qquad (4\text{-}2\text{-}1)$$

As an example, consider a thermocouple that has been calibrated against a standard with a systematic standard uncertainty of 0.10°C. When the calibration correction is applied, the fixed error of the thermocouple is replaced by the calibration uncertainty and the systematic standard uncertainty of the calibration curve — for this example taken to be 0.05°C. If the thermocouple is then used to measure the mean temperature of a flow field, an additional uncertainty might need to be applied to account for how well the thermocouple measurement actually represents the mean temperature. If this conceptual uncertainty (estimated by taking multiple measurements or by analytical modeling) were 0.20°C, then the systematic standard uncertainty for the thermocouple measurement would be

$$b_T = \sqrt{(0.10°C)^2 + (0.05°C)^2 + (0.20°C)^2} = 0.23°C \qquad (4\text{-}2\text{-}2)$$

Estimates of systematic uncertainties are usually made at some confidence level rather than at the standard deviation level. Typically, these systematic uncertainty estimates are representative of the 95% limits of the possible values of the systematic error. To obtain the systematic standard uncertainty, a distribution is assumed for this 95% estimate (i.e. normal, rectangular, triangular), and the estimate is divided by the appropriate distribution

ASMENORMDOC.COM : Click to view the full PDF of ASME V&V 20-2009

factor (2 for normal, 1.65 for rectangular, etc.) to convert the 95% estimate to a standard deviation [1].

An estimate of the range of random error for measurements of a variable X_i is the sample standard deviation, s_i, also called the random standard uncertainty. Unlike the systematic error, the random error varies from measurement to measurement. To reflect the entire range of possible measured values of a variable, the measurements used to calculate the random standard uncertainty must be taken over the time frame and conditions that cover the variations in the variable. For example, taking multiple samples of data as a function of time while holding all other conditions constant will identify the random variation associated with the measurement system and the unsteadiness of the test condition. If the random standard uncertainty of the variable being measured is also expected to be representative of other possible variations in the measurement (repeatability of test conditions for example), then these additional error sources will have to be varied while the multiple data samples are taken to determine the standard uncertainty. If repeatability of test conditions is not represented in the experiment, then this effect will have to be estimated as an additional systematic standard uncertainty.

4-2.2 Uncertainty of a Result

Consider an experimental result that is determined from J measured variables as

$$r = r\,(X_1, X_2, \ldots, X_i, \ldots, X_J) \qquad (4\text{-}2\text{-}3)$$

The standard uncertainty of the result, u_r, is found as

$$u_r = \sqrt{b_r^2 + s_r^2} \qquad (4\text{-}2\text{-}4)$$

where b_r is the systematic standard uncertainty of the result

$$b_r^2 = \sum_{i=1}^{J} \left(\frac{\partial r}{\partial X_i} b_i\right)^2 + 2\sum_{i=1}^{J-1}\sum_{k=i+1}^{J} \frac{\partial r}{\partial X_i}\frac{\partial r}{\partial X_k} b_{ik} \qquad (4\text{-}2\text{-}5)$$

and s_r is the random standard uncertainty of the result

$$s_r^2 = \sum_{i=1}^{J} \left(\frac{\partial r}{\partial X_i} s_i\right)^2 + 2\sum_{i=1}^{J-1}\sum_{k=i+1}^{J} \frac{\partial r}{\partial X_i}\frac{\partial r}{\partial X_k} s_{ik} \qquad (4\text{-}2\text{-}6)$$

where

b_i = systematic standard uncertainties of the measurements

s_i = random standard uncertainties of the measurements

The terms b_{ik} and s_{ik} in eqs. (4-2-5) and (4-2-6) are the covariance of the systematic and random standard uncertainties, respectively. When the elemental systematic errors for two separately measured variables are related (e.g., when the transducers used to measure different variables are each calibrated against the same standard), the systematic errors are said to be correlated and the covariance of the systematic errors is nonzero. The significance of correlated systematic errors is that they can have the effect of either decreasing or increasing the uncertainty in the result. The covariance term, b_{ik}, is determined by summing the products of the elemental systematic standard uncertainties for variables i and k that arise from the same source [3].

Usually the random standard uncertainties are considered to be independent so that s_{ik} is taken as zero. However, there can be situations where the measured variables, X_i, in eq. (4-2-3) can be affected by a common, time-varying, nonrandom error source, such as a drift in inlet flow rate to a test configuration. In this case, calculating the random standard uncertainties for each variable and calculating s_r from eq. (4-2-6) with s_{ik} taken as zero can lead to an incorrect determination of the random standard uncertainty of the result. These cases of correlated random errors can easily be handled [4] by calculating the result from eq. (4-2-3) each time the X_is are measured and then directly calculating the standard deviation, s_r, of the set of results and using that s_r in eq. (4-2-4) rather than using eq. (4-2-6).

Monte Carlo methods can be used to find the standard uncertainty of the result [5] instead of the propagation approach given by eqs. (4-2-4) through (4-2-6). The Monte Carlo method is illustrated in Sections 3, 5, and 7.

4-3 UNCERTAINTY OF VALIDATION EXPERIMENT

The experimental uncertainty, u_D, used in the validation process is the u_r obtained above,

$$u_D = u_r \qquad (4\text{-}3\text{-}1)$$

Even though the experiment will have both systematic and random errors and associated standard uncertainties, the uncertainty of the experimental result for the validation process will be fossilized as a systematic standard uncertainty [3]. Thus for the purposes of the validation process, the experimental result has a single value, a fixed (but unknown) error, and only a systematic component of uncertainty.

4-4 SUMMARY

This section has presented the basic concepts necessary to determine the uncertainty of the experimental result. As noted at the beginning of this section, the ASME standard [1] on this subject, PTC 19.1-2005, *Test Uncertainty*, is considered to be a companion document for V&V 20. PTC 19.1-2005 provides detailed examples of the application of uncertainty analysis to the determination of the uncertainty of test results and gives practical considerations for uncertainty analysis in general.

4-5 REFERENCES

[1] ASME PTC 19.1-2005, *Test Uncertainty*.

[2] ISO *Guide to the Expression of Uncertainty in Measurement* (1995), ISO, Geneva, Switzerland.

ASMENORMDOC.COM : Click to view the full PDF of ASME V V 20 2009

[3] Coleman, H. W. and Steele, W. G., *Experimentation, Validation, and Uncertainty Analysis for Engineers*. 3rd ed., John Wiley & Sons, New York, 2009.

[4] Coleman, H. W. and Lineberry, D. L., "Proper Estimation of Random Uncertainties in Steady State Testing," *AIAA J.*, Vol. 44, No. 3, 2006.

[5] Joint Committee for Guides in Metrology, "Evaluation of Measurement Data — Supplement 1 to the 'Guide to the Expression of Uncertainty in Measurement' — Propagation of Distributions using a Monte Carlo Method," JCGM 101:2008, France, 2008.

ASMENORMDOC.COM : Click to view the full PDF of ASME V V 20 2009

Section 5
Evaluation of Validation Uncertainty

5-1 OVERVIEW

This Section describes how the validation uncertainty u_{val} is determined once estimates of u_{num} and the uncertainty contributors to u_{input} and u_D have been made as discussed in previous sections.

Discussed in this Section are two approaches for determining u_{val} that differ in the manner of propagation with which estimates for u_{input} and u_D are obtained. The first is use of a sensitivity coefficient (local) method, and the second is use of a Monte Carlo (sampling, global) method. Both approaches are illustrated for four example cases that cover a wide range of V&V applications.

The first three cases considered are for the finned-tube heat transfer example (discussed in Section 1 and in Mandatory Appendix I and shown schematically in Fig. 1-4-1) in which the following occur.

5-1.1 Case 1

The validation variable T_o is directly measured.

5-1.2 Case 2

The validation variable q is a result defined by a data reduction equation that combines variables measured in the experiment (and no measured variables share the same error sources).

5-1.3 Case 3

The validation variable q is a result defined by a data reduction equation that combines variables measured in the experiment *and* the measurements of T_i and T_o share identical error sources.

In these cases, specification of the validation condition (set point) requires experimental determination of the value of Reynolds number ($4\rho Q/\pi\mu d_1$), and since the simulation is performed for actual experimental conditions, the values of the variables from the experiment will be inputs to the simulation. The errors in these inputs are assumed to be uncorrelated for all cases, with the exception of T_i and T_o for Case 3.

The fourth case considers a combustion flow with the validation variable being duct wall heat flux q at a given location (Fig. 5-1 -1). The experimental q is inferred from temperature–time measurements at the outside combustor duct wall using a data reduction equation that is itself a model. The predicted q is from a simulation using a turbulent chemically reacting flow code to model the flow through the duct.

5-2 ESTIMATING u_{val} WHEN THE EXPERIMENTAL VALUE, D, OF THE VALIDATION VARIABLE IS DIRECTLY MEASURED (CASE 1)

This case is one in which the experimental value D of the validation variable is directly measured. A key feature of such cases is that D and S have no shared variables, which leads to a straightforward evaluation of u_{input} and u_D. The

Fig. 5-1-1 Schematic for Combustion Gas Flow Through a Duct With Wall Heat Flux Being the Validation Variable (Case 4)

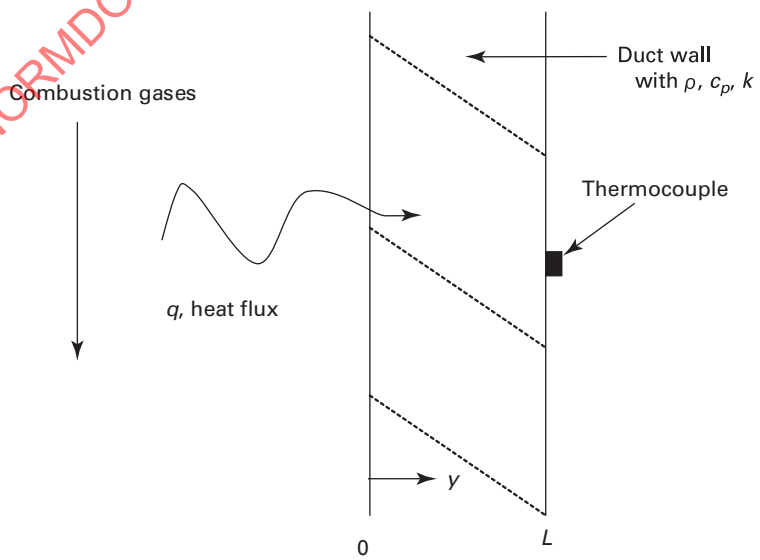

ASMENORMDOC.COM : Click to view the full PDF of ASME V V 20-2009

analysis is more complex in cases for which D and S have shared variables as shown in subsection 5-3.

For the finned-tube heat transfer experiment shown in Fig. 1-4-1, consider a case in which the validation variable is defined as the directly measured downstream bulk fluid temperature T_o. Then

$$S = T_{o,S} \tag{5-2-1}$$

$$D = T_{o,D} \tag{5-2-2}$$

$$E = S - D = T_{o,S} - T_{o,D} \tag{5-2-3}$$

The functional dependence of the simulation result is represented by

$$T_{o,S} = T_{o,S}(T_i, T_\infty, Q, \rho, \mu, C_P, h_1, h_2, h_f, h_c, k_f, k_t, d_1, d_2, L, a, w_f, w_{nf}) \tag{5-2-4}$$

where the simulation models the conditions of the experiment, so that values from the experiment are used as inputs to the simulation. The expression for the comparison error is then

$$E = T_{o,S}(T_i, T_\infty, Q, \rho, \mu, C_P, h_1, h_2, h_f, h_c, k_f, k_t, d_1, d_2, L, a, w_f, w_{nf}) - T_{o,D} \tag{5-2-5}$$

5-2.1 Sensitivity Coefficient Approach (Case 1)

As discussed in subsection 1-5, since the validation variable T_o is directly measured, the assumption of effectively independent errors δ_{input} and δ_D is reasonable. The expression for u_{val} is from eq. (1-5-10)

$$u_{\text{val}}^2 = u_{\text{num}}^2 + u_{\text{input}}^2 + u_{T_{o,D}}^2$$

with u_{input} given by eq. (3-2-1) with its correlation terms equal to zero

$$u_{\text{input}}^2 = \sum_{i=1}^{n} \left(\frac{\partial T_{o,S}}{\partial X_i} u_{X_i} \right)^2$$

which for this particular case yields

$$\begin{aligned} u_{\text{input}}^2 = {} & \left(\frac{\partial T_{o,S}}{\partial T_i}\right)^2 u_{T_i}^2 + \left(\frac{\partial T_{o,S}}{\partial T_\infty}\right)^2 u_{T_\infty}^2 + \left(\frac{\partial T_{o,S}}{\partial Q}\right)^2 u_Q^2 + \left(\frac{\partial T_{o,S}}{\partial \rho}\right)^2 u_\rho^2 \\ & + \left(\frac{\partial T_{o,S}}{\partial \mu}\right)^2 u_\mu^2 + \left(\frac{\partial T_{o,S}}{\partial C_P}\right)^2 u_{C_P}^2 + \left(\frac{\partial T_{o,S}}{\partial h_1}\right)^2 u_{h_1}^2 + \left(\frac{\partial T_{o,S}}{\partial h_2}\right)^2 u_{h_2}^2 \\ & + \left(\frac{\partial T_{o,S}}{\partial h_f}\right)^2 u_{h_f}^2 + \left(\frac{\partial T_{o,S}}{\partial h_c}\right)^2 u_{h_c}^2 + \left(\frac{\partial T_{o,S}}{\partial k_f}\right)^2 u_{k_f}^2 + \left(\frac{\partial T_{o,S}}{\partial k_t}\right)^2 u_{k_t}^2 \\ & + \left(\frac{\partial T_{o,S}}{\partial d_1}\right)^2 u_{d_1}^2 + \left(\frac{\partial T_{o,S}}{\partial d_2}\right)^2 u_{d_2}^2 + \left(\frac{\partial T_{o,S}}{\partial L}\right)^2 u_L^2 + \left(\frac{\partial T_{o,S}}{\partial a}\right)^2 u_a^2 \\ & + \left(\frac{\partial T_{o,S}}{\partial w_f}\right)^2 u_{wf}^2 + \left(\frac{\partial T_{o,S}}{\partial w_{nf}}\right)^2 u_{wnf}^2 \end{aligned} \tag{5-2-6}$$

The derivatives in eq. (5-2-6) are evaluated using the procedures of Section 3. The standard uncertainty, $u_{T_{o,D}}$, is determined using the techniques discussed in Section 4.

The sensitivity coefficient method requires knowledge about only the nominal values of the input parameters and their associated standard uncertainties. Knowledge about the form of the distributions is not required.

Uncertainty exists in the validation condition set point due to uncertainties in the parameters defining the set point. Applying the sensitivity coefficient approach to eq. (1-4-2) leads to

$$u_{\text{Re}}^2 = \left(\frac{\partial \text{Re}}{\partial \rho}\right)^2 u_\rho^2 + \left(\frac{\partial \text{Re}}{\partial Q}\right)^2 u_Q^2 + \left(\frac{\partial \text{Re}}{\partial \mu}\right)^2 u_\mu^2 + \left(\frac{\partial \text{Re}}{\partial d_1}\right)^2 u_{d_1}^2 \tag{5-2-7}$$

The derivatives in eq. (5-2-7) can be evaluated analytically due to the simple form of Re.

A graphical summary of the procedures used to evaluate u_{val} using the sensitivity coefficient propagation approach is illustrated in Fig. 5-2-1. The procedures defined in previous sections are used to estimate all standard uncertainties and the partial derivatives.

5-2.2 Monte Carlo Approach (Case 1)

Figure 5-2-2 illustrates the Monte Carlo approach for this case. In contrast to the sensitivity coefficient approach, the Monte Carlo method requires that probability distributions be assumed for the errors in the input parameters. The standard uncertainties, u, are generally taken to be the standard deviations of the assumed distributions. For a given "run" i of the simulation, a random sample is taken from each of these distributions and the simulation result, S_i, experimental result, D_i, validation comparison error, E_i, and validation point, Re_i, are calculated. This process is repeated N times, and the resulting means and standard deviations of the N values of E_i and Re_i evaluated.

Note that since each S_i includes (essentially) the same δ_{num}, the effect of δ_{num} is not observed in the variability of the distribution of the N values of S_i or E_i. The effect of the numerical uncertainty is accounted for when u_{num} is included in the calculation of u_{val}.

The number of samples N can be reduced using the techniques discussed in Section 3.

5-3 ESTIMATING u_{val} WHEN THE EXPERIMENTAL VALUE, D, OF THE VALIDATION VARIABLE IS DETERMINED FROM A DATA REDUCTION EQUATION (CASES 2 AND 3)

When the validation variable is not directly measured but is determined from a data reduction equation using other measured variables, the estimation of u_{input} and u_D (and subsequently u_{val}) becomes more complex. Example Cases 2 and 3 illustrate the application of the validation approach in such circumstances. The most general form of the sensitivity coefficient propagation equation as it applies to these cases is presented first, with the form for each of the two specific cases then presented in the subsections following.

ASME NORMDOC.COM : Click to view the full PDF of ASME V&V 20 2009

Fig. 5-2-1 Sensitivity Coefficient Propagation Approach for Estimating u_{val} When the Validation Variable (T_o) Is Directly Measured (Case 1)

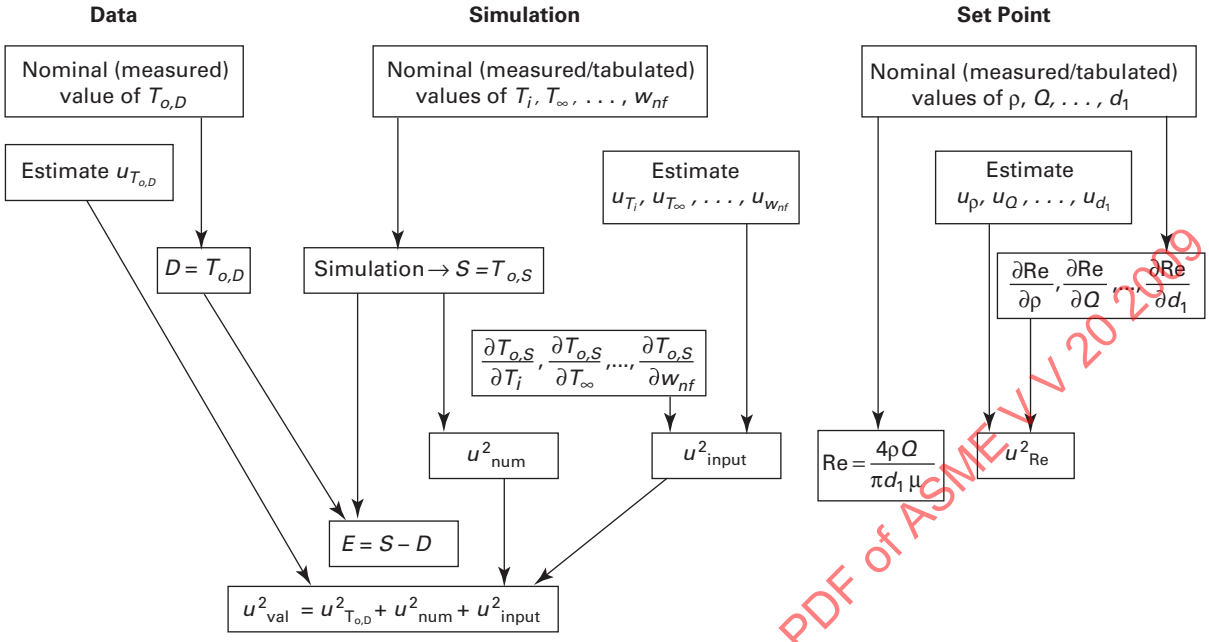

Fig. 5-2-2 Monte Carlo Approach for Estimating u_{val} When the Validation Variable (T_o) Is Directly Measured (Case 1)

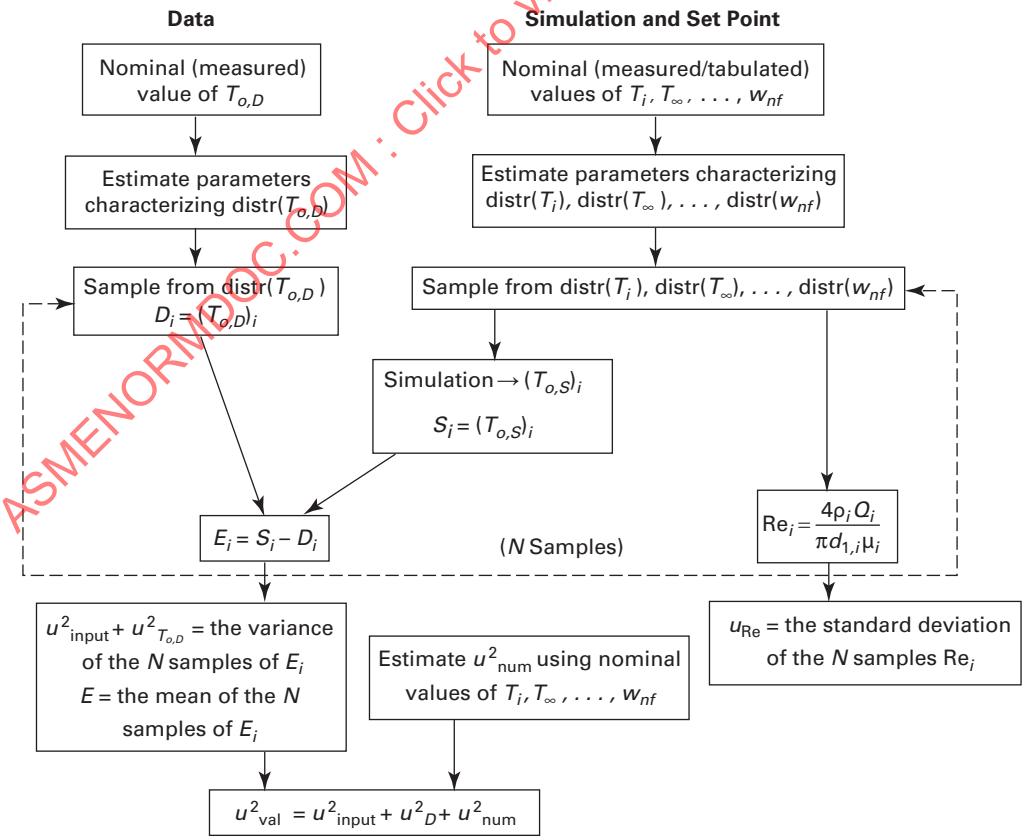

ASMENORMDOC.COM : Click to view the full PDF of ASME V V 20 2009

Consider the general situation in which the validation variable is a result determined from a data reduction equation containing j variables x_j, and some of the measured variables may share identical error sources. The equation for the comparison error is then [recalling eqs. (1-5-4) and (1-5-6)]

$$E = S(x_1, x_2, \ldots x_j) - D(x_1, x_2, \ldots x_j) = \delta_{\text{model}} + \delta_{\text{num}} + \delta_{\text{input}} - \delta_D \quad (5\text{-}3\text{-}1)$$

In this instance, δ_{input} and δ_D cannot reasonably be assumed to be independent since S and D share a dependence on the same measured variables. Application of the sensitivity coefficient propagation approach to obtain an expression for u_{val} yields

$$u_{\text{val}}^2 = \left[\left(\frac{\partial S}{\partial x_1}\right) - \left(\frac{\partial D}{\partial x_1}\right)\right]^2 u_{x_1}^2 + \left[\left(\frac{\partial S}{\partial x_2}\right) - \left(\frac{\partial D}{\partial x_2}\right)\right]^2 u_{x_2}^2 + \cdots + \left[\left(\frac{\partial S}{\partial x_j}\right) - \left(\frac{\partial D}{\partial x_j}\right)\right]^2 u_{x_j}^2 + 2\left[\left(\frac{\partial S}{\partial x_1}\right) - \left(\frac{\partial D}{\partial x_1}\right)\right] \times \left[\left(\frac{\partial S}{\partial x_2}\right) - \left(\frac{\partial D}{\partial x_2}\right)\right] u_{x_1 x_2} + \cdots + u_{\text{num}}^2 \quad (5\text{-}3\text{-}2)$$

where there is a covariance term containing a $u_{x_i x_2}$ factor for each pair of x variables that share identical error sources [1]. There is no explicit expression for u^2_{input}, as its components combine implicitly with components of u^2_D. Equation (5-3-2) can be expressed in a form analogous to eq. (1-5-10) as

$$u_{\text{val}}^2 = u_{\text{num}}^2 + u_{\text{input}+D}^2 \quad (5\text{-}3\text{-}3)$$

where

$$u_{\text{input}+D}^2 = \left[\left(\frac{\partial S}{\partial x_1}\right) - \left(\frac{\partial D}{\partial x_1}\right)\right]^2 u_{x_1}^2 + \left[\left(\frac{\partial S}{\partial x_2}\right) - \left(\frac{\partial D}{\partial x_2}\right)\right]^2 u_{x_2}^2 + \cdots + \left[\left(\frac{\partial S}{\partial x_j}\right) - \left(\frac{\partial D}{\partial x_j}\right)\right]^2 u_{x_j}^2 + 2\left[\left(\frac{\partial S}{\partial x_1}\right) - \left(\frac{\partial D}{\partial x_1}\right)\right] \times \left[\left(\frac{\partial S}{\partial x_2}\right) - \left(\frac{\partial D}{\partial x_2}\right)\right] u_{x_1 x_2} + \cdots + 2\left[\left(\frac{\partial S}{\partial x_{j-1}}\right) - \left(\frac{\partial D}{\partial x_{j-1}}\right)\right] \times \left[\left(\frac{\partial S}{\partial x_j}\right) - \left(\frac{\partial D}{\partial x_j}\right)\right] u_{x_{j-1} x_j} \quad (5\text{-}3\text{-}4)$$

Methods for evaluating the sensitivity coefficients of the simulation predicted value with respect to the variables ($\partial S/\partial x_i$) are discussed in Section 3. The estimate of u_{num} is made using the techniques in Section 2.

5-3.1 No Measured Variables Share Identical Error Sources (Case 2)

Again, using the finned-tube heat transfer experiment as an example, consider now a case in which the validation variable of interest is q, the rate of heat transfer given by the 1-D averaged conservation of energy equation as

$$q = \rho Q C_p (T_i - T_o) \quad (5\text{-}3\text{-}5)$$

and no measurements share any error sources. It is important to note several points. First, the rate of heat transfer is not directly measured — it is an experimental result determined from measured variables and others whose values are found from reference sources (the properties, for example). Second, since eq. (5-3-5) is a 1-D statement of conservation of energy with T_i and T_o taken as the mean inlet and outlet temperatures, there is no modeling error for q_D incurred when it is used as contrasted with the situation to be discussed in Case 4. However, there will likely be spatial nonuniformity uncertainties for $T_{i,D}$ and $T_{o,D}$ to account for how well they represent the mean temperatures. Since there are no error sources shared by different variables, all covariance terms in eq. (5-3-2) are zero. In this example, it is assumed that the simulation predicts T_o and calculates q using the input values of ρ, Q, C_p, and T_i.

The comparison error expression is

$$E = S - D = q_S - q_D \quad (5\text{-}3\text{-}6)$$

where

$$q_S = \rho Q C_p [T_{i,D} - T_{o,S}(T_i, T_\infty, Q, \rho, \mu, C_p, h_1, h_2, h_f, h_c, k_f, k_t, d_1, d_2, L, a, w_f, w_{nf})] \quad (5\text{-}3\text{-}7)$$

and

$$q_D = \rho Q C_p (T_{i,D} - T_{o,D}) \quad (5\text{-}3\text{-}8)$$

5-3.1.1 Sensitivity Coefficient Approach (Case 2). For this case u_{val} is given by eqs. (5-3-3) and (5-3-4) where $u_{\text{input}+D}$ is expressed as

$$u_{\text{input}+D}^2 = \left[\left(\frac{\partial q_S}{\partial \rho}\right) - \left(\frac{\partial q_D}{\partial \rho}\right)\right]^2 u_\rho^2 + \left[\left(\frac{\partial q_S}{\partial Q}\right) - \left(\frac{\partial q_D}{\partial Q}\right)\right]^2 u_Q^2 + \left[\left(\frac{\partial q_S}{\partial C_p}\right) - \left(\frac{\partial q_D}{\partial C_p}\right)\right]^2 u_{C_P}^2 + \left[\left(\frac{\partial q_S}{\partial T_i}\right) - \left(\frac{\partial q_D}{\partial T_i}\right)\right]^2 u_{T_i}^2 + \left(\frac{\partial q_S}{\partial T_\infty}\right)^2 u_{T_\infty}^2 + \left(\frac{\partial q_S}{\partial \mu}\right) u_\mu^2 + \left(\frac{\partial q_S}{\partial h_1}\right)^2 u_{h_1}^2 + \left(\frac{\partial q_S}{\partial h_2}\right)^2 u_{h_2}^2 + \left(\frac{\partial q_S}{\partial h_f}\right)^2 u_{h_f}^2 + \left(\frac{\partial q_S}{\partial h_c}\right)^2 u_{h_c}^2 + \left(\frac{\partial q_S}{\partial k_f}\right)^2 u_{k_f}^2 + \left(\frac{\partial q_S}{\partial k_t}\right)^2 u_{k_t}^2 + \left(\frac{\partial q_S}{\partial d_1}\right)^2 u_{d_1}^2 + \left(\frac{\partial q_S}{\partial d_2}\right)^2 u_{d_2}^2 + \left(\frac{\partial q_S}{\partial L}\right)^2 u_L^2 + \left(\frac{\partial q_S}{\partial a}\right)^2 u_a^2 + \left(\frac{\partial q_S}{\partial w_f}\right)^2 u_{w_f}^2 + \left(\frac{\partial q_S}{\partial w_{nf}}\right)^2 u_{w_{nf}}^2 + \left(\frac{\partial q_D}{\partial T_{o,D}}\right)^2 u_{T_{o,D}}^2 \quad (5\text{-}3\text{-}9)$$

Equation (5-2-7) is used to evaluate the uncertainty in the set point, Re. Figure 5-3-1 illustrates the application of the sensitivity equation approach to this case.

5-3.1.2 Monte Carlo Approach (Case 2). The Monte Carlo approach is illustrated in Fig. 5-3-2. Probability distributions for the errors in the experimentally measured variables and the errors in the other input parameters are assumed; the standard uncertainties u are taken to be the standard deviations of the assumed distributions, and the variance of the sample of N values of E_i is taken as the estimate of $u^2_{\text{input}+D}$.

ASMENORMDOC.COM : Click to view the full PDF of ASME V V 20 2009

Fig. 5-3-1 Sensitivity Coefficient Propagation Approach for Estimating u_{val} When the Validation Variable Is Defined by a Data Reduction Equation That Combines Variables Measured in the Experiment (Case 2)

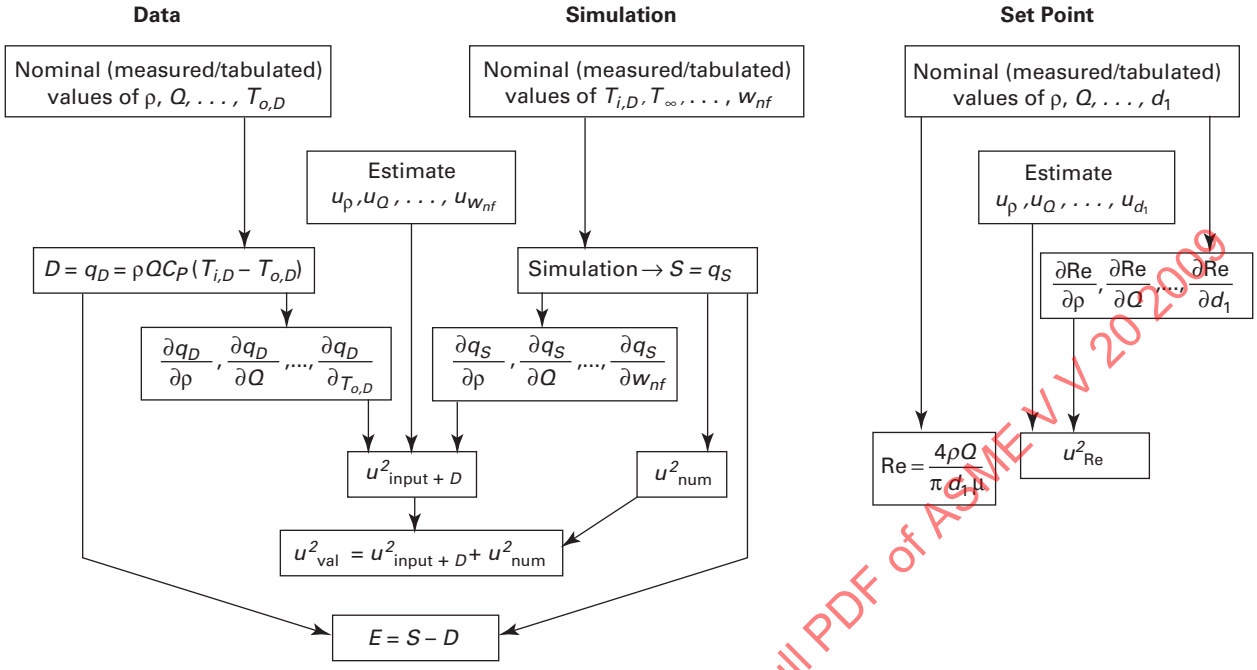

Fig. 5-3-2 Monte Carlo Approach for Estimating u_{val} When the Validation Variable Is Defined by a Data Reduction Equation That Combines Variables Measured in the Experiment (Case 2)

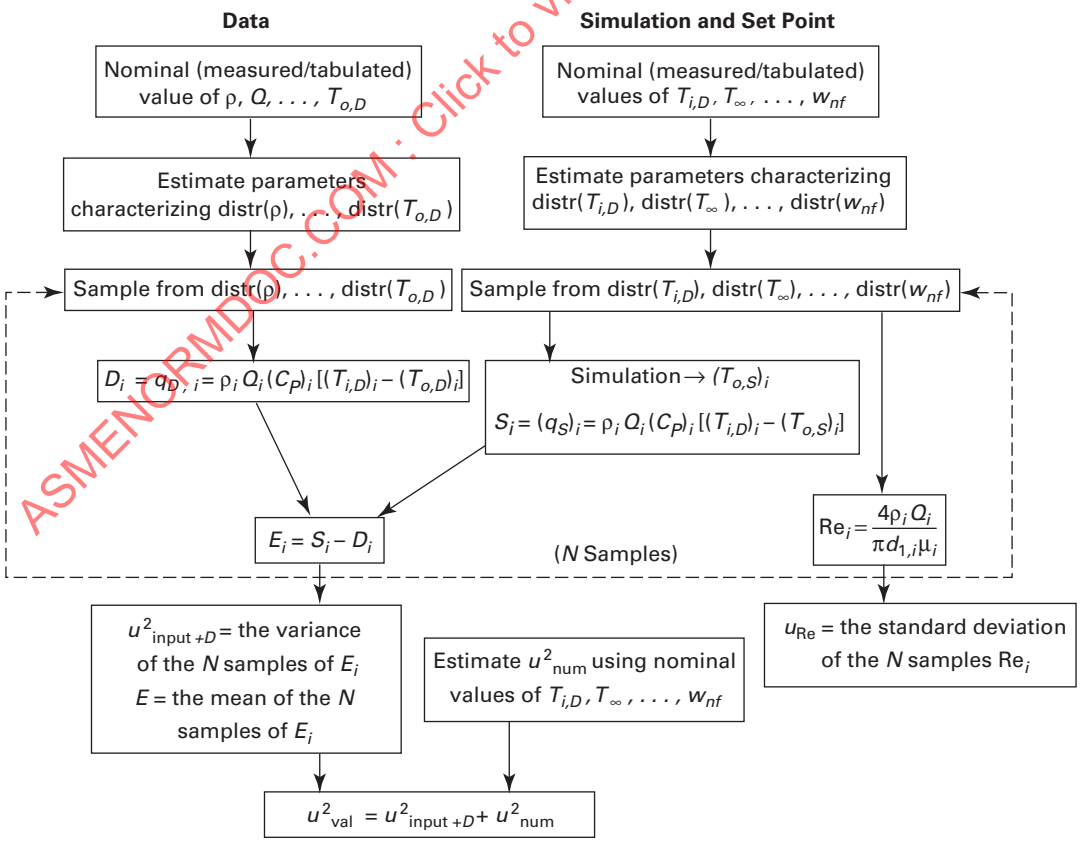

ASMENORMDOC.COM : Click to view the full PDF of ASME V V 20 2009

Fig. 5-3-3 Sensitivity Coefficient Propagation Approach for Estimating u_{val} When the Validation Variable Is Defined by a Data Reduction Equation That Combines Variables Measured in the Experiment and Two Measured Variables Share an Identical Error Source (Case 3)

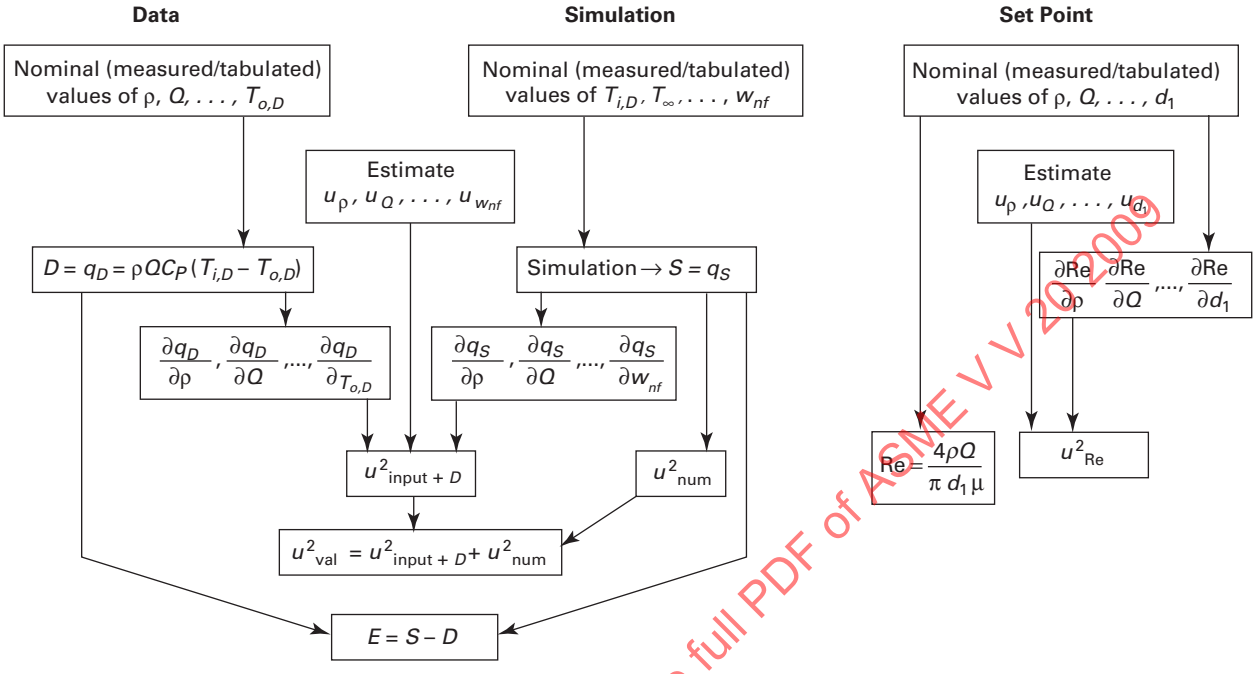

5-3.2 Measured Variables Share Identical Error Sources (Case 3)

Now consider that the measured temperatures T_i and T_o share an identical error source (such as both temperature transducers being calibrated against the same standard and therefore, after making the calibration corrections, leaving each transducer with the error of the standard in common). The comparison error expressions are as given in eqs. (5-3-6) through (5-3-8) in para. 5-3.1.

5-3.2.1 Sensitivity Coefficient Approach (Case 3). For this case u_{val} is given by eqs. (5-3-3) and (5-3-4) where $u_{input+D}$ is expressed as

$$
\begin{aligned}
u^2_{input+D} = {} & \left[\left(\frac{\partial q_S}{\partial \rho}\right) - \left(\frac{\partial q_D}{\partial \rho}\right)\right]^2 u^2_\rho + \left[\left(\frac{\partial q_S}{\partial Q}\right) - \left(\frac{\partial q_D}{\partial Q}\right)\right]^2 u^2_Q \\
& + \left[\left(\frac{\partial q_S}{\partial C_P}\right) - \left(\frac{\partial q_D}{\partial C_P}\right)\right]^2 u^2_{C_P} + \left[\left(\frac{\partial q_S}{\partial T_i}\right) - \left(\frac{\partial q_D}{\partial T_i}\right)\right]^2 u^2_{T_i} \\
& + \left(\frac{\partial q_S}{\partial T_\infty}\right)^2 u^2_{T_\infty} + \left(\frac{\partial q_S}{\partial \mu}\right) u^2_\mu + \left(\frac{\partial q_S}{\partial h_1}\right)^2 u^2_{h_1} + \left(\frac{\partial q_S}{\partial h_2}\right)^2 u^2_{h_2} \\
& + \left(\frac{\partial q_S}{\partial h_f}\right)^2 u^2_{h_f} + \left(\frac{\partial q_S}{\partial h_c}\right)^2 u^2_{h_c} + \left(\frac{\partial q_S}{\partial k_f}\right)^2 u^2_{k_f} + \left(\frac{\partial q_S}{\partial k_t}\right)^2 u^2_{k_t} \\
& + \left(\frac{\partial q_S}{\partial d_1}\right)^2 u^2_{d_1} + \left(\frac{\partial q_S}{\partial d_2}\right)^2 u^2_{d_2} + \left(\frac{\partial q_S}{\partial L}\right)^2 u^2_L + \left(\frac{\partial q_S}{\partial a}\right)^2 u^2_a \\
& + \left(\frac{\partial q_S}{\partial w_f}\right)^2 u^2_{w_f} + \left(\frac{\partial q_S}{\partial w_{nf}}\right)^2 u^2_{w_{nf}} + \left(\frac{\partial q_D}{\partial T_{o,D}}\right)^2 u^2_{T_{o,D}} \\
& + 2\left[\left(\frac{\partial q_S}{\partial T_i}\right) - \left(\frac{\partial q_D}{\partial T_i}\right)\right]\left[\left(\frac{\partial q_S}{\partial T_{o,D}}\right) - \left(\frac{\partial q_D}{\partial T_{o,D}}\right)\right] u_{T_i T_{o,D}} \qquad (5\text{-}3\text{-}10)
\end{aligned}
$$

where the final term in the equation is the covariance term that takes into account the fact that the measured values of T_i and $T_{o,D}$ share an error from the same source. Since q_S does not depend on $T_{o,D}$, that derivative in the final term is zero.

Equation (5-2-7) is used to evaluate the uncertainty in the set point, Re. Figure 5-3-3 illustrates the application of the sensitivity coefficient propagation approach to this example case.

5-3.2.2 Monte Carlo Approach (Case 3). In the Monte Carlo approach, probability distributions for the errors in the experimentally measured variables and the errors in the other input parameters are assumed; the standard uncertainties u are taken to be the standard deviations of the assumed distributions; and the variance of the sample of N values of E_i is taken as the estimate of $u^2_{input+D}$. The procedure is shown in Fig. 5-3-4. In this case the error from $distr(\delta T_b)$ is from the shared identical systematic error source and the same error is assigned to both $(T_{i,D})$ and $(T_{o,D})$ for a given iteration.[9]

[9] In general, only some elemental systematic error sources will be the same for $T_{i,D}$ and $T_{o,D}$, and the other elemental sources will not be the same. Such situations are discussed in detail in reference [1].

ASME NORMDOC.COM : Click to view the full PDF of ASME V V 20-2009

Fig. 5-3-4 Monte Carlo Propagation Approach for Estimating u_{val} When the Validation Variable Is Defined by a Data Reduction Equation That Combines Variables Measured in the Experiment and Two Measured Variables Share an Identical Error Source (Case 3)

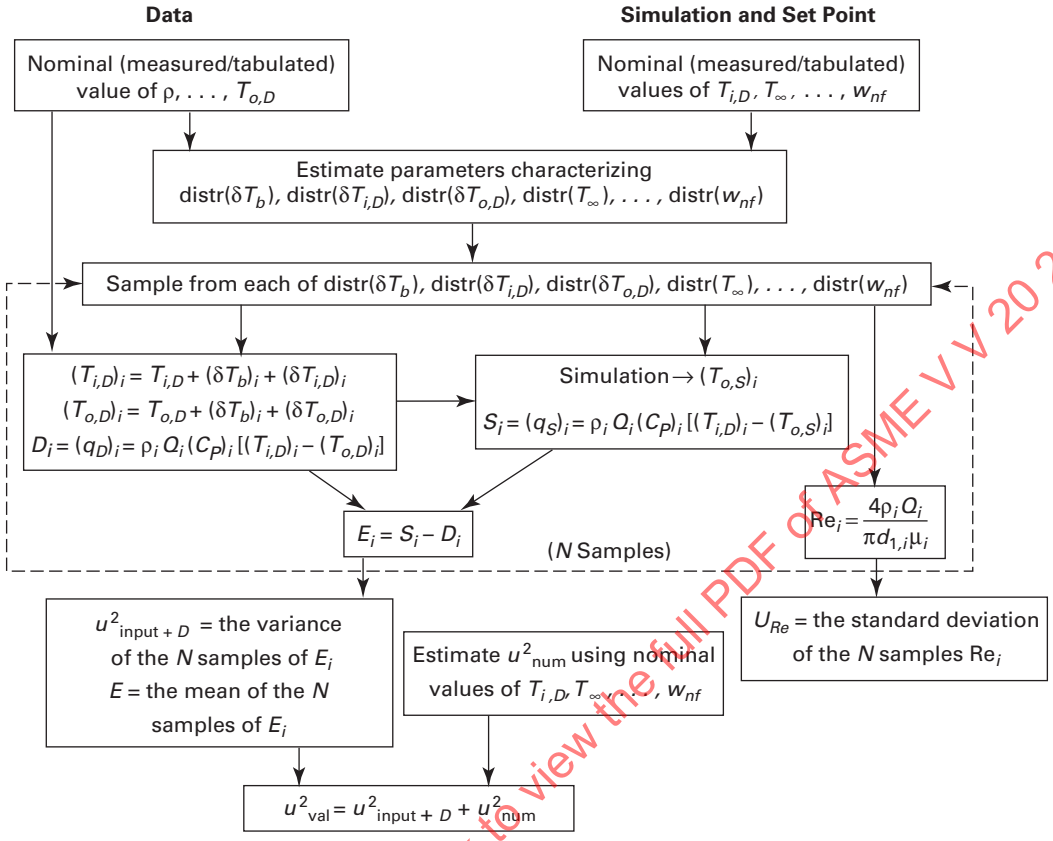

5-4 ESTIMATING u_{val} WHEN THE EXPERIMENTAL VALUE, *D*, OF THE VALIDATION VARIABLE IS DETERMINED FROM A DATA REDUCTION EQUATION THAT ITSELF IS A MODEL (CASE 4)

Consider the case of combustion gases flowing through a duct, with the validation variable of interest being the heat flux q incident on a particular area of the duct wall. The situation is shown schematically in Fig. 5-1-1. The simulation result q_S is predicted using a code that models a turbulent chemically reacting flow at the conditions of the experiment. Inputs would be geometry, propellant and oxidizer flow rates, etc. The chemical equilibrium code that calculates the combustion gas properties might be considered to be a part of the simulation model (similar to the common treatment of turbulence models and their parameters in a CFD analysis) or it might be considered to be part of the input parameters with uncertainty contributions taken into account in u_{input}.

The experimental heat flux is determined by measuring the temperature of the back wall ($y = L$) of the duct as a function of time, t. The measured $T(t)$ history is then used in an inverse conduction data reduction model [2] to infer the incident heat flux at $y = 0$. The data reduction model might assume 1-D conduction, constant or variable wall properties, incident heat flux constant with time, adiabatic wall at $y = L$, etc. In this approach, the experimental result, q_D, now contains errors from categories analogous to those in the simulation (i.e., the error due to assumptions and approximations in the data reduction model is denoted $\delta_{D,\text{model}}$); the error in the data reduction model output due to the errors in the inputs (measured and from reference sources) is denoted $\delta_{D,\text{input}}$; and the error due to the numerical solution of the data reduction model is denoted $\delta_{D,\text{num}}$.

The validation comparison error in this case is given by

$$E = S - D = q_S - q_D = \delta_{S,\text{model}} + \delta_{S,\text{input}} + \delta_{S,\text{num}} - \delta_{D,\text{model}} - \delta_{D,\text{input}} - \delta_{D,\text{num}} \quad (5\text{-}4\text{-}1)$$

If $\delta_{D,\text{model}}$ is not (or cannot be) estimated with an uncertainty, then the two modeling errors are not distinguishable individually and a total modeling error is given by

$$\delta_{\text{model,total}} = (\delta_{S,\text{model}} - \delta_{D,\text{model}}) = E - (\delta_{S,\text{input}} + \delta_{S,\text{num}} - \delta_{D,\text{input}} - \delta_{D,\text{num}}) \quad (5\text{-}4\text{-}2)$$

Now u_{val} is defined as the standard uncertainty corresponding to the standard deviation of the parent population of the combination of $(\delta_{S,\text{input}} + \delta_{S,\text{num}} - \delta_{D,\text{input}} - \delta_{D,\text{num}})$.

ASMENORMDOC.COM : Click to view the full PDF of ASME V V 20 2009

The functional relationships for q_S and q_D are given by

$$q_S = q_S(x_1, x_2, \ldots x_j) \tag{5-4-3}$$

where the j different x_i are the inputs to the simulation model, and

$$q_D = q_D(\rho, c_p, k, L, T, t) \tag{5-4-4}$$

Realizing that the simulation is of the flow field and the experimental data reduction model is of the duct wall, the expressions for the results q_S and q_D do not contain shared variables as in Cases 2 and 3.

5-4.1 Sensitivity Coefficient Approach (Case 4)

The sensitivity coefficient approach in this case yields

$$u_{\text{val}}^2 = \left(\frac{\partial q_S}{\partial x_1}\right)^2 u_{x_1}^2 + \ldots + \left(\frac{\partial q_S}{\partial x_j}\right)^2 u_{x_j}^2 + u_{S,\text{num}}^2 + \left(\frac{\partial q_D}{\partial \rho}\right)^2 u_\rho^2 + \left(\frac{\partial q_D}{\partial c_p}\right)^2 u_{c_p}^2 + \left(\frac{\partial q_D}{\partial k}\right)^2 u_k^2 + \left(\frac{\partial q_D}{\partial L}\right)^2 u_L^2 + \left(\frac{\partial q_D}{\partial T}\right)^2 u_T^2 + \left(\frac{\partial q_D}{\partial t}\right)^2 u_t^2 + u_{D,\text{num}}^2 \tag{5-4-5}$$

Defining

$$u_{S,\text{input}}^2 = \left(\frac{\partial q_S}{\partial x_1}\right)^2 u_{x_1}^2 + \ldots + \left(\frac{\partial q_S}{\partial x_j}\right)^2 u_{x_j}^2 \tag{5-4-6}$$

and

$$u_{D,\text{input}}^2 = \left(\frac{\partial q_D}{\partial \rho}\right)^2 u_\rho^2 + \left(\frac{\partial q_D}{\partial c_p}\right)^2 u_{c_p}^2 + \left(\frac{\partial q_D}{\partial k}\right)^2 u_k^2 + \left(\frac{\partial q_D}{\partial L}\right)^2 u_L^2 + \left(\frac{\partial q_D}{\partial T}\right)^2 u_T^2 + \left(\frac{\partial q_D}{\partial t}\right)^2 u_t^2 \tag{5-4-7}$$

the expression for u_{val} becomes

$$u_{\text{val}}^2 = u_{S,\text{input}}^2 + u_{S,\text{num}}^2 + u_{D,\text{input}}^2 + u_{D,\text{num}}^2 \tag{5-4-8}$$

Figure 5-4-1 illustrates this case.

5-4.2 Monte Carlo Approach (Case 4)

As in the previous cases, probability distributions of the errors in the experiment and the errors in the input parameters are assumed, and the standard uncertainties, u, are taken to be the standard deviations of the assumed distributions. The validation uncertainty is determined as shown in Fig. 5-4-2.

5-5 ASSUMPTIONS AND ISSUES

A summary of relevant assumptions and issues concerning the two methods to propagate uncertainty through the data reduction equations and simulations and multipoint model validation follows.

5-5.1 Sensitivity Coefficient Propagation Approach

Assumptions and issues associated with the sensitivity coefficient propagation approach, as related to model validation, are summarized below.

(a) While the sensitivity coefficient propagation approach generally requires fewer evaluations of the simulation model than the Monte Carlo approach, the

Fig. 5-4-1 Sensitivity Coefficient Propagation Approach for Estimating u_{val} When the Validation Variable Is Defined by a Data Reduction Equation That Itself Is a Model (Case 4)

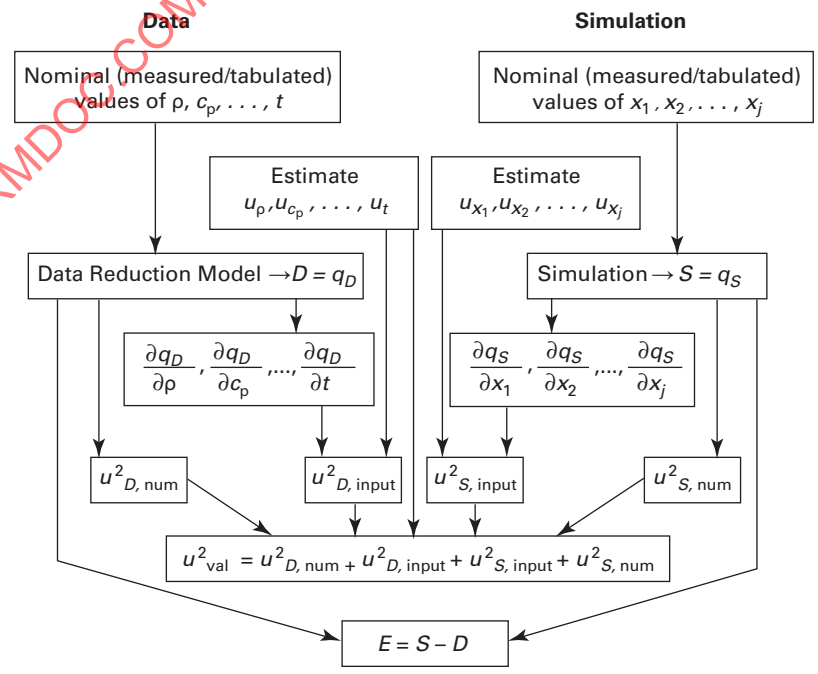

ASMENORMDOC.COM : Click to view the full PDF of ASME V V 20 2009

Fig. 5-4-2 Monte Carlo Propagation Approach for Estimating u_{val} When the Validation Variable Is Defined by a Data Reduction Equation That Itself Is a Model (Case 4)

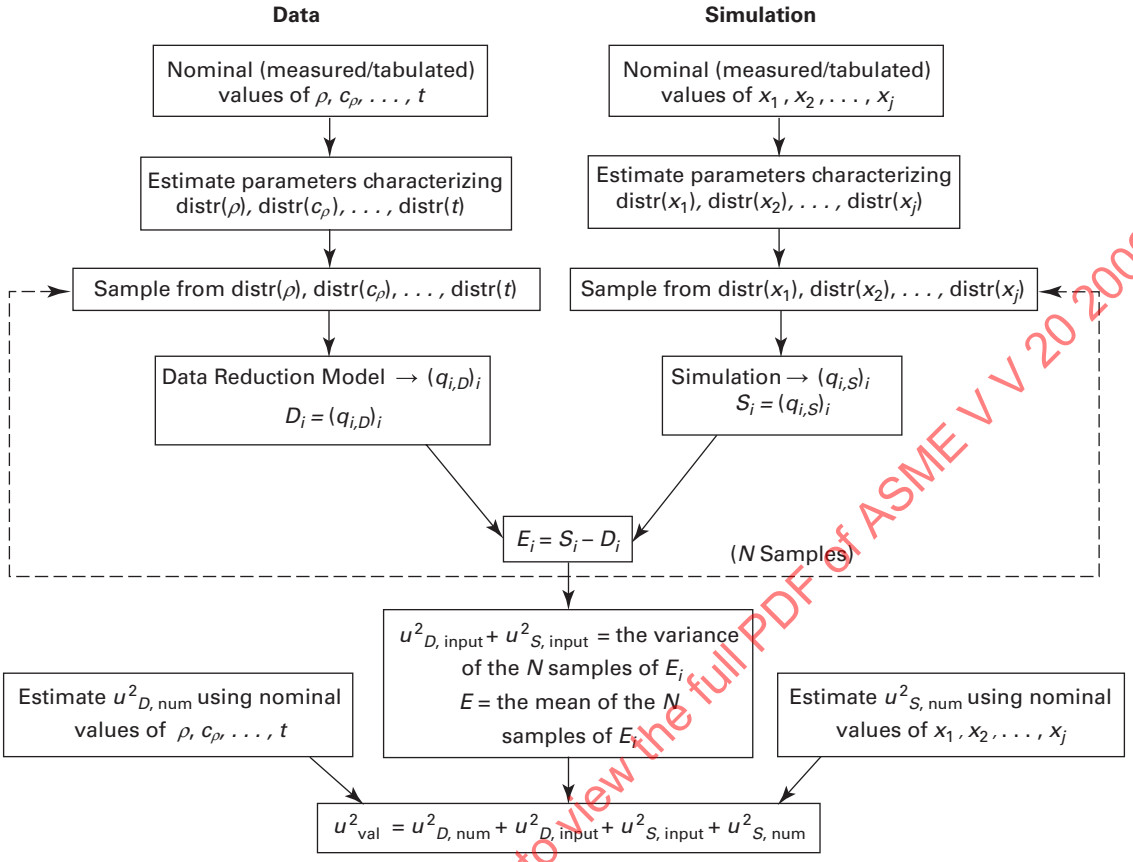

ASMENORMDOC.COM: Click to view the full PDF of ASME V V 20 2009

number of evaluations can be significant. For models with a very large number of input parameters, some effort may be needed to identify those parameters that have a significant effect on the model predictions for the conditions (set point) of the validation experiment. The sensitivity propagation analysis can then be limited to these parameters.

(b) The method, as presented, assumes that the mean simulation model output, mean (S), and the uncertainty of the model output due to the input parameters, u_{input}, can be evaluated from the nominal values of the input parameters, and from a first order sensitivity analysis. These assumptions may not be appropriate if the model is highly nonlinear in the input parameters, over the parameter ranges associated with the standard uncertainty of the parameters about the set point. Note that validation experiments are often performed under carefully controlled conditions, leading to smaller ranges for the uncertainties in the input parameters than may occur in the field.

(c) An advantage of the sensitivity coefficient propagation method is it requires only that the nominal value (or mean value) and standard uncertainty (standard deviation) of the model input parameters and data be characterized. The Monte Carlo approach requires the full specification of the uncertainty distributions unless one adopts the approach outlined in subpara. (b) of para. 5-5.2.

(d) One cannot, without further assumption, characterize the interval within which δ_{model} falls, to a fixed level of probability. The method characterizes only E and u_{val}, and not the distribution associated with the uncertainty in $(\delta_{input} + \delta_{num} - \delta_D)$.

5-5.2 Monte Carlo Propagation Approach

Assumptions and issues associated with the Monte Carlo approach, as they relate to model validation, are summarized below.

(a) The Monte Carlo approach requires that the number of evaluations of the simulation model be sufficiently large [3] such that the mean model prediction and the standard uncertainty u_{input} can be resolved.

(b) The distributions of the important model parameters must be specified. If sufficient knowledge does not

exist to specify any of these distributions, a range of distributions and associated distributional parameters can be utilized (normal, uniform, etc.) to evaluate the sensitivity of the validation analysis to the distributional choices.

(c) While the number of simulation evaluations required by the Monte Carlo approach to adequately estimate mean (S) and u_{input} is at most a weak function of the number of model parameters (not a function if the random samples are from independent, identical distributions [3]), one must specify the distributions of the parameters used in the analysis. As in the case of the uncertainty propagation method, some effort may be needed to identify those parameters that have a significant effect on the model predictions for the conditions (set point) of the validation experiment, so that the distributions associated with those parameters that are not important need not be characterized.

(d) The Monte Carlo simulations can be performed on a coarser grid if it is established that u_{num} for that grid is significantly smaller than u_{input}. The use of a simulation based on grid for which u_{num} is on the order of u_{input} will significantly increase u_{val}, leading to a situation where a significant part of the estimated standard uncertainty, u_{val} is due to limitations in the computation rather than due to uncertainties in the validation experiment (i.e., those that are due to uncertainties associated with measurements and the parameters used in the simulation of the experiment).

(e) The method provides an estimated distribution for the uncertainty in δ_{model} based on the uncertainty in (δ_{input} + δ_{num} − δ_D). The distribution can be used to estimate the interval in which the δ_{model} falls, with a given probability. As the probability increases (say, from 95% to 99%), the number of simulation evaluations required to resolve the tails of the distribution increases.

5-5.3 Implications for Multipoint Validation

The procedure documented here can be applied to characterize model error for multiple set points. This Standard, however, does not provide guidance on how the results can be interpolated (or extrapolated) to other set points. Several issues arise in interpolation. These include the choice of the interpolation function and the characterization of the statistics of the residuals (i.e., the form of the distribution, correlation between residuals at different set points, and the estimation of the distributional parameters). Such issues are beyond the scope of this Standard.

5-6 REFERENCES

[1] Coleman, H. W. and Steele, W. G., *Experimentation, Validation, and Uncertainty Analysis for Engineers*, 3rd ed., John Wiley & Sons, New York (2009).

[2] Beck, J. V., Blackwell, B. F., and St. Clair, C. R., *Inverse Heat Conduction*, Wiley, New York (1985).

[3] Fishman, G. S., *Monte Carlo: Concepts, Algorithms, and Applications*, Springer, New York (1995).

ASMENORMDOC.COM : Click to view the full PDF of ASME V&V 20-2009

Section 6
Interpretation of Validation Results

6-1 INTRODUCTION

Previous sections of this document have presented a validation methodology based on determining the validation comparison error, E, and the validation uncertainty, u_{val}, and this Section discusses the interpretation of the comparison of these metrics. Note that once a validation effort reaches the point where the simulation value, S, and the experimental value, D, of a validation variable have been determined, the sign and magnitude of $E\ (= S - D)$ are known.

The validation uncertainty u_{val} is an estimate of the standard deviation of the parent population of the combination of all errors except the modeling error $(\delta_{num} + \delta_{input} - \delta_D)$ in S and D. Techniques for estimation of the uncertainty components u_{num}, u_{input}, and u_D that combine to give u_{val} have been discussed in Sections 2, 3, and 4, respectively. Evaluation of u_{val} from those uncertainty components has been demonstrated in Section 5 for four separate cases that represent practical validation scenarios. For each of the cases, the contributions of u_{input} and u_D to u_{val} are determined by propagation of the simulation input standard uncertainties and the experimental standard uncertainties using two techniques: a sensitivity coefficient (local) approach and a Monte Carlo (sampling, global) approach that requires specification of error distributions.

Recalling eq. (1-5-7)

$$\delta_{model} = E - (\delta_{num} + \delta_{input} - \delta_D) \qquad (1\text{-}5\text{-}7)$$

and considering the definition of u_{val}, it is evident that

$$(E \pm u_{val})$$

then characterizes an interval within which δ_{model} falls, or

$$\delta_{model} \in [E - u_{val},\ E + u_{val}]$$

Thus, E is an estimate of δ_{model}, and u_{val} is the standard uncertainty of that estimate. The validation uncertainty can thus be viewed as the standard uncertainty, $u_{\delta_{model}}$, of the estimate of δ_{model}.

6-2 INTERPRETATION OF VALIDATION RESULTS USING E AND u_{val} WITH NO ASSUMPTIONS MADE ABOUT ERROR DISTRIBUTIONS

If one has only an estimate for the validation uncertainty, u_{val}, and not an estimate of the probability distribution associated with $(\delta_{num} + \delta_{input} - \delta_D)$, an interval within which the value of δ_{model} falls with a given probability cannot be estimated without further assumption. One can make the following statements, however:

(a) If

$$|E| >> u_{val} \qquad (6\text{-}2\text{-}1)$$

then probably $\delta_{model} \approx E$.

(b) If

$$|E| \leq u_{val} \qquad (6\text{-}2\text{-}2)$$

then probably δ_{model} is of the same order as or less than $(\delta_{num} + \delta_{input} - \delta_D)$.

From a practical standpoint, in the first case one has information that can possibly be used to improve the model (reduce the modeling error). In the second case, however, the modeling error is within the "noise level" imposed by the numerical, input, and experimental uncertainties, and formulating model "improvements" is more problematic.

6-3 INTERPRETATION OF VALIDATION RESULTS USING E AND u_{val} WITH ASSUMPTIONS MADE ABOUT ERROR DISTRIBUTIONS

To estimate an interval within which δ_{model} falls with a given degree of confidence, an assumption about the probability distribution of the combination of all errors, except the modeling error, must be made. This then allows the choice of a coverage factor [1, 2] k such that

$$U_{\%} = k\,u \qquad (6\text{-}3\text{-}1)$$

where $U_{\%}$ is called the *expanded uncertainty* and one can say, for instance, that $(E \pm U_{95})$ then defines an interval within which δ_{model} falls about 95 times out of 100 (i.e., with 95% confidence) when the coverage factor has been chosen for a level of confidence of 95%.

6-3.1 Parent Error Distributions

To obtain a perspective on the order of magnitude of k, consider the following three parent error distributions used as examples in the ISO Guide [1]:

(a) a uniform (rectangular) distribution with equal probability that δ lies at any value between $-A$ and $+A$, so that $\sigma = A/\sqrt{3}$.

(b) a triangular distribution symmetric about $\delta = 0$ with base from $-A$ to $+A$, so that $\sigma = A/\sqrt{6}$.

(c) a Gaussian distribution with standard deviation σ.

ASMENORMDOC.COM : Click to view the full PDF of ASME V V 20 2009

6-3.2 Coverage Factor

Choose a coverage factor, k, such that $(\delta_{num} + \delta_{input} - \delta_D)$ certainly (or almost certainly) falls within $\pm k(u_{val})$.

(a) If $(\delta_{num} + \delta_{input} - \delta_D)$ is from the uniform distribution, 100% of the population is covered for $k = 1.73$.

(b) If $(\delta_{num} + \delta_{input} - \delta_D)$ is from the triangular distribution, 100% of the population is covered for $k = 2.45$.

(c) If $(\delta_{num} + \delta_{input} - \delta_D)$ is from the Gaussian distribution, 95.5% of the population is covered for $k = 2.0$, 99.7% for $k = 3.0$, 99.95% for $k = 3.5$, and 99.99% for $k = 4.0$.

With these comparisons, one can conclude that, for error distributions in the "family" of the three distributions considered, δ_{model} certainly (or almost certainly) falls within the interval $E \pm k(u_{val})$, where k is typically a number in the range of 2 to 3.

In the case of the Monte Carlo approach, a direct calculation of a coverage interval can be performed for sufficiently large number of samples N using the distribution of the N calculated values of E, if one has sufficient confidence in the choices of the input distributions. Alternatively, this distribution can also be used to evaluate an equivalent k if the distribution is symmetric.

6-4 REFERENCES

[1] *Guide to the Expression of Uncertainty in Measurement* (corrected and reprinted, 1995), International Organization for Standardization, Geneva, Switzerland, (1995).

[2] Coleman, H.W. and Steele, W.G., *Experimentation, Validation, and Uncertainty Analysis for Engineers,* 3rd ed., John Wiley & Sons, New York (2009).

ASMENORMDOC.COM : Click to view the full PDF of ASME V&V 20 2009

Section 7
Examples

7-1 OVERVIEW

To demonstrate the validation approach in this Standard, an example problem is presented. The example applies the approaches described in this Standard to address code verification, solution verification, uncertainty in model input parameters, uncertainty in experimental data, validation uncertainty, and interpretation of the validation comparison. The example is based on validating a model for the heat transfer rate from a fin-tube heat exchanger.

This Section is divided into two main subsections covering the code verification example (subsection 7-2) and validation example (subsection 7-3). The code verification example includes a description of the problem (para. 7-2.1), presentation of a manufactured solution (para. 7-2.2), and discussion of the results (para. 7-2.3). The validation example includes an end-to-end demonstration of the approach with paragraphs on the experimental data (para. 7-3.2), simulation (para. 7-3.3), and validation comparison (para. 7-3.4); an additional paragraph (para. 7-3.5) summarizes applying the validation approach to a second simulation model. In the experimental data section, experimental uncertainty (para. 7-3.2.1) is estimated. The simulation section includes a discussion of the simulation model (para. 7-3.3.1), presentation of the simulation results (para. 7-3.3.2), and estimation of simulation uncertainty (solution verification in para. 7-3.3.3 and input parameter uncertainty in para. 7-3.3.4). The paragraph for assessing the validation comparison presents two approaches for calculating the validation uncertainty (propagation equation approach in para. 7-3.4.1, and a Monte Carlo approach in para. 7-3.4.2) and discusses the interpretation of the validation results (para. 7-3.4.3). The validation approach is repeated for a second simulation model, with simulation results and simulation uncertainty summarized in para. 7-3.5.1 and the validation comparison results summarized in para. 7-3.5.2.

7-2 CODE VERIFICATION EXAMPLE

Verification is performed for the code features in the simulation model applied in the validation assessment. That simulation model (described later in subsection 7-3) includes numerically solving the partial differential equation for linear heat conduction with convection boundary conditions. Two analytical solutions for code verification are developed in Nonmandatory Appendix A using the method of manufactured solutions. Both solutions are applicable to the simulation model used in the validation example, but differ in the code features that are tested. A variation of MMS #1 in Nonmandatory Appendix A is used in this Section to demonstrate code verification. The solution is briefly described here. The solution was specifically designed so that the mathematical operations required for developing the manufactured solution (MS) could be carried out by hand. However, symbolic mathematics software can make this task easier and is typically necessary for more complex applications.

7-2.1 Problem Description

Linear steady heat conduction is to be verified for a two-dimensional domain. The domain is taken as one-eighth of a square (2.7 m × 2.7 m) with a circular hole (1.11 m in diameter) in the center as shown in Fig. 7-2-1. The boundary surfaces of the two-dimensional domain are labeled as s_1 to s_4. Although the two-dimensional domain selected for the verification problem is similar to the two-dimensional domain used in the validation, this is not required for code verification. It is done for convenience here.

The partial differential equation in the code to be verified is that for linear steady heat conduction and is given by

$$k\left[\frac{\partial^2 T}{\partial x^2} + \frac{\partial^2 T}{\partial y^2}\right] = 0 \qquad (7\text{-}2\text{-}1)$$

Fig. 7-2-1 Problem Domain With (*x*, *y*) Coordinates Shown for Domain Corners

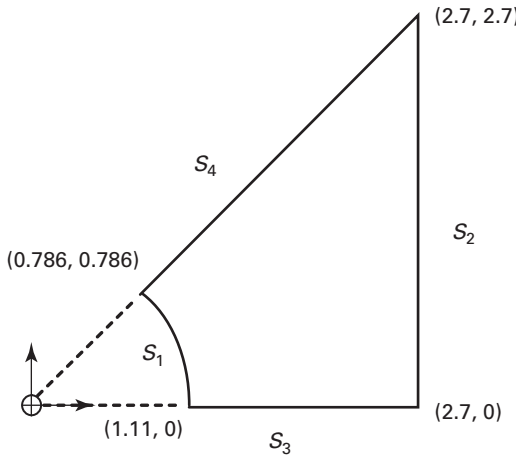

ASMENORMDOC.COM : Click to view the full PDF of ASME V&V 20-2009

The boundary conditions to be verified are convective boundary conditions defined on surfaces s_1 and s_2 as

$$-k\left.\frac{\partial T}{\partial n}\right|_{s_1} = q_n(r,\theta)|_{s_1} = h_i\left(T|_{s_1} - T_f\right)$$
$$-k\left.\frac{\partial T}{\partial n}\right|_{s_2} = q_n(r,\theta)|_{s_2} = h_o\left(T|_{s_2} - T_\infty\right) \quad (7\text{-}2\text{-}2)$$

where n is the normal to the surface.

7-2.2 Manufactured Solution

The processes described in Section 2 are applied to derive an analytical solution using the method of manufactured solutions and perform code verification. The selected analytical solution is

$$M(r,\theta) = T_m + \cos(4\theta)\exp(r) \quad (7\text{-}2\text{-}3)$$

where
(r, θ) = the polar coordinates
T_m = a constant, nominal temperature

The solution is constructed in polar coordinates, but the finite element code being verified will solve the problem in the Cartesian coordinate system. Similarly, the solution is developed in dimensionless variables for convenience; the code could be set up to use these or the MS converted to dimensional variables.

The steady heat conduction equation in polar coordinates is used to derive the manufactured solution.

$$L(T) = k\left[\frac{1}{r}\frac{\partial}{\partial r}\left(r\frac{\partial T}{\partial r}\right) + \frac{1}{r^2}\frac{\partial}{\partial \theta}\left(\frac{\partial T}{\partial \theta}\right)\right] = 0 \quad (7\text{-}2\text{-}4)$$

The thermal conductivity is a constant in eq. (7-2-4), $k = K$. Note that a more general analytical solution is developed in Nonmandatory Appendix A to verify nonlinear heat conduction where thermal conductivity, k, is a function of temperature.

By operating on the manufactured solution, M, in eq. (7-2-3), with operator, L, in eq. (7-2-4), the following set of equations can be defined.

$$L(T) = k\left[\frac{1}{r}\frac{\partial}{\partial r}\left(r\frac{\partial T}{\partial r}\right) + \frac{1}{r^2}\frac{\partial}{\partial \theta}\left(\frac{\partial T}{\partial \theta}\right)\right] = Q(r,\theta)$$
$$Q(r,\theta) = KM\left[1 + \frac{1}{r} - \frac{16}{r^2}\right] \quad (7\text{-}2\text{-}5)$$

The solution of eq. (7-2-5) is by definition

$$T(r,\theta) = M(r,\theta) \quad (7\text{-}2\text{-}6)$$

The boundary conditions are derived from the analytical solution and discussed next.

The boundary conditions are evaluated from the solution in eq. (7-2-3) at the boundary surfaces of the problem domain (Fig. 7-2-1). Along boundary surfaces s_3 and s_4, it can be shown that the normal flux is zero because the gradient of the MS is zero. On boundary surfaces s_1 and s_2, temperature, normal flux, or convective conditions, which are typical in a thermal analysis, could be specified from this manufactured solution. The analytical forms of these boundary conditions are given next.

For a specified temperature boundary condition the value is applied from the analytical solution.

$$T(r,\theta)|_{s_1} = M(r,\theta)|_{s_1}$$
$$T(r,\theta)|_{s_2} = M(r,\theta)|_{s_2} \quad (7\text{-}2\text{-}7)$$

A specified normal heat flux boundary condition applies gradients of the analytical solution.

$$q_n(r,\theta)|_{s_1} = -k\left.\frac{\partial T}{\partial n}\right|_{s_1} = -K\frac{\partial M}{\partial r} = -KM$$
$$q_n(r,\theta)|_{s_2} = -k\left.\frac{\partial T}{\partial n}\right|_{s_2} = -K\left[\frac{\partial M}{\partial r}\cos(\theta) - \frac{1}{r}\frac{\partial M}{\partial \theta}\sin(\theta)\right]$$
$$= -KM\left[\cos(\theta) + \frac{4}{r}\tan(4\theta)\sin(\theta)\right] \quad (7\text{-}2\text{-}8)$$

A convective boundary condition can be prescribed in two ways. First, a form is selected for the convective temperature and the required convection coefficient to satisfy the boundary condition is calculated.

$$h(r,\theta)|_{s_1} = q_n(r,\theta)|_{s_1} / [T_f(r,\theta) - M(r,\theta)]$$
$$h(r,\theta)|_{s_2} = q_n(r,\theta)|_{s_2} / [T_\infty(r,\theta) - M(r,\theta)] \quad (7\text{-}2\text{-}9)$$

where the normal flux, q_n, is computed from eq. (7-2-8). Notice that for this manufactured solution the convection coefficient on surface s_2 will have negative values if a constant convection temperature is selected. This is due to the sign change in the normal flux on surface s_2, which can be demonstrated from eq. (7-2-8). *Parameters taking nonphysical values should be avoided*. In this case, either the convection temperature can be made to vary spatially or the boundary condition can be specified in a different manner, as discussed next. Alternatively, the convection coefficient can be selected, and the convection temperature to satisfy the boundary condition is calculated.

$$T_f(r,\theta)|_{s_1} = q_n(r,\theta)|_{s_1} / h_i(r,\theta) + M(r,\theta)|_{s_1}$$
$$T_\infty(r,\theta)|_{s_2} = q_n(r,\theta)|_{s_2} / h_o(r,\theta) + M(r,\theta)|_{s_2} \quad (7\text{-}2\text{-}10)$$

Because the boundary conditions are derived from the analytical solution, various combinations of the boundary conditions can be verified with the same analytical solution. Separate verification problems that test the combinations of temperature, normal heat flux, and convective heat flux boundary conditions could all be tested with this one analytical solution. In most cases, a general form of the boundary condition, allowing for spatial variation of the specified quantity, is verified. Results are presented for one combination of boundary conditions, that being specified convective heat flux on both surfaces s_1 and s_2. Convective boundary conditions are applied in the simulation model used in the validation.

In practice if a particular form of a boundary condition is not performing as expected, using a different form of the boundary condition is useful to diagnose whether the performance is being caused by a particular form of the boundary condition. Specifying the dependent variable, in this case temperature, is a good starting point in a

ASMENORMDOC.COM : Click to view the full PDF of ASME V V 20 2009

code verification study to debug setting up and running a code verification problem.

7-2.3 Code Verification Results

An unstructured mesh (grid) heat transfer code applying the finite element method is used to perform calculations [1]. A series with four meshes is used in the code verification study. The meshes are refined in an unstructured manner on the interior of the domain; the boundary of the domain is refined in a structured manner. The unstructured refinement gives meshes that do not have common nodes on the interior of the domain. An unstructured refinement is not required for code verification. However, in general, an unstructured refinement is a more rigorous test of the code verification procedure than a structured refinement, the reason being that an unstructured refinement does not have a uniform refinement factor over the mesh while a structured refinement does. Furthermore, for commercial software it may be easier to obtain a series of meshes refined in an unstructured manner. The series of meshes used in the example is shown in Fig. 7-2-2. The mesh is refined such that the total number of elements over the domain increased by approximately a factor of four with each mesh refinement. A characteristic mesh size, h, based on the edge length of the average element (discussed later) is reduced by approximately a factor of two in each refinement.

A finite element computer code is set up to solve the previously described differential equation with the addition of a source term on the right hand side. The code solves the following differential equation

$$L(T) = k\left[\frac{\partial^2 T}{\partial x^2} + \frac{\partial^2 T}{\partial y^2}\right] = Q(r, \theta) \tag{7-2-11}$$

with the convective boundary conditions.

$$\begin{aligned} -k\left.\frac{\partial T}{\partial n}\right|_{s_1} &= q_n(r, \theta)\big|_{s_1} = h_i\left(T|_{s_1} - T_f\right) \\ -k\left.\frac{\partial T}{\partial n}\right|_{s_2} &= q_n(r, \theta)\big|_{s_2} = h_o\left(T|_{s_2} - T_\infty\right) \end{aligned} \tag{7-2-12}$$

Fig. 7-2-2 Finite Element Meshes Used in the Code Verification Refinement Study

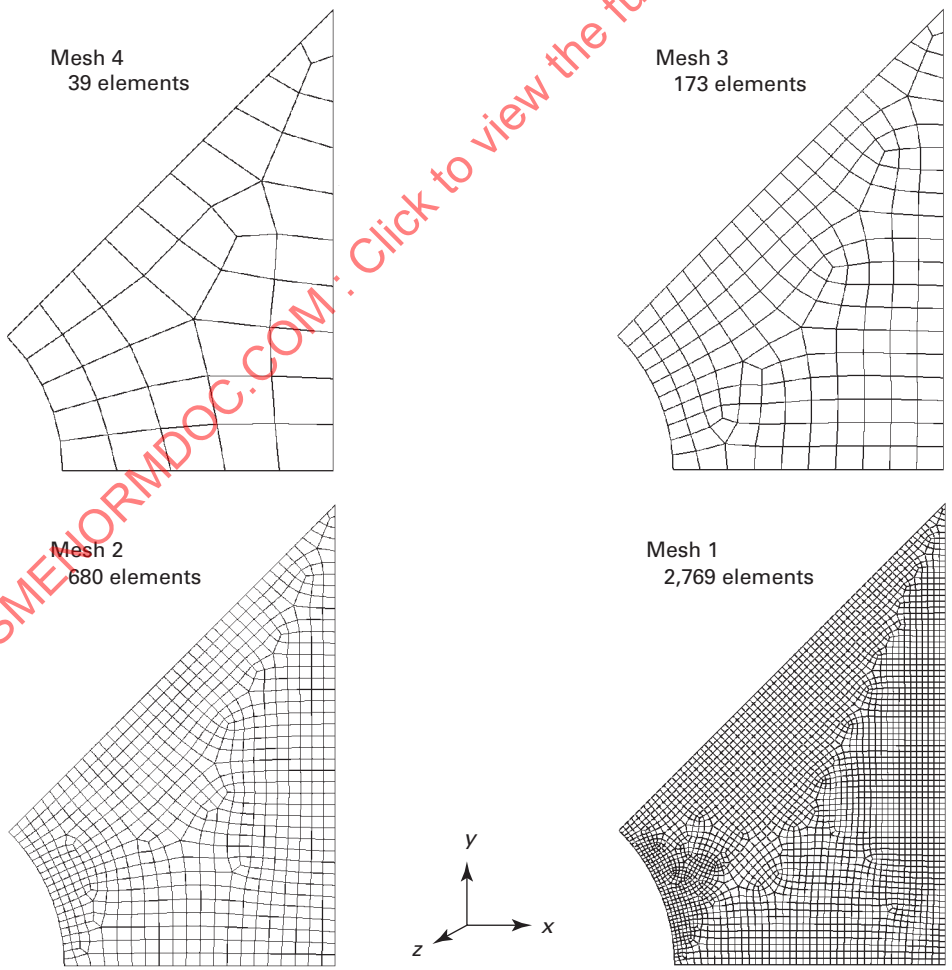

ASMENORMDOC.COM : Click to view the full PDF of ASME V&V 20 2009

The code is required to have functionality for applying a spatially varying source term, $Q(r, \theta)$, in the differential equation. The functional form of the source term in polar coordinates is given in eq. (7-2-5). The convective boundary conditions are specified with constant convection coefficients, h_i and h_o, and the convection temperature calculated from eqs. (7-2-10) and (7-2-8).

$$T_f(r,\theta)\big|_{s_1} = \frac{q_n(r,\theta)\big|_{s_1}}{h_i} + M(r,\theta)\big|_{s_1} = -\frac{K\,M(r,\theta)\big|_{s_1}}{h_i} + M(r,\theta)\big|_{s_1}$$

$$T_\infty(r,\theta)\big|_{s_2} = \frac{q_n(r,\theta)\big|_{s_2}}{h_o} + M(r,\theta)\big|_{s_2} \qquad (7\text{-}2\text{-}13)$$

$$= -\frac{K\,M(r,\theta)\big|_{s_2}}{h_o}\left[\cos(\theta) + \frac{4}{r}\tan(4\theta)\sin(\theta)\right] + M(r,\theta)\big|_{s_2}$$

Because the code is solving in Cartesian coordinates (x, y), the polar coordinates for computing the source term and convection temperatures are calculated from standard transformations.

$$r = \sqrt{x^2 + y^2}$$
$$\theta = \tan^{-1}(y/x) \qquad (7\text{-}2\text{-}14)$$

The differential equation defined in eqs. (7-2-11) to (7-2-13) is solved in a thermal analysis code [1]. This code, and most commercial codes, uses an iterative method (e.g., conjugate gradient method) to solve a linear system of equations. The tolerance for the iterative method needs to be set appropriately for a verification study. The tolerance should be set small enough so that the approximation error in the linear system is less (2 to 3 orders or magnitude; see Section 2) than the error obtained by comparing the code's solution to the analytical solution. If the problem were nonlinear, the tolerance for the nonlinear solution would similarly need to be appropriately set. The tolerance for the linear solution was set to 1e-8 using a generalized minimum residual (GMRES) method in these calculations.

Four code solutions of eqs. (7-2-11) to (7-2-13) were obtained using the parameter values in Table 7-2-1 and the meshes shown in Fig. 7-2-2. Code verification evaluates the error through comparison of the code's solution to the analytical solution in eq. (7-2-3). Code verification can be performed for different code outputs. When verification is being conducted as a precursor to validation the output used in the validation activity is of primary interest. Other code outputs could also be studied, and in general should be studied when possible, in a code verification activity. As a demonstration, code verification results are shown for the temperature at two locations, the integrated heat flux along surface s_1 (the output used in the validation study) and for the L_2 norm of the temperature field.

Table 7-2-1 Parameter Values Used for the Code Verification Example

Input Parameter	Value
Thermal conductivity ($k = K$)	5 W/m K
Convection coefficient, h_i	200 W/m^2 K
Convection coefficient, h_o	10 W/m^2 K

Code verification using the temperature at two locations on surface s_1 is considered first. The locations are near the midpoint of surface s_1 and have the (x, y) coordinates listed below:

	x	y
Location 1:	0.990131,	0.5044969
Location 2:	1.056862,	0.3433951

Note that the mesh sequence was defined to have a node at both these locations in all four meshes. If the mesh sequence is not defined with a node at these locations, the code output must be interpolated from the nodal solution to give the solution at the prescribed locations. Comparison with the analytical solution in this case will include mesh discretization error and interpolation error. Generally, it is preferred to study the discretization error separately from the interpolation error. As long as the dependence of the interpolation error on the discretization is of equal or higher order than the mesh discretization error, the two errors can be studied simultaneously. However, only the lower ordered error will be observed in the code verification.

Integrated code outputs are also of interest in code verification. In this example the integrated heat flux along surface s_1 is considered. This output is used in the validation example. The code's solutions of the local temperature and the integrated heat flux for the four meshes are listed in Table 7-2-2 with details of the element count in the meshes. The analytical solutions are listed at the bottom of Table 7-2-2. The analytical solution for the temperature is obtained from eq. (7-2-3). The analytical solution of the integrated flux is obtained by

Table 7-2-2 Code Verification Results

Solution	Total Number of Elements	Elements Along s_1	Temperature at Loc 1, °C	Temperature at Loc 2, °C	Integrated Flux Along s_1, W
Mesh 4	39	5	99.03772	100.96471	3.126 e-3
Mesh 3	173	10	99.05491	100.94549	6.123 e-4
Mesh 2	690	20	99.05954	100.94048	6.903 e-5
Mesh 1	2,769	40	99.06078	100.93926	1.571 e-5
Analytical	...	...	99.0611593	100.9388433	0.0

ASMENORM.COM : Click to view the full PDF of ASME V&V 20-2009

integrating the analytical expression for the normal flux in eq. (7-2-8) along surface s_1.

The error in the code's solution is defined as

$$E_h = f(h) - f^{\text{exact}} \tag{7-2-15}$$

where

f^{exact} = analytical solution

$f(h)$ = code solution for that mesh

h = characteristic mesh size

The error can be evaluated for selected code outputs, like temperature at selected locations or integrals of outputs. Norms of the error are also of interest, as theoretical proofs of the error's dependence on mesh are typically in terms of norms of the error [2]. For example, the L_2 norm is the integral of the error over the problem domain (A_Ω).

$$L_2^2 = \frac{1}{A_\Omega}\int_{A_\Omega} E_h^2 dA_\Omega \tag{7-2-16}$$

Other error measures are the H_1 semi-norm that integrates the error in the gradient and L_∞ norm that is the maximum error over the domain [2]. As an example, the L_2 norm of the temperature is evaluated in this example. To evaluate the norm the error is integrated over the domain. Gauss-quadrature has been used to calculate the L_2 norm here. Other numerical approximations could be used, but the approximation error in evaluating the integral should be relatively small compared to E_h.

The dependence of the error on a characteristic mesh size is studied. The characteristic mesh size in this study is taken as the edge length for an average element area (for this two-dimensional problem)

$$h = \sqrt{\frac{\sum_{i=1}^{N_{\text{elements}}} A_{\Omega_i}}{N_{\text{elements}}}} \tag{7-2-17}$$

where

A_{Ω_i} = the area of element i

The total area of the domain (A_Ω) is 3.16 m^2 for the domain in Fig. 7-2-1. Other characteristics of the mesh are the diagonal length across the element with the maximum area (volume in 3-D) in the mesh [2].

The error in the code solutions for local (point) temperatures, integrated flux, and L_2 norm are listed in Table 7-2-3 as a function of the mesh and characteristics mesh size. All three code outputs demonstrate convergence to the analytical solution. The errors are decreasing monotonically as the code's solution converges to the analytical solution. The absolute value of the error is plotted as a function of characteristic mesh size in Fig. 7-2-3. The error (on log scale) in Fig. 7-2-3 demonstrates approximately a linear dependence on log(h) for all three code outputs considered. As discussed in Section 2, for consistent numerical solution methods (like finite element) on well-behaved problems, the error in the solution is asymptotically proportional to h^p, and

$$E_h = f(h) - f^{\text{exact}} = Ch^p + H.O.T \tag{7-2-18}$$

where

$H.O.T$ = higher order terms

In addition to checking that the code is converging to the correct solution, code verification checks the rate of convergence of the error. A reference line (Ch^2) is plotted in Fig. 7-2-3. The error in temperature at locations 1 and 2 and the L_2 norm are visually parallel to the reference line (Ch^2) indicating these errors have a second order dependence on the mesh size (h). The integrated flux appears to decrease at a higher rate than second order ($p = 2$).

The observed order of convergence can be estimated from the error on any two meshes (see para. 2-4.1)

$$p^{\text{obs}} = \frac{\ln\left(\left|\frac{E_{h_2}}{E_{h_1}}\right|\right)}{\ln(r_{21})} \tag{7-2-19}$$

where

$E_{h_i} = E_h(h_i)$

$r_{21} = h_2/h_1$ with $h_1 < h_2$

The observed order of convergence is listed in Table 7-2-4. In the table the observed order of convergence between subsequent meshes from eq. (7-2-19) is listed in the first three rows. The coarsest mesh (mesh 4) may not be in the asymptotic region for the local temperature; the higher order terms ($H.O.T$) in eq. (7-2-18) may not be negligible in comparison to the first-order term. Convergence rates involving Mesh 4 are slightly less than 2, but increase to values near 2 as the mesh is refined. The convergence rate for the integrated flux along surface s_1 is slightly larger than 2 for the results from meshes 3 and 4 and meshes 1 and 2. It is not clear why the rate increases to more than 3 for meshes 2 and 3. The errors are so small for this linear

ASMENORMDOC.COM : Click to view the full PDF of ASME V&V 20 2009

Table 7-2-3 Error (E_h) in the Code Simulation During Mesh Refinement

Mesh	Characteristic Mesh Size, h_i, m	Refinement Factor, h_{i+1}/h_i	Temp Error at Loc 1, °C	Temp Error at Loc 2, °C	Integrated Flux Error Along s_1, W	L_2 Norm Temp Error, °C
4	0.2847	...	−2.343 e-2	2.586 e-2	3.126 e-3	3.175 e-1
3	0.1352	2.11	−6.249 e-3	6.647 e-3	6.123 e-4	6.642 e-2
2	0.0677	2.00	−1.619 e-3	1.636 e-3	6.903 e-5	1.717 e-2
1	0.0338	2.00	−3.793 e-4	4.167 e-4	1.571 e-5	4.366 e-3

Fig. 7-2-3 Error as a Function of Characteristic Mesh Size

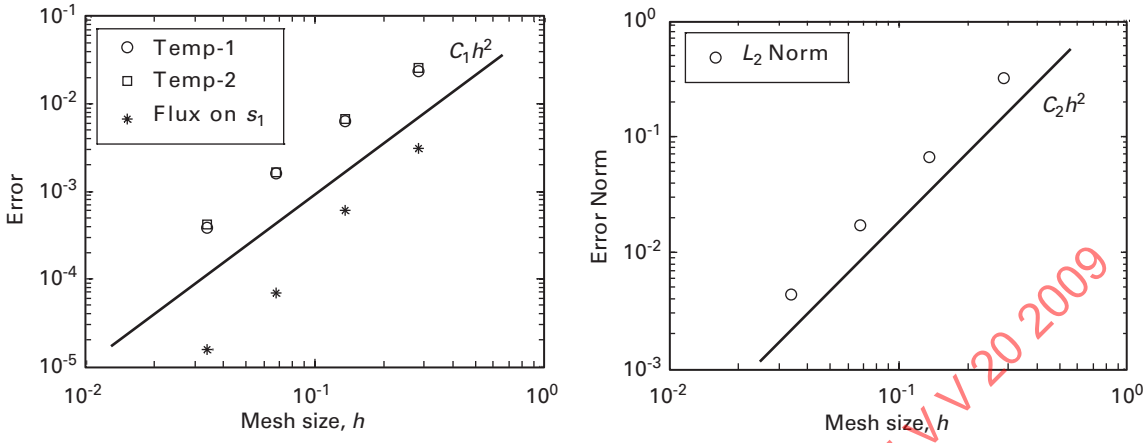

problem that the noise in the observed p could be due to roundoff error.

Alternately, the convergence rate for the sequence of meshes can be estimated with standard regression on the observed [log(h), log(E_h)] data. The coefficients C and p can be estimated from eq. (7-2-18) while neglecting higher order terms. The observed convergence rate for the four meshes using regression on the results from all four meshes is listed in the last row of Table 7-2-4. The observed convergence rate is approximately two (second order) for the local temperature and L_2 temperature norm when estimated from the results with meshes 4 to 1.

The code verification results support that the computer code gives (at least) second order accuracy in the local temperature, the L_2 norm of temperature, and the integrated flux along a surface. Note that this is a relatively easy problem. Even for the coarsest discretization (mesh 4), the code is very accurate. The numerical error at locations 1 and 2 is less than 0.026°C (out of 100°C) and the L_2 norm of the error less than 0.32°C. In this case of an unstructured refinement, the refinement factor is not uniform over the domain. The characteristic size of each element in the coarse mesh is not uniformly halved when the element is refined to produce the subsequent mesh. However, the numerical error convergences in a monotonic and consistent manner and convergence rates based on an average refinement factor do not appear to be affected.

The results have established that the computer code is verified to (at least) second order accuracy in the local temperature, L_2 norm of the temperature, and integrated flux along a surface. An additional step can be taken to confirm that code is converging at an observed rate and that rate is correct. The additional step involves comparing the observed convergence rate to the anticipated convergence rate, with the objective being to establish that code is free of coding mistakes (for the code features tested in the verification problem). The difficulty is in identifying the anticipated rate. Under certain conditions the convergence rate for selected error measures can be theoretically determined. For example, the convergence rates for various norms of the error with a finite element method can be theoretically derived [2]. The theoretical convergence rates, however, are derived for simplified cases, typically linear differential equations and for norm-based error measures. In the absence of theoretical convergence rates, judgment is required. Based on the numerical algorithms in the code there may be an expectation for the order of a code output. If code verification indicates the observed order is less than expected, then the results should be communicated to the code developers.

For the code verification results obtained in this study, the L_2 norm of the temperature can be theoretically shown to be second order, and the observed convergence rate confirms that second order accuracy

ASMENORMDOC.COM : Click to view the full PDF of ASME V V 20 2009

Table 7-2-4 Observed Order of Convergence (p^{obs}) From Mesh Refinement

Meshes	Temperature at Loc 1	Temperature at Loc 2	Integrated Flux on s_1	L_2 Norm of Temperature
3 and 4	1.77	1.82	2.19	2.10
2 and 3	1.96	2.03	3.16	1.96
1 and 2	2.07	1.97	2.13	1.97
All (1 to 4)	1.93	1.94	2.55	2.01

is obtained. There is not a known theoretical basis for the convergence rates of the local temperature or the integrated surface heat flux (for a finite element method). Given that both outputs demonstrate second order convergence, there is little concern that a code mistake may be degrading the (order of) accuracy of the code. If, however, the convergence rate of local temperature was first order, further investigation may be warranted to understand why first order convergence was obtained. Paragraph 2-3.3.3 provides additional discussion on possible causes for lower than expected convergence rates.

7-3 VALIDATION EXAMPLE

In this Section, the validation procedure presented in this document is demonstrated through its application to an example problem. The example involves quantifying the accuracy of a model to predict the heat transfer rate in a fin-tube heat exchanger. Each aspect of the validation procedure is demonstrated. The steps in the procedure are demonstrated with the example of this Section for

(a) estimating uncertainty in experimental data

(b) estimating uncertainty for the numerical error in a simulation (solution verification)

(c) estimating uncertainty in the simulation due to input parameter uncertainty

(d) evaluating the validation uncertainty

(e) interpreting the validation comparison

True validation requires experimental data. However, the example validation exercise presented here uses synthetic data for good reason. The validation procedure is presented without ambiguities, clearly described with controlled sources of error, and the parameters can be manipulated to elucidate behavior of interest.

The remainder of this Section provides an overview of the example problem. The experimental configuration and measured experimental data for validation of the model are described in the para. 7-3.2. Uncertainty in the experimental data is also estimated in this Section. The model is discussed in para. 7-3.3, including the effects of uncertainty in the model input parameters and solution verification. The validation uncertainty and interpretation of the comparison are discussed in para. 7-3.4. Both propagation equation and Monte Carlo approaches are applied for computing the validation uncertainty. Paragraphs 7-3.2 through 7-3.4 apply the validation approach of this document from beginning to end on the example problem. In para. 7-3.5 the assessment of a second simulation model is summarized. The second model has been updated to include additional physics that the first model did not include. Model updating is not considered part of the validation approach. However, if additional information becomes available and an update to the model is proposed, the validation procedure can be repeated to assess the updated model.

7-3.1 Validation Problem Overview

The objective of this exercise is the validation assessment of a simulation model for predicting the heat transfer rate from a horizontal fin-tube heat exchanger. A schematic of the fin-tube heat exchanger assembly is shown in Fig. 7-3-1. A heated fluid is circulated through the tube with attached fins. Heat from the fluid is exchanged with cooler ambient air surrounding the fin-tube heat exchanger. The fluid flows with a volume flow rate Q, enters with a bulk temperature of T_i, and exits at a bulk temperature of T_o. The tube has a circular geometry defined by an inner radius (r_1), outer radius (r_2), and length (L). The fins have a thickness w_f and are equally spaced along the length of the heat exchanger at a distance w_{nf}. The ambient air temperature is constant along the length of the heat exchanger with value T_∞. The fins are square in profile with an edge length of a.

A simulation model of the total heat transfer rate is compared to experimental data in the validation assessment. The total heat transfer rate is simulated with an energy balance on the fluid and requires numerically

Fig. 7-3-1 Schematic of Fin-Tube Heat Exchanger Assembly

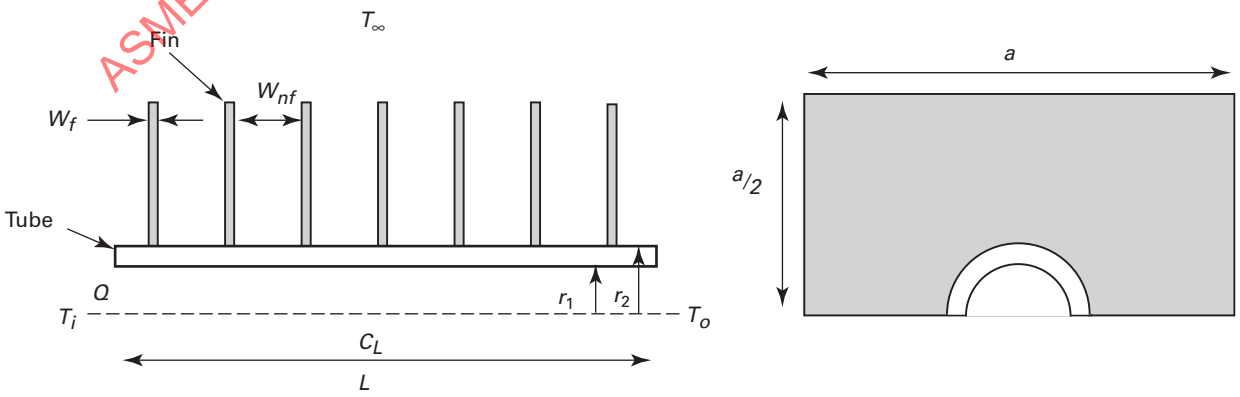

ASMENORMDOC.COM : Click to view the full PDF of ASME V V 20 2009

solving the partial differential equation for linear steady heat conduction with convective boundary conditions. Total heat transfer rate in the experiment is calculated from measurements of the fluid flow rate and bulk fluid temperatures at the inlet and outlet through a data reduction equation.

7-3.2 Experimental Data

The experimental data are based on a fin-tube heat exchanger with a copper tube and aluminum fins using heated water as the working fluid. Synthetic experimental data are generated based on the materials, dimensions, and nominal settings listed in Table 7-3-1. The synthetic process to generate the experimental data represents building an experimental apparatus and conducting the experiments.

A suite of 10 repeat experiments is conducted on a single fin-tube heat exchanger. In each experiment the bulk fluid temperatures at the inlet and outlet, the volume flow rate, and ambient air temperature are measured. The ambient air temperature, while not needed to experimentally calculate the total heat transfer rate in the experiment, is needed to simulate the total heat transfer rate with the model. It is important that the modeler communicate with the experimentalist to ensure that all conditions necessary for modeling the experiment are measured (such as the ambient temperature). The total heat transfer rate in the experiment can be calculated as

$$q_D = \rho Q C_p (T_i - T_o) \qquad (7\text{-}3\text{-}1)$$

where

C_p = specific heat
Q = volume flow rate
q_D = overall heat transfer rate, W
$(T_i - T_o)$ = bulk fluid temperature drop along the heat exchanger
ρ = density of the fluid

The measured data for the suite of 10 experiments and the calculated total heat transfer rate in the experiment are given in Table 7-3-2. The average of the measurement over the 10 experiments is given in the last row of Table 7-3-2.

Table 7-3-1 Details of the Fin-Tube Assembly and Flow Conditions

Material	Value
Internal fluid	Water
Tube material	Copper
Fin material	Aluminum
Tube inner radius, r_1, m	1.03e-2
Tube outer radius, r_2, m	1.11e-2
Fin edge length, a, m	5.40e-2
Fin thickness, w_f, m	2.54e-4
Fin spacing, w_{nf}, m	4.8e-3
Number of fins, N_f	500
Length, L, m	2.54
Volume flow rate, Q(m^3/s)	6.34e-6 (nominal)
Fluid inlet temperature, T_i, °C	70 (nominal)
Ambient temperature, T_∞, °C	22 (nominal)

There is variation in the measurements and total heat transfer rate derived from the 10 experiments in Table 7-3-2. The experiments were (synthetically) run on the same fin-tube heat exchanger. Thus, no variation is due to changes in the heat exchanger materials or geometry. The variation is due to

(a) repeating the experimental conditions
(b) random measurement error

The 10 experiments had nominally identical flow conditions. However, the driving flow conditions, the inlet fluid temperature, volume flow rate, and ambient temperature, are replicated between experiments to the accuracy that they are controlled and measured. For example, the inlet temperature was specified to be nominally 70°C. The true inlet temperature for one experiment may be 70.1°C. The measured inlet temperature is 70.1°C plus measurement error. In validation applications where the driving conditions vary due to lack of repeatability of the experiment, this variation can be accounted for by using the measured driving conditions of the experiment in the model. If the experimental conditions can be effectively replicated (i.e., the same driving conditions for repeated experiments), the effect of the random contribution to the measurement error can be reduced by averaging over multiple experiments.

Several measurements are used to compute the total heat transfer rate and all measurements have an associated uncertainty. Uncertainty estimates for measurements may be obtained from the manufacturer's specifications or through device calibration. For physical properties, such as density and specific heat of water, judgment may be required. With uncertainty estimates for the random and systematic contributions to the measurement uncertainty, the uncertainty in the total heat transfer rate can be estimated. Estimates of the experimental standard uncertainties are provided in Table 7-3-3. The bulk fluid temperatures and volumetric flow rate have random and systematic uncertainties associated with the measurements. The sensors for measuring the bulk fluid inlet and outlet temperatures have been calibrated to provide the accuracy listed in the table. Furthermore, the calibration was performed to the same standard for the inlet and outlet bulk fluid temperature sensors. By calibrating with same standard, the systematic errors for the inlet and outlet fluid temperature are identical (perfectly correlated). In this case, the covariance of the systematic uncertainty [i.e, b_{ik} in the propagation equation shown in eq. (7-3-2)], for the inlet and outlet bulk fluid temperatures is the product of the systematic uncertainties, b_i, of the two measurements. The other systematic uncertainties are uncorrelated, $b_{ik} = 0$. Properties of water are taken from a database [3] and estimated to have standard uncertainties of 0.5% and 1% for density and specific heat. Uncertainties in the dimensions of the physical hardware are considered to be negligible.

ASMENORMDOC.COM : Click to view the full PDF of ASME V&V 20 2009

Table 7-3-2 Measured Flow Conditions and Calculated Total Heat Transfer Rate

Experiment	ρ, kg/m³	Q, m³/s	C_p, J/kg°C	T_i, °C	T_o, °C	T_∞, °C	q_D, W
1	990	6.21 e-06	4,180	70.09	67.21	21.66	74.0
2	990	6.24 e-06	4,180	70.14	67.22	22.31	75.4
3	990	6.21 e-06	4,180	70.09	67.17	22.02	75.0
4	990	6.24 e-06	4,180	70.01	67.25	22.14	71.3
5	990	6.22 e-06	4,180	70.12	67.29	21.99	72.8
6	990	6.25 e-06	4,180	70.02	67.04	22.10	77.1
7	990	6.22 e-06	4,180	70.19	67.11	21.88	79.3
8	990	6.25 e-06	4,180	69.97	67.18	21.94	72.2
9	990	6.23 e-06	4,180	70.17	67.25	22.08	75.3
10	990	6.26 e-06	4,180	70.17	67.23	22.11	76.2
Average	990	6.23e-06	4,180	70.10	67.20	22.02	74.9

7-3.2.1 Experimental Uncertainty, u_D. The effect of uncertainty in the values used to calculate the total heat transfer rate from eq. (7-3-1) can be estimated with the propagation equation. The approach to estimate experimental uncertainty in the total heat transfer rate due to uncertainty in the measurements used to compute it is presented in Section 4. The propagation equation for systematic uncertainties is

$$b_{q_D}^2 = \sum_{i=1}^{J} \left(\frac{\partial q_D}{\partial X_i} b_i \right)^2 + \sum_{i=1}^{J-1} \sum_{k=i+1}^{J} \frac{\partial q_D}{\partial X_i} \frac{\partial q_D}{\partial X_k} b_{ik} \quad (7\text{-}3\text{-}2)$$

where $J = 5$ is the number of uncertain variables in the experimental data reduction equation. Terms for independent and correlated systematic uncertainties are included in eq. (7-3-2) because the experiment has correlated systematic input uncertainty in the measured bulk fluid temperatures.

The propagation equation for random uncertainties is

$$s_{q_D}^2 = \sum_{i=1}^{J} \left(\frac{\partial q_D}{\partial X_i} s_i \right)^2 \quad (7\text{-}3\text{-}3)$$

The propagation equations require

(a) partial derivatives (sensitivity coefficients) of the total heat transfer rate with respect to the measurements used to compute it

(b) estimates of the random and systematic uncertainties in those measurements

As discussed later in this Section, the effect of random uncertainty on the total heat transfer rate can also be estimated directly from the 10 experiments.

Table 7-3-3 Estimates of the Experimental Measurement Standard Uncertainties

Variable, X_i	Uncertainty (Standard)	
	Random, s_i	Systematic, b_i
T_i, °C	0.05°C	0.1°C
T_o, °C	0.05°C	0.1°C
Q, m³/sec	0.5%	1.0%
ρ, kg/m³	...	0.5%
C_p, J/kg °C	...	1.0%
T_∞, °C	...	0.22°C

For the simple data reduction equation in eq. (7-3-1), the partial derivatives needed in eqs. (7-3-2) and (7-3-3) can be analytically derived (other approaches for obtaining partial derivatives for more complex cases are discussed in Section 3). The sensitivities of the total heat transfer rate to each of the five inputs needed to calculate it are as follows.

$$\begin{aligned} \frac{\partial q_D}{\partial T_i} &= \rho Q C_p \\ \frac{\partial q_D}{\partial T_o} &= -\rho Q C_p \\ \frac{\partial q_D}{\partial Q} &= \rho C_p (T_i - T_o) \\ \frac{\partial q_D}{\partial \rho} &= Q C_p (T_i - T_o) \\ \frac{\partial q_D}{\partial C_p} &= \rho Q (T_i - T_o) \end{aligned} \quad (7\text{-}3\text{-}4)$$

As discussed in Section 3, multiplying the partial derivatives by the parameters to give scaled sensitivity coefficients is useful. Numerical values of the scaled sensitivity coefficients are listed in Table 7-3-4, and these were computed using the average of measurements over the 10 experiments (last row of Table 7-3-2). Because the partial derivatives depend on the magnitude of the measurements, the magnitudes of the partial derivatives will vary between the experiments. However, given the small differences in the measurements between experiments, the magnitudes of the partial derivatives for other experiments are within 1% of the values (evaluated with the average measurements) listed in Table 7-3-4.

Table 7-3-4 Sensitivity Coefficients for Average Conditions

X_i	$X_i \frac{\partial q_D}{\partial X_i}$	Standard Uncertainty	
		Random, s_i	Systematic, b_i
T_i	1,808, W	0.07 %	0.14 %
T_o	−1,734, W	0.07 %	0.14 %
Q	74.9, W	0.5 %	1.0 %
ρ	74.9, W	...	0.5 %
C_p	74.9, W	...	1.0 %

ASMENORMDOC.COM : Click to view the full PDF of ASME V&V 20 2009

The magnitudes of the scaled sensitivity coefficients can be compared to identify the parameters that have the largest impact on the total heat transfer rate. The inlet and outlet fluid temperature are seen as the parameters that have the largest scaled sensitivity coefficients and hence will have the largest impact on the total heat transfer rate.

The uncertainty in the total heat transfer rate derived from the experiment can be estimated with eqs. (7-3-2) and (7-3-3) using the partial derivatives and the uncertainty estimates (repeated from Table 7-3-3) in Table 7-3-4. [Note that the uncertainty estimates are provided in relative magnitudes so that the propagation can be readily evaluated with the scaled sensitivity coefficients. While generally not a good practice to provide uncertainty in (nonabsolute) temperature measurements in relative terms, it is done here for convenience.]

The random and systematic uncertainties in the total heat transfer rate estimated with the propagation equation are listed in the last row of Table 7-3-5. The random contribution to the measurement uncertainty can also be estimated from the 10 experiments directly instead of using the propagation approach. The random uncertainty is estimated as the standard deviation in the total heat transfer rate from the 10 experiments. The random contribution estimated from the variation among the 10 experiments is shown near the middle of Table 7-3-5. Estimating the random uncertainty directly from multiple experiments assumes that random measurement error is causing the variation between the experiments. The random uncertainty estimated from the 10 experiments is about 30% larger than the random uncertainty estimated from the propagation equation. The systematic uncertainty can only be estimated with the propagation equation.

The random and systematic contributions to the uncertainty in the total heat transfer rate are listed separately in Table 7-3-5. The uncertainty values are based on using the sensitivity coefficients evaluated at the average of the measurements over the 10 experiments. If the sensitivity coefficients are evaluated at the measurement values of each experiment, the uncertainty values change less than 1%. The overall uncertainty in the measured total heat transfer rate is

$$u_D = \sqrt{s_{q_D}^2 + b_{q_D}^2} \tag{7-3-5}$$

The measured total heat transfer rate with standard uncertainty limits of u_D are plotted in Fig. 7-3-2. The uncertainty in each experiment and the average of the 10 experiments (dash line) and its uncertainty are shown in the figure. The standard uncertainty on the experimentally measured total heat transfer rate is approximately 3% and has a larger contribution from the random uncertainties than from the systematic uncertainties. An additional step could be taken to identify the parameters that are the main contributors to the uncertainty in total heat transfer rate using importance factors. Importance factors are discussed in Nonmandatory Appendix B.

Table 7-3-5 Experimental Values of Total Heat Transfer Rate and Its Standard Uncertainties

Experiment	q_D, W	s_{q_o}, W	b_{q_o}, W	$u_D = \sqrt{s_{q_o}^2 + b_{q_o}^2}$, W
1	74.0			
2	75.6			
3	75.1			
4	71.4			
5	72.8			
6	77.0	2.39	1.15	2.65
7	79.3			
8	72.1			
9	75.1			
10	76.2			
Average	74.9	1.84	1.15	2.17

Fig. 7-3-2 Experimental Total Heat Transfer Rate and Its Standard Uncertainty, u_D

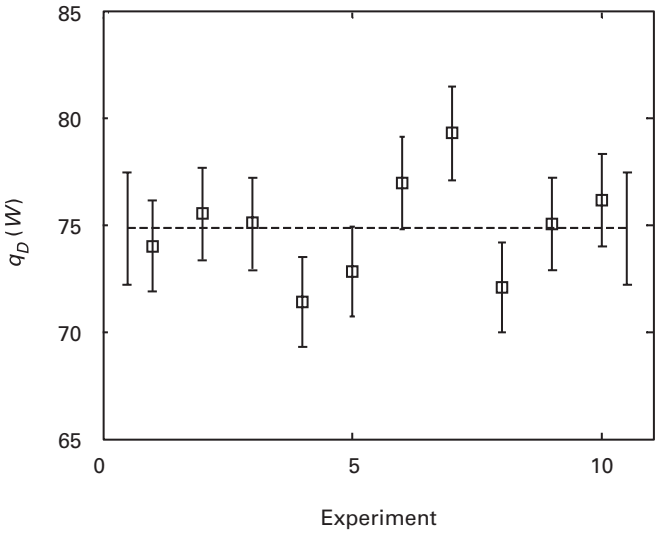

ASMENORMDOC.COM : Click to view the full PDF of ASME V V 20 2009

7-3.3 Simulation

7-3.3.1 Simulation Model. The model to simulate the total heat transfer rate from the fin-tube heat exchanger is summarized here. Details of the model development are given in Mandatory Appendix I. The model of the total heat transfer from the fin-tube heat exchanger is

$$q_S = \rho Q C_p (T_o - T_\infty)\left[\exp\left(\frac{\overline{U}_1 A_1}{\rho Q C_p}\right) - 1\right] \quad (7\text{-}3\text{-}6)$$

where

A_1 = wetted area of the tube's inner surface ($A_1 = 2\pi r_1 L$)
C_p = specific heat
Q = volume flow rate
q_S = overall heat transfer rate, W
T_o = bulk fluid temperature at the outlet
T_∞ = ambient air temperature
$\overline{U}_1$ = axially averaged overall heat transfer coefficient
ρ = density of the fluid

The axially averaged overall heat transfer coefficient is computed from the heat transfer coefficients on the finned (subscript *f*) and unfinned (subscript *nf*) portions of the tube

$$\overline{U}_1 = \frac{U_{f_1} w_f + U_{nf_1} w_{nf}}{w_f + w_{nf}} \quad (7\text{-}3\text{-}7)$$

The expression for the overall heat transfer coefficients through the unfinned region of the heat exchanger is

$$U_{nf_1} = \frac{1}{\frac{1}{h_1} + \frac{r_1 \ln(r_2/r_1)}{2\pi k_t} + \frac{r_1}{h_2 r_2}} \quad (7\text{-}3\text{-}8)$$

In eq. (7-3-8), h_1 and h_2 are the convective heat transfer coefficients on the inside and outside of the bare tube, respectively, k_t is the thermal conductivity of the tube, and r_1 and r_2 are the inner and outer radius of the tube, respectively. The heat transfer coefficient on the unfinned region (U_{nf_1}) is calculated with the thermal properties and dimensions of the tube and convection coefficients on the inside and outside of the tube. Convection coefficients are estimated based on empirical correlations for flow in a pipe and natural convection from a horizontal cylinder.

The overall heat transfer coefficient for the finned region (U_{f_1}) is calculated by solving for the heat transfer through a section of the fin-tube heat exchanger. The heat transfer model for the finned region of the heat exchanger is shown in Fig. 7-3-3. Symmetry is applied so that one-eighth of the cross section is modeled. The model is three-dimensional with a single element through the thickness of the fin and tube.[10] The partial differential equation for steady heat conduction is numerically solved over the cross section.

$$\frac{\partial}{\partial x}\left(k_t \frac{\partial T_t}{\partial x}\right) + \frac{\partial}{\partial y}\left(k_t \frac{\partial T_t}{\partial y}\right) + \frac{\partial}{\partial z}\left(k_t \frac{\partial T_t}{\partial z}\right) = 0 \quad \text{tube} \quad (7\text{-}3\text{-}9)$$

$$\frac{\partial}{\partial x}\left(k_f \frac{\partial T_f}{\partial x}\right) + \frac{\partial}{\partial y}\left(k_f \frac{\partial T_f}{\partial y}\right) + \frac{\partial}{\partial z}\left(k_f \frac{\partial T_f}{\partial z}\right) = 0 \quad \text{fin}$$

The thermal properties and convection coefficient are constant. Perfect contact is imposed at the interface of the tube and fin

$$-k_t \left.\frac{\partial T_t}{\partial r}\right|_{r_{2,\theta}^-} = -k_f \left.\frac{\partial T_f}{\partial r}\right|_{r_{2,\theta}^+} \quad (7\text{-}3\text{-}10)$$

$$T_t(r_2^-, \theta) = T_f(r_2^+, \theta)$$

Boundary conditions are applied at the inner surface of the tube and at outer the edge of the fin. The boundary condition form at the inner surface of the tube is

$$-k_t \left.\frac{\partial T_t}{\partial r}\right|_{r_1,\theta} = h_1 [T_{fl} - T_t(r_1, \theta)] \quad (7\text{-}3\text{-}11)$$

where

r_1 = inner radius of the tube
T_{fl} = bulk fluid temperature
θ = traditional polar coordinate for cylindrical geometry

The front and back surfaces of the fin (s_f) have convection to the ambient air.

$$-k_f \left.\frac{\partial T_f}{\partial n}\right|_{s_f} = h_f (T_f | s_f - T_\infty) \quad (7\text{-}3\text{-}12)$$

Fig. 7-3-3 Heat Transfer Model for the Fin-Tube Assembly

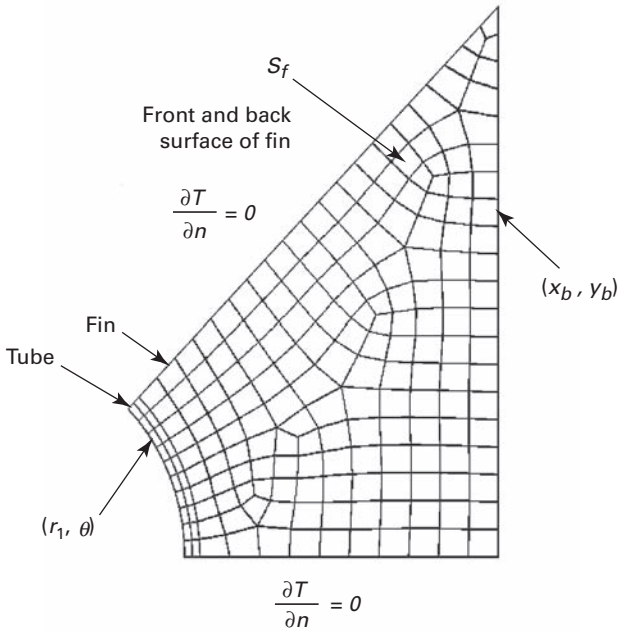

[10] An equivalent two-dimensional model of the heat transfer could also be developed for the configuration.

ASMENORMDOC.COM : Click to view the full PDF of ASME V&V 20 2009

The form of the boundary condition at the edge of the fin is

$$-k_f \left.\frac{\partial T_f}{\partial n}\right|_{(x_b, y_b)} = h_f [T_f(x_b, y_b) - T_\infty] \qquad (7\text{-}3\text{-}13)$$

where

n = outward normal at this surface

(x_b, y_b) = boundary surface of the fin (fin edge opposite the tube)

Adiabatic conditions are applied along the lines of symmetry.

The heat flux over the inner surface of the tube is integrated to calculate the overall heat transfer coefficient.

$$U_{f_i} = \frac{4}{\pi(T_{fl} - T_\infty)} \int_0^{\pi/4} h_1 \left[T_{fl} - T_t(r_i, \theta)\right] d\theta \qquad (7\text{-}3\text{-}14)$$

The model for simulating the heat transfer rate requires 10 parameters for eqs. (7-3-6) to (7-3-14). The values and standard uncertainty for parameters used in the simulations are listed in Table 7-3-6, and all other parameters (associated with the geometry) are held constant with no uncertainty. Thermal conductivities of the tube and fin are taken from database values for copper and aluminum [3]. Uncertainty (systematic) in the thermal conductivities is assigned a 5% standard uncertainty. Convection coefficients are estimated for the conditions of internal flow in a pipe and for natural convection from a cylinder and fin. Convection coefficients are assigned a 10% standard uncertainty. The ambient temperature, fluid temperature (taken as the inlet bulk fluid temperature), and flow rate are measured in the experiment (values are given in Table 7-3-2). Uncertainties in these parameters are assigned from the measurement uncertainty in Table 7-3-3. Density and specific heat of water are taken from database values. The same values and standard uncertainties for computing the total heat transfer rate in the experiment are applied in the model. The uncertainties assigned in the example are realistic, but should not be taken as universally applicable to other situations.

Table 7-3-6 Simulation Model Input Parameters and Standard Uncertainties

Parameter	Value	Uncertainty (Standard)	
		Random, s_i	Systematic, b_i
k_t (W/m °C)	386	...	5%
k_f (W/m °C)	204	...	5%
h_1 (W/m² °C)	150	...	10%
h_2 (W/m² °C)	6	...	10%
h_f (W/m² °C)	6	...	10%
T_∞ (°C)	Measured	...	1%
T_{fl} (°C)	Measured, T_i	0.05°C	0.1°C
Q (m³/ sec)	Measured	0.5%	1.0%
ρ (kg/m³)	990	...	0.5%
C_p (J/kg °C)	4,180	...	1%

The simulation value for the total heat transfer rate is calculated as follows. The two-dimensional heat transfer in a fin-tube section, defined by eqs. (7-3-9) to (7-3-13), is solved, and the overall heat transfer coefficient for the finned region of the heat exchanger, U_{f_i}, is calculated with eq. (7-3-14). This solution is done in a finite element code that directly computes the integral of the flux in eq. (7-3-14). The overall heat transfer coefficient on the unfinned region of the heat exchanger, U_{nf_i}, is calculated with eq. (7-3-8). The overall heat transfer coefficients are used in eq. (7-3-7) to calculate the axially averaged overall heat transfer coefficient and the simulated value of the total heat transfer rate is calculated from eq. (7-3-6).

7-3.3.2 Simulation Results. Ten experiments were conducted in this validation activity. Simulation results could be generated for each experiment, or a representative simulation could be generated for the set of experiments. Deciding what simulation results are needed depends on

(a) what is varying in the experiments and what impact does the variation have on the model

(b) what is feasible given the computational expense of the simulation

The experimental outcome may vary due to random measurement error, variation in the driving conditions of the experiment, and variation in the physical hardware (e.g., experiments conducted on different physical hardware). In this example, only the first two sources exist. As a demonstration, two approaches are considered for simulating the experiments. First, a simulation is generated using the measurements from each experiment. Second, a single simulation is generated using the average of the measurements from each experiment. Additional comments are provided below on the issue.

In experimental applications where the initiating or driving conditions vary due to lack of repeatability, but these conditions can be measured, each experiment may be simulated using the measured conditions. Simulating each experiment at the measured conditions aligns each simulation with each experiment. This may not always be feasible given the computation expense or may not be needed. In some cases, the variation in the driving experimental conditions may have negligible impact on the simulation. The sensitivity to the experimental conditions can be studied by running the simulation at bounding values of the experimental conditions or through an uncertainty analysis.

The simulation values of the total heat transfer rate are listed in the second column of Table 7-3-7 for individually simulating each experiment in the suite of experiments. In addition, the simulation using the average measured conditions is shown in the last row. In this case, noting that the variation among the individual simulations of total heat transfer rate is small, it is concluded that the

ASMENORMDOC.COM : Click to view the full PDF of ASME V&V 20 2009

Table 7-3-7 Simulation Values of Total Heat Transfer Rate

Experiment	q_S, W
1	97.9
2	96.7
3	97.2
4	96.8
5	97.3
6	96.9
7	97.7
8	97.1
9	97.2
10	97.2
Average	97.2

variation in the experimental conditions that are input to the model had a small effect on the simulation.

7-3.3.3 Solution Verification, u_{num}. The simulated total heat transfer rate has a dependence on the mesh used in solving for the heat transfer in the fin-tube cross section. All simulations were run with the mesh shown in Fig. 7-3-3. This mesh was the second mesh from a series of meshes generated for the simulation. The series started with a coarse mesh and approximately doubled the mesh density three times in an unstructured manner to create the series of four meshes. The series of meshes is used to estimate the numerical uncertainty in the simulated heat transfer rate. The numerical error could have been estimated prior to selecting a mesh to simulate the experiments. In this manner, the mesh required for a numerical uncertainty that was negligible compared to other uncertainties (e.g., experimental uncertainty or input parameter uncertainty) could be selected. If numerical uncertainty is to be made small relative to the uncertainty due to input parameter uncertainty, some iteration may be required to select the required mesh. This is because a mesh is needed to evaluate the uncertainty due to input parameter uncertainty.

The approach described in subsection 2-4 for solution verification is used to estimate an uncertainty for the numerical error. The simulation was run for the mesh series that successively refined the finite element mesh. The refined mesh sequence doubled the mesh density in the tube and approximately doubled the mesh density in the fin. The simulation was run for each of the four meshes. The relative characteristic mesh size in the tube and fin and the simulated heat transfer rate are listed in Table 7-3-8. The average element edge length is selected as the characteristic mesh size. This mesh characteristic is halved as the mesh is refined in the tube and approximately halved in the fin. The characteristic mesh size for the combined fin-tube assembly is within round-off of the characteristic mesh size for the fin.

The simulated total heat transfer rate as the mesh was refined is plotted in Fig. 7-3-4. The simulated total heat

Table 7-3-8 Solution Verification Results for Total Heat Transfer Rate

Mesh	h-Tube (Relative)	h-Fin (Relative)	q_S, W
1	0.125	0.119	97.89981
2	0.25	0.239	97.89765
3	0.5	0.477	97.88894
4	1	1	97.85440

transfer rate had a monotonic dependence on the characteristic mesh size. The procedure outlined in para. 2-4.1 is applied to estimate the numerical uncertainty. The procedure uses a sequence of three meshes. The numerical uncertainty is estimated with two sequences of three meshes from the four meshes. First, uncertainty is estimated using the sequence of meshes from Mesh 2 (fine) to Mesh 4 (coarse). Then, the estimates are calculated using the sequence from Mesh 1 (fine) to Mesh 3 (coarse). With these two sequences the constancy of the convergence rate can be checked.

The results of the solution verification are listed in Table 7-3-9. The order of convergence is listed in the second column, representative error estimates are listed in columns three and four, and the numerical uncertainty estimate from the Grid Convergence Index (GCI) is listed in the final column. The observed order of convergence is 2 for both mesh sequences. The relative differences are order 10^{-4} or smaller. The GCI is order of 10^{-3} and 10^{-4} for the two mesh sequences. From eq. (2-4-12), the dimensional numerical uncertainty estimate, u_{num}, is related to the dimensionless GCI as

$$u_{num} = \frac{GCI^{21}_{fine}}{2} q_S \qquad (7\text{-}3\text{-}15)$$

where the dimensional scaling value q_S = 97.2 W is taken as the simulation of the total heat transfer rate at the average conditions. The magnitude of u_{num} is given in the final column of Table 7-3-9.

Mesh 3 was used to generate the simulation results in the previous section. The numerical error estimate from the first mesh sequence (in Table 7-3-9) is applicable for Mesh 3. The magnitude of the numerical uncertainty could be argued as negligible given the magnitude of the experimental uncertainty. The numerical uncertainty is over an order of magnitude smaller than the experimental uncertainty. For completeness, the numerical uncertainty value is included in the remainder of the analysis.

7-3.3.4 Simulation Input Parameter Uncertainty, u_{inp}. The parameters required to simulate the total heat transfer have uncertainty in their values. Estimates of the standard uncertainty in the parameter values are provided in Table 7-3-6. Both random and systematic uncertainties are present. The effect of uncertainty in the values used to simulate the total heat transfer rate can be estimated with the propagation equation. The approach discussed in Section 3 is applied to estimate the effect of

ASMENORMDOC.COM : Click to view the full PDF of ASME V&V 20-2009

Fig. 7-3-4 Mesh Refinement Study for Solution Verification

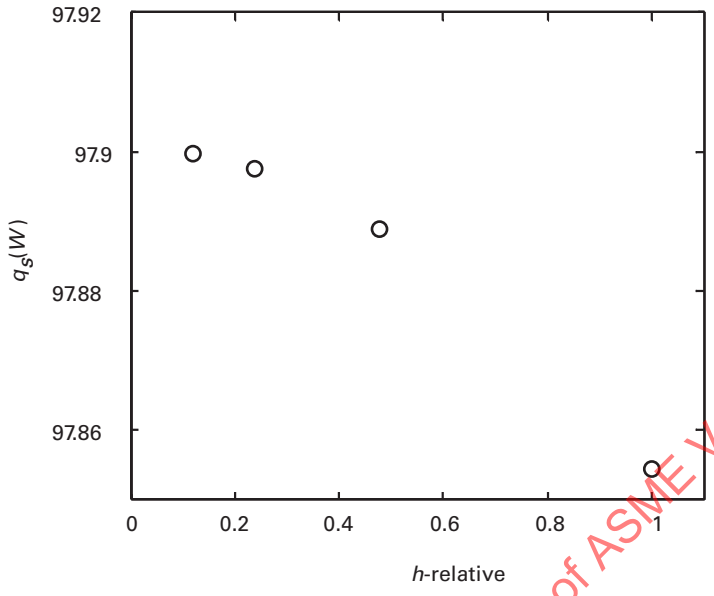

input parameter uncertainty. The propagation equation for systematic uncertainties is

$$b_{q_s}^2 = \sum_{i=1}^{J} \left(\frac{\partial q_S}{\partial X_i} b_i \right)^2 \quad (7\text{-}3\text{-}16)$$

The propagation equation for random uncertainties is

$$s_{q_s}^2 = \sum_{i=1}^{J} \left(\frac{\partial q_S}{\partial X_i} s_i \right)^2 \quad (7\text{-}3\text{-}17)$$

The propagation equation requires partial derivatives of the simulated total heat transfer rate with respect to the uncertain parameters. These partial derivatives are calculated with a second order central finite difference approximation.

$$\frac{\partial q_S}{\partial X_i} = \frac{q_S(X_i + \delta X_i) - q_S(X_i - \delta X_i)}{2\delta X_i} \quad (7\text{-}3\text{-}18)$$

The simulation is run while individually perturbing each parameter to approximate the gradients. The central difference approximation requires a positive and negative perturbation in each parameter. The total number of additional simulations needed for this approximation is 2 times the number of parameters. Alternatively, a forward or backward difference could have been used and required one-half as many additional simulation. The advantage of a central difference approximation is that

(a) it is a second order approximation

(b) the linearity of the simulation (in parameter space) can be checked

Although not shown in the document, the total heat transfer was closely approximated as linear with respect to the parameters over the range of the standard uncertainty. The values at the nominal, forward perturbation, and backward perturbation were plotted for each parameter, and adherence to a linear relationship over the three values was observed. The magnitude of the parameter perturbation was equal to the standard uncertainty in each parameter. This gives an approximation to the partial derivative over the range of the standard uncertainty. If the heat transfer rate is approximately linear, the partial derivative is independent of the parameter perturbation magnitude.

The partial derivatives (sensitivity coefficients), which are computed using a central difference approximation, are listed in Table 7-3-10. The derivatives are evaluated using the average measured input conditions (inlet temperature, flow rate, ambient temperature) over the 10 experiments. The simulation partial derivatives do vary with experiment because the input variables vary between experiments. The variation in input variables, which is due to the measured inputs used in the simulation, is not significant, and partial derivatives for the average measured conditions are representative of those for the individual experiments. If the variation in simulating the separate experiments is significant, the partial derivatives may need to be computed separately for the simulation of each experiment.

Table 7-3-9 Measures of the Numerical Error and Numerical Uncertainty for Total Heat Transfer Rate

Mesh Sequence	*p(observed)*	e_a^{21},%	e_{ext}^{21},%	GCI_{fine}^{21},%	u_{num},W
Mesh 2 to Mesh 4	1.99	3.530 e-4	4.718 e-4	1.416 e-3	0.07
Mesh 1 to Mesh 3	2.01	8.898 e-5	1.183 e-4	3.550 e-4	0.02

ASMENORMDOC.COM : Click to view the full PDF of ASME V V 20 2009

Table 7-3-10 Partial Derivatives of the Total Heat Transfer Rate for the Simulation Model With Respect to Uncertain Model Inputs for the Average of Measured Experimental Conditions and Standard Uncertainty for the Inputs

X_i	$X_i \frac{\partial q_S}{\partial X_i}$, W	Uncertainty (Standard)	
		Random, s_i	Systematic, b_i
k_t (W/m °C)	0.015	...	5%
k_f (W/m °C)	0.19	...	5%
h_1 (W/m² °C)	48.21	...	10%
h_2 (W/m² °C)	41.16	...	10%
h_f (W/m² °C)	3.77	...	10%
T_∞ (°C)	-44.53	...	1%
T_{fl} (°C)	141.72	0.07 %	0.14%
Q (m³/ sec)	3.91	0.5%	1.0%
ρ (kg/m³)	3.91	...	0.5%
C_p (J/kg °C)	3.91	...	1%

The standard uncertainty in the parameters for the simulation is propagated through the simulation model with eqs. (7-3-16) and (7-3-17) using the partial derivatives and input parameter uncertainty in Table 7-3-10. (Note that these standard uncertainties are the same as the values listed in Table 7-3-6 and repeated here for convenience.) The random contribution to the uncertainty can be estimated by propagation through the model or in the case that a simulation is computed for each experiment by estimating the standard deviation among the 10 experiments as was discussed for the experimental uncertainty in para. 7-3.2.1.

The magnitudes of the random and systematic standard uncertainties in the simulation of total heat transfer rate are listed at the bottom of Table 7-3-11 from the propagation approach. If a single simulation at the average conditions and its uncertainty due to uncertain inputs were estimated, the values at the bottom of the table would be obtained. If, however, a simulation were generated for each experiment, the random contribution to the uncertainty could be estimated from the uncertainty in the 10 simulations. The random uncertainty listed for the individual experiments is the standard deviation among the simulated total heat transfer of the 10 experiments.

The effect of random uncertainty is relatively small compared to the systematic uncertainty. The uncertainty due to model input uncertainty is computed by combining the random and systematic contributions.

$$u_{\text{input}} = \sqrt{s_{q_s}^2 + b_{q_s}^2} \tag{7-3-19}$$

The simulation of the total heat transfer rate and the uncertainty in the simulation due to model input uncertainty is shown in Fig. 7-3-5. The uncertainty in the simulation of each experiment and the uncertainty in the simulation using average inputs from the 10 experiments (dashed line) and its uncertainty are shown.

The standard uncertainty in the total heat transfer rate due to input parameter uncertainty is approximately 6.6%. The contribution of each parameter to the uncertainty in the simulation can be identified with importance factors. Importance factors are discussed in Nonmandatory Appendix B. Importance factors indicate that the convection coefficients on the inner surface of the tube (h_1) and outer surface (h_2) account for 99% of the simulated systematic uncertainty in the total heat transfer rate. The convection coefficient on the inner surface accounts for about 57%, and the coefficient on the outer surface accounts for about 42%.

7-3.4 Assessing the Validation Comparison

At this point in the analysis, the magnitudes of difference between the simulation and experimental measurements are known

$$E = S - D = q_S - q_D \tag{7-3-20}$$

The validation uncertainty u_{val} is an estimate of the standard deviation of the parent population of the combination of all errors except the modeling error in S and D. Standard uncertainty components u_{num}, u_{input}, and u_D that combine to give u_{val} have been estimated. If the uncertainties in the experiment and simulation are effectively independent, then combining the uncertainties is simple.

$$u_{\text{val}} = \sqrt{u_D^2 + u_{\text{input}}^2 + u_{\text{num}}^2} \tag{7-3-21}$$

However, in this example the uncertainties in the experiment and simulation are *not independent*. The reason that the uncertainties are not independent is discussed in the following section where the approach for computing u_{val} is presented.

7-3.4.1 Propagation Approach for Evaluating the Validation Uncertainty, u_{val}. The simulation and experimental uncertainties are not independent because parameters are common between the simulation and experiment. This

Table 7-3-11 Simulation Values of Total Heat Transfer Rate and Its Standard Uncertainty From Input Parameter Uncertainty

Experiment	q_S, W	Uncertainty (Standard)		
		s_{qs}, W	b_{qs}, W	u_{input}, W
1	97.9			
2	96.7			
3	97.2			
4	96.8			
5	97.3			
6	96.9	0.37	6.37	6.38
7	97.7			
8	97.1			
9	97.2			
10	97.2			
Average	97.2	0.10	6.37	6.37

ASMENORMDOC.COM : Click to view the full PDF of ASME V V 20 2009

Fig. 7-3-5 Simulation Values of Total Heat Transfer Rate and Its Uncertainty, u_{input}

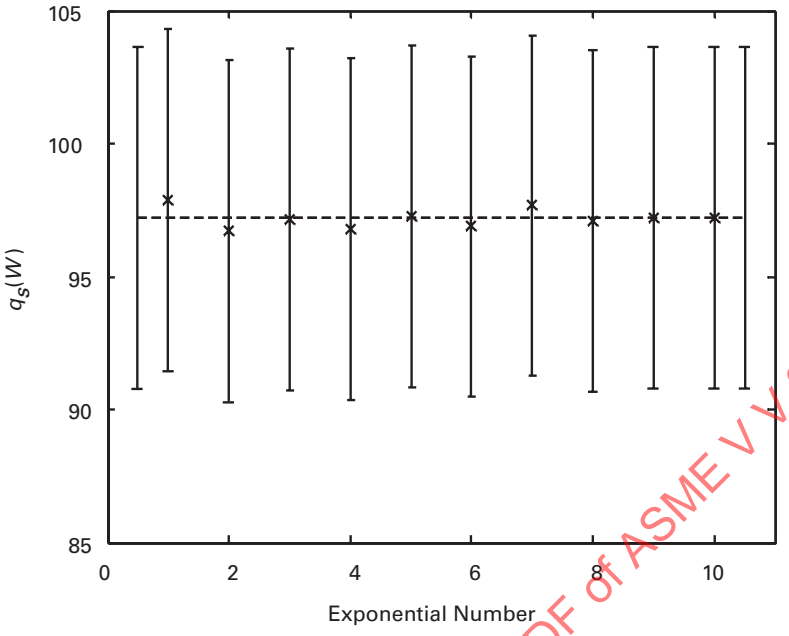

means that the simulation and experiment share identical error sources. The uncertain experimental variables (Table 7-3-3) and uncertain simulation input variables (Table 7-3-6) contain several common uncertain variables. All uncertain parameters that impact the difference $E = S - D$ are listed in Table 7-3-12. The second column identifies whether the (uncertain) parameter affects the simulation (S), experiment (D), or both (D and S). Uncertain parameters that impact both are inlet bulk fluid temperature, volume flow rate, density of the fluid, and specific heat of the fluid. For cases with common shared identical error source, the propagation equations for the simulation uncertainty and experimental uncertainty must be combined to calculate u_{val}. This example is Case 3 in Section 5 and the general expression for computing u_{val} is given in para. 5-3.2.1.

$$
\begin{aligned}
u_{\text{val}}^2 = {} & \left[\left(\frac{\partial q_S}{\partial \rho}\right) - \left(\frac{\partial q_D}{\partial \rho}\right)\right]^2 u_\rho^2 + \left[\left(\frac{\partial q_S}{\partial Q}\right) - \left(\frac{\partial q_D}{\partial Q}\right)\right]^2 u_Q^2 \\
& + \left[\left(\frac{\partial q_S}{\partial C_p}\right) - \left(\frac{\partial q_D}{\partial C_p}\right)\right]^2 u_{C_p}^2 + \left[\left(\frac{\partial q_S}{\partial T_i}\right) - \left(\frac{\partial q_D}{\partial T_i}\right)\right]^2 u_{T_i}^2 \\
& + \left(\frac{\partial q_S}{\partial T_\infty}\right)^2 u_{T_\infty}^2 + \left(\frac{\partial q_S}{\partial \mu}\right) u_\mu^2 + \left(\frac{\partial q_S}{\partial h_1}\right) u_{h_1}^2 + \left(\frac{\partial q_S}{\partial h_2}\right)^2 u_{h_2}^2 \\
& + \left(\frac{\partial q_S}{\partial h_f}\right)^2 u_{h_f}^2 + \left(\frac{\partial q_S}{\partial h_c}\right)^2 u_{h_c}^2 + \left(\frac{\partial q_S}{\partial k_f}\right)^2 u_{k_f}^2 + \left(\frac{\partial q_S}{\partial k_t}\right)^2 u_{k_t}^2 \\
& + \left(\frac{\partial q_S}{\partial d_1}\right)^2 u_{d_1}^2 + \left(\frac{\partial q_S}{\partial d_2}\right)^2 u_{d_2}^2 + \left(\frac{\partial q_S}{\partial L}\right)^2 u_L^2 + \left(\frac{\partial q_S}{\partial a}\right)^2 u_a^2 \\
& + \left(\frac{\partial q_S}{\partial_{W_f}}\right)^2 u_{W_f}^2 + \left(\frac{\partial q_S}{\partial W_{nf}}\right)^2 u_{W_{nf}}^2 + \left(\frac{\partial q_D}{\partial T_{o,D}}\right)^2 u_{T_{o,D}}^2 + u_{\text{num}}^2 \\
& + 2\left[\left(\frac{\partial q_S}{\partial T_i}\right) - \left(\frac{\partial q_D}{\partial T_i}\right)\right]\left[\left(\frac{\partial q_S}{\partial T_{o,D}}\right) - \left(\frac{\partial q_D}{\partial T_{o,D}}\right)\right] b_{T_i T_{o,D}} \qquad (7\text{-}3\text{-}22)
\end{aligned}
$$

The general expression has been simplified for this example. Contact conductance (h_c) and viscosity (μ) are not included in the simulation. Also, uncertainties associated with the geometry (d_1, d_2, L, a, w_f, and w_{nf}) are neglected. After removing terms associated with these parameters, eq. (7-3-22) can be simplified.

$$
\begin{aligned}
u_{\text{val}}^2 = {} & \left[\left(\frac{\partial q_S}{\partial \rho}\right) - \left(\frac{\partial q_D}{\partial \rho}\right)\right]^2 u_\rho^2 + \left[\left(\frac{\partial q_S}{\partial Q}\right) - \left(\frac{\partial q_D}{\partial Q}\right)\right]^2 u_Q^2 \\
& + \left[\left(\frac{\partial q_S}{\partial C_p}\right) - \left(\frac{\partial q_D}{\partial C_p}\right)\right]^2 u_{C_p}^2 + \left[\left(\frac{\partial q_S}{\partial T_i}\right) - \left(\frac{\partial q_D}{\partial T_i}\right)\right]^2 u_{T_i}^2 + \left(\frac{\partial q_S}{\partial T_\infty}\right)^2 u_{T_\infty}^2 \\
& + \left(\frac{\partial q_S}{\partial_{h_1}}\right)^2 u_{h_1}^2 + \left(\frac{\partial q_S}{\partial h_2}\right)^2 u_{h_2}^2 + \left(\frac{\partial q_S}{\partial h_f}\right)^2 u_{h_f}^2 + \left(\frac{\partial q_S}{\partial_{k_f}}\right)^2 u_{k_f}^2 + \left(\frac{\partial q_S}{\partial_{k_t}}\right)^2 u_{k_t}^2 \\
& + \left(\frac{\partial q_D}{\partial T_{o,D}}\right)^2 u_{T_{o,D}}^2 + u_{\text{num}}^2 \\
& + 2\left[\left(\frac{\partial q_S}{\partial T_i}\right) - \left(\frac{\partial q_D}{\partial T_i}\right)\right]\left[\left(\frac{\partial q_S}{\partial T_{o,D}}\right) - \left(\frac{\partial q_D}{\partial T_{o,D}}\right)\right] b_{T_i}\, b_{T_o} \qquad (7\text{-}3\text{-}23)
\end{aligned}
$$

There are several notable issues concerning eq. (7-3-23). The first four terms and the last term in eq. (7-3-23) represent the contribution from uncertain parameters that impact both the simulation and experimental values of the total heat transfer rate. The contribution of these parameters to u_{val} depends on the difference in the partial derivatives from the simulation and experiment (squared). The uncertain parameters that only impact the simulation are included in term five

ASMENORMDOC.COM : Click to view the full PDF of ASME V V 20 2009

Table 7-3-12 Parameters Included in Evaluating u_{val}, Parameter Standard Uncertainty Estimates, and Parameter Sensitivity Coefficients

		Standard Uncertainty			Scaled Sensitivity Coefficients	
Parameter	Impact	Random, s_i	Systematic, b_i	Total, u_i	$X_i \frac{\partial q_D}{\partial X_i}$, W	$X_i \frac{\partial q_S}{\partial X_i}$, W
T_i (°C)	*D* and *S*	0.07%	0.14%	0.16%	1808	141.72
T_o (°C)	*D*	0.07%	0.14%	0.16%	−1734	...
Q (m³/ s)	*D* and *S*	0.5%	1.0%	1.12%	74.9	3.91
ρ (kg/m³)	*D* and *S*	...	0.5%	0.5%	74.9	3.91
C_p (J/kg °C)	*D* and *S*	...	1.0%	1.0%	74.9	3.91
k_i (W/m °C)	*S*	...	5%	5%	...	0.015
k_f (W/m °C)	*S*	...	5%	5%	...	0.19
h_1 (W/m² °C)	*S*	...	10%	10%	...	48.21
h_2 (W/m² °C)	*S*	...	10%	10%	...	41.16
h_f (W/m² °C)	*S*	...	10%	10%	...	3.77
T_∞ (°C)	*S*	...	1%	1%	...	−44.53

through ten. The fourth line has a term for the uncertain parameter that impacts the experiment and the numerical uncertainty. The final term of the equation accounts for correlated bias errors between the input and output fluid temperatures that impact both the simulation and experiment.

The parameter uncertainties and parameter sensitivity coefficients (from Table 7-3-4 and Table 7-3-10) for the simulation and experiment that are required for evaluating u_{val} are listed in Table 7-3-12. (Note that relative uncertainties should be used with the scaled sensitivity coefficients.)

The results listed in Table 7-3-13 summarize the total heat transfer from the experiment and its uncertainty, the simulation result and its uncertainty from input uncertainty and numerical uncertainty, the comparison error, and the validation uncertainty u_{val} from eq. (7-3-23). A single value of u_{val} is calculated and does not depend on whether each experiment is modeled or the average experiment is modeled. In both cases, the sensitivity coefficients were evaluated at the average conditions of the 10 experiments.

In this example, though the simulation and the experiment have shared error sources, the magnitude of u_{val} is negligibly different from the values obtained from assuming independence and using eq. (7-3-21). This outcome depends on

(*a*) the magnitude of the difference in the scaled sensitivity coefficients in the simulation and experiment for the shared parameters

(*b*) the relative importance of the shared parameters to the uncertainty in the simulation and experiment

This outcome is problem specific and other problems could have a larger difference.

7-3.4.2 Monte Carlo Approach for Evaluating the Validation Uncertainty, u_{val}. The validation uncertainty can also be computed with a Monte Carlo approach. In this example, the simulation and the experiment have identical error sources and correlated errors (in the inlet and outlet fluid temperature). This is Case 3 in Section 5, and the procedure for evaluating u_{val} by Monte Carlo is discussed in para. 5-3.2.2.

Table 7-3-13 Experimental and Simulation Values of Total Heat Transfer Rate and Associated Standard Uncertainties

Experiment	q_D, W	u_D, W	q_S, W	u_{input}, W	u_{num}, W	E, W	u_{val}, W
1	74.0	2.65	97.9	6.38	0.07	23.9	6.69
2	75.6		96.7			21.1	
3	75.1		97.2			22.1	
4	71.4		96.8			25.4	
5	72.8		97.3			24.5	
6	77.0		96.9			19.9	
7	79.3		97.7			18.4	
8	72.1		97.1			25.0	
9	75.1		97.2			22.1	
10	76.2		97.2			22.3	
Average	74.9	2.17	97.2	6.37	0.07	22.3	6.69

ASMENORMDOC.COM : Click to view the full PDF of ASME V V 20 2009

A Monte Carlo procedure involves sampling over range of uncertain parameters that are inputs to the simulation and experimental data reduction equation. The simulation model and experimental data reduction equation are evaluated with samples of the parameters to estimate the effect of parameter uncertainty. A Latin hypercube sampling (LHS) procedure is applied in this Section to evaluate u_{val}. The LHS procedure is discussed in Section 3 as applied to the simulation model for u_{input} and in Section 4 for the experimental uncertainty, u_D. Because the simulation and experiment have shared error sources, the sampling of parameters in the experimental data reduction equation and parameters for the simulation is done jointly to evaluate u_{val}. In cases that do not share error sources, the Monte Carlo sampling can be done independently on the simulation and experimental data reduction equation.

All of the parameters required for calculating the total heat transfer rate in the experiment and simulation and their standard uncertainties are listed Table 7-3-14. When applying a sampling-based procedure, in addition to specifying the standard uncertainty of each parameter, a (probability) distribution function is required for each parameter. For example, the uncertainty in the parameter might be distributed as a Gaussian function defined by a mean and standard deviation. In most cases there is not sufficient data to assign a distribution function and judgment is required. For this demonstration example a Gaussian distribution function is assigned to all inputs. The mean of the Gaussian distribution is taken as the nominal parameter value (averaged over the 10 experiments for measured inputs), and the standard deviation is the standard uncertainty; these values are listed in Table 7-3-14.

Twenty LHS samples of the inputs are generated for the example. Two of the LHS parameter sample sets (from 20) are listed in last two columns of Table 7-3-14. The simulation and experimental values of total heat transfer rate, and their difference, for each of the 20 LHS parameter sample sets is given in Table 7-3-15. The LHS samples of total heat transfer rate are also plotted in Fig. 7-3-6. The samples of the total heat transfer rate are analyzed with standard statistics to get uncertainty from the LHS samples. The mean and standard deviation are listed at the bottom of the table for each column. The means are the nominal (expected value) of the simulated (q_S) total heat transfer rate, experimental (q_S) total heat transfer rate, and difference (E). The estimated standard deviations (of columns 3, 4, and 5) are the standard uncertainties in the simulation due to input parameter uncertainty (u_{input}), the experimental uncertainty due to measurement uncertainty (u_D), and contributions of both these uncertainties to u_{val}.

The nominal values of q_S and q_D and their standard uncertainty estimates computed with an LHS approach can be compared to the previous estimates from a propagation approach (in paras. 7-3.2.1 and 7-3.3.4). A fundamental difference between the LHS and propagation approaches is the assumption of linearity in a propagation approach, which is not necessary in an LHS approach. Some insight into the impact of this assumption can be obtained through comparing the results of the two approaches. The comparison is not solely due to the assumption of linearity because the LHS approach has a dependence on sample size. The comparison is shown in Table 7-3-16. Note that in the example u_{num} is of negligible magnitude and u_{val} only has contributions from simulation input uncertainty and experimental measurement uncertainty.

The results in Table 7-3-16 indicate that the LHS and propagation approaches give consistent results for the nominal total heat transfer rates and uncertainties. The values for the experiment should be in close agreement because the experimental data reduction equation is a linear function of the parameters [see eq. (7-3-1)]. The difference between the values from the LHS approach and propagation equation is small and only due to the sample size dependence for the

ASMENORMDOC.COM : Click to view the full PDF of ASME V&V 20-2009

Table 7-3-14 Parameter Standard Uncertainty and Example Latin Hypercube Samples

Parameter	Impact	Nominal	Standard Uncertainty			Latin Hypercube Samples	
			Random, s_i	Systematic, b_i	Total, u_i	1	2
T_i (°C)	*D* and *S*	70.01	0.07%	0.14%	0.16%	70.183	70.116
T_o (°C)	*D*	67.20	0.07%	0.14%	0.16%	67.288	67.072
Q (m³/ sec)	*D* and *S*	6.23 e-06	0.5%	1.0%	1.12%	6.334 e-06	6.265 e-06
ρ (kg/m³)	*D* and *S*	990	...	0.5%	0.5%	984.5	992.0
C_p (J/kg°C)	*D* and *S*	4180	...	1.0%	1.0%	4118	4211
k_t (W/m°C)	*S*	386	...	5%	5%	391.1	388.9
k_f (W/m°C)	*S*	204	...	5%	5%	239.7	215.9
h_1 (W/m²°C)	*S*	150	...	10%	10%	140.8	160.7
h_2 (W/m²°C)	*S*	6	...	10%	10%	7.008	4.760
h_f (W/m²°C)	*S*	6	...	10%	10%	6.732	5.886
T_∞ (°C)	*S*	22.02	...	1%	1%	22.02	22.19

Fig. 7-3-6 LHS Samples of Simulated and Experimental Values of Total Heat Transfer Rate

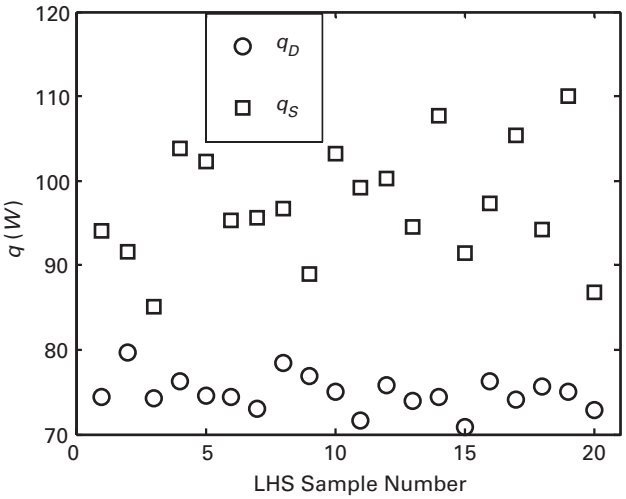

LHS. The simulation has approximately a linear dependence on the parameters. The two approaches give the same nominal value of the total heat transfer rate, but the estimate of the standard uncertainty is larger (6.6%) for the LHS than that for the propagation approach. The estimates of the validation uncertainty for the two approaches are similarly consistent in the nominal value of the difference in total heat transfer rate, with LHS estimating a larger standard uncertainty than the propagation approach. The consistency between the LHS and propagation approaches addresses concerns that may arise in the applicability of the linear assumption required for the propagation approach. Agreement between the two approaches is problem specific, and the other problems may demonstrate a larger difference.

Table 7-3-15 LHS Samples for the Simulated and Experimental Values of the Total Heat Transfer Rate

Sample Number	q_S, W	q_D, W	$E = q_S - q_D$, W
1	94.08	74.33	19.74
2	91.58	79.66	11.92
3	85.06	74.25	10.81
4	103.84	76.34	27.51
5	102.25	74.50	27.75
6	95.33	74.49	20.84
7	95.60	73.09	22.51
8	96.73	78.49	18.24
9	89.02	76.84	12.18
10	103.17	75.00	28.16
11	99.16	71.57	27.59
12	100.27	75.84	24.43
13	94.46	73.90	20.56
14	107.69	74.39	33.30
15	91.49	70.91	20.58
16	97.33	76.24	21.09
17	105.41	74.12	31.28
18	94.27	75.66	18.61
19	109.94	75.09	34.85
20	86.83	72.79	14.04
Mean	97.18	74.88	22.03
Standard Deviation	6.79	2.08	7.03

7-3.4.3 Interpretation of the Validation Results. The previous sections have presented the approach for determining the comparison error E and the validation uncertainty u_{val}. (The experimental uncertainty and simulation uncertainty due to input parameter uncertainty and numerical uncertainty were also estimated.) The validation uncertainty u_{val} is an estimate of the standard deviation of the parent population of the combination of the errors $(\delta_{num} + \delta_{input} - \delta_D)$ where δ_{model} has been excluded. The expression for δ_{model}, the error due to modeling assumptions and approximations, was derived in Section 1.

$$\delta_{model} = E - (\delta_{num} + \delta_{input} - \delta_D) \qquad (7\text{-}3\text{-}24)$$

Thus, $E \pm u_{val}$ defines an interval within which δ_{model} falls with an unspecified probability, or

$$E - u_{val} \le \delta_{model} \le E + u_{val} \qquad (7\text{-}3\text{-}25)$$

The comparison is interpreted in two ways. First, with no assumptions on the distribution of parent population of the errors $(\delta_{num} + \delta_{input} - \delta_D)$, the magnitudes of E and u_{val} can be compared to make approximate inferences about δ_{model}. Second, by making an assumption on the distribution of the parent population of the errors $(\delta_{num} + \delta_{input} - \delta_D)$, an interval can be estimated within which δ_{model} falls with a specified probability. Section 6 discusses interpreting the validation results.

With no assumptions on distributions, the magnitudes of E and u_{val} can be compared to indicate if δ_{model} might be present. The values for E and u_{val} in Table 7-3-13 indicate that E is approximately a factor of 3 larger than u_{val} over the suite of experiments. A magnitude of E that is a factor of 3 larger than u_{val} is in the range that E can be

Table 7-3-16 Comparison of Nominal Values and Standard Uncertainties Computed With the Propagation and LHS Approaches

Quantity Simulation	LHS	Propagation
q_S, W	97.2	97.2
u_{input}, W	6.79	6.37
Experiment		
q_D, W	74.9	74.9
u_D, W	2.08	2.17
Difference		
$E = q_S - q_D$, W	22.3	22.3
u_{val}, W	7.03	6.69

ASMENORMDOC.COM : Click to view the full PDF of ASME V&V 20 2009

directly related to δ_{model}. Given the difference in magnitudes of E and u_{val}, E probably includes a contribution from δ_{model}.

By assuming a probability distribution for the combination of all errors except the modeling error δ_{model}, an interval can be estimated within which δ_{model} falls. With an assumed distribution for the combination of all errors except the modeling error, a coverage factor, k, can be specified to define an expanded uncertainty, $U_{val,\alpha} = k\, u_{val}$, that defines the interval $(E \pm U_{val,\alpha})$ within which δ_{model} with level of confidence α. The magnitude of k depends on the probability distribution and level of confidence α. Magnitudes for k are discussed in subsection 6-3 for various probability distributions and confidence levels. For a Gaussian distribution with $\alpha \cong 95\%$ confidence level, k is 2.0. The interval within which δ_{model} falls with ~95% probability, $E \pm 2u_{val}$, is plotted in Fig. 7-3-7. In the case that a single simulation is generated at the average conditions the dashed line is obtained with shown bounds [10.4, 37.3]. If each experiment were individually simulated, the variation in the magnitude of δ_{model} can be observed. If the expanded uncertainty is for a 99% probability ($k = 3$) the average interval for δ_{model} expands to [3.7, 44.0] W.

The validation procedure outlined in this document is complete at this point. The approach in this document is a procedure to objectively assess and quantify the accuracy of a simulation. The approach resulted in an estimated range characterizing the error δ_{model}. The question as to whether the simulation model is adequate depends on the accuracy required for an application. Given the outcome or the validation procedure, however, there may be a desire to improve the accuracy of the model or better understand the source of δ_{model}. What is done as follow-on to the validation procedure of this document would be considered model development and not validation. However, as will be seen, the possibility of improving the model is informed by the validation. If the originally assessed model is improved or modified to include additional physics, it can be assessed with the same procedure. The assessment of a second model with the same experimental data is summarized in the following section. The experimental data was not involved in updating the model. Additional comments are provided below on the issue of the next step after a validation assessment.

The validation procedure can include some insight into the possible source of δ_{model}. Potential areas to consider are discussed next. It would be beneficial to consider these even if the outcome of the validation were favorable or acceptable.

(a) The inputs — both the nominal values and uncertainty estimates — for the experimental data reduction equation and simulation could be re-evaluated. The nominal inputs or uncertainty estimates may not be applicable to the validation experiment. Importance factors (see Nonmandatory Appendix B) identify the relative contribution of each parameter to the uncertainty in the experimental data reduction equation and uncertainty in the simulation due to input uncertainty. Obtaining additional data for the nominal value or uncertainty of an input parameter identified as important could impact δ_{model}.

(b) Review the adequacy of the approaches used to propagate the uncertainties.

ASMENORMDOC.COM : Click to view the full PDF of ASME V V 20 2009

Fig. 7-3-7 Interval for δ_{model} ($E \pm 2u_{val}$) Assuming a Gaussian Distribution for the Errors and 95% Probability

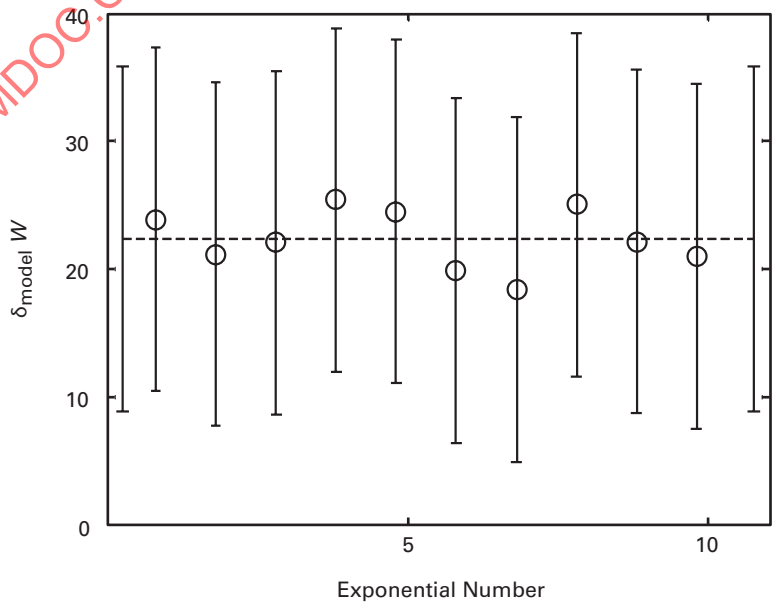

(c) The critical assumptions that form the basis for the selected simulation model should be reviewed. Additional studies (through simulation and/or experimentation) may indicate that an assumption is not appropriate.

7-3.5 Assessing a Second Model

The initial model for simulating the total heat transfer rate from the fin tube heat exchanger assumed perfect contact (an infinite contact conductance, h_c) at the interface between the tube and fin. Further investigation and testing has shown that the contact conductance between the fin and tube is smaller than initially believed. To investigate the effect of a finite contact conductance, the simulated model results including a contact conductance at the fin/tube interface are calculated. The simulation uncertainty with contact conductance in the model is also estimated. The validation comparison to the experimental data is repeated to assess the model with a contact conductance.

Once a model has been assessed and the experimental data observed, there are many ways that a model can be updated to more closely match the experimental data. Updates to the model can be physically motivated, but just because the updated model more closely matches experimental data does not necessarily mean the update to the model physically represents the true δ_{model}. Some caution must be exercised in updating a model and the claims that can be made when the updated model is assessed. The intent of this Section is to demonstrate how the updated model can be assessed and the outcome of that assessment. The validation approach can demonstrate whether the second (updated) model is more accurate than the first model, but justifying the appropriateness of the updates is an issue to be discussed among the modeler, experimentalist, and perhaps others.

7-3.5.1 Simulation Model With Contact Conductance and Uncertainty Simulation Model. The simulation model is the same as that discussed in para. 7-3.3, except that a contact conductance is defined at the fin/tube interface when solving for the two-dimensional heat transfer in the fin-tube cross section. Instead of perfect contact at the fin/tube interface, defined by eq. (7-3-11), a contact conductance is defined at the interface.

$$-k_t \left.\frac{\partial T_t}{\partial r}\right|_{r_2^-,\theta} = h_c\left[T_t(r_2^-,\theta) - T_f(r_2^+,\theta)\right] = -k_f \left.\frac{\partial T_f}{\partial r}\right|_{r_2^+,\theta} \tag{7-3-26}$$

This is the only change in the simulation model. The same parameter values and uncertainty values given in Table 7-3-6 are used in the simulation. The contact conductance in eq. (7-3-26) is h_c = 150 W/m^2°C with a standard systematic uncertainty of 20%.

7-3.5.1.1 Code Verification. The code verification process described earlier did not include the option for a finite contact conductance. This verification could be accomplished, using the exact MMS solution including contact conductance as described in Nonmandatory Appendix B. The results will not be presented here in the interest of space.

7-3.5.1.2 Simulation Results. The simulated values of the total heat transfer rate with a contact conductance are listed in Table 7-3-17. As was done previously and discussed in para. 7-3.3.2, two approaches were taken to simulate the experiments. Each experiment was simulated, and a single simulation at the average of the conditions measured over the 10 experiments was conducted. The simulation at the average conditions is provided at the bottom of Table 7-3-17. Notice that the magnitude of the simulated total heat transfer with a contact conductance decreased to 73.8 W from a value of 97.2 when perfect contact was assumed.

7-3.5.1.3 Solution Verification. The simulation model adds the effect of a contact conductance between the fin and tube. Given the outcome of the previous mesh refinement study in para. 7-3.3.3, and furthermore arguing that contact conductance may have a small dependence on the mesh, the solution verification may not need to be repeated. The previous evidence may be convincing that the numerical error due to mesh is negligible. In the interest of demonstrating the approach, the solution verification process is repeated for the second model. The same sequence of meshes discussed in para. 7-3.3.3 is used to perform solution verification. The results of the study are provided in Tables 7-3-19 and 7-3-20 for the model with contact conductance included.

The dependence of the simulated total heat transfer rate on the mesh is monotonic. The estimated observed convergence rate for the two mesh sequences is 2.0. The uncertainty for the numerical uncertainty is negligibly

Table 7-3-17 Simulation Values of the Total Heat Transfer Rate for the Model With Contact Conductance

Experiment	q_s, W
1	74.3
2	73.4
3	73.7
4	73.5
5	73.8
6	73.5
7	74.1
8	73.7
9	73.8
10	73.8
Average	73.8

ASMENORMDOC.COM: Click to view the full PDF of ASME V&V 20 2009

Table 7-3-18 Simulation Values of the Total Heat Transfer Rate and the Standard Uncertainty for the Model With Contact Conductance

		Uncertainty (Standard)		
Experiment	q_S, W	s_{q_S}, W	b_{q_S}, W	u_{input}, W
1	74.3			
2	73.4			
3	73.7			
4	73.5			
5	73.8			
6	73.5	0.28	5.18	5.19
7	74.1			
8	73.7			
9	73.8			
10	73.8			
Average	73.8	0.08	5.18	5.18

small; the numerical uncertainty is two orders of magnitude smaller than the experimental uncertainty in the total heat transfer rate.

7-3.5.1.4 Simulation Input Parameter Uncertainty. The uncertainty due to input uncertainty is propagated through the simulation in the same manner as discussed in para. 7-3.3.4. In addition to the input parameters listed in para. 7-3.3.4, uncertainty in the contact conductance is included. The simulation model with a contact conductance will have different partial derivatives with respect to the parameters. The partial derivatives are numerically calculated with the central difference approximation. The scaled sensitivity coefficients and standard uncertainties for the parameters are listed in Table 7-3-21. The uncertainty in the simulation of the total heat transfer rate can be estimated from the propagation equations in para. 7-3.3.4 using the data in Table 7-3-21. Both the random and systematic contributions to the uncertainty can be estimated.

The magnitudes of the random and systematic contributions to the standard uncertainty in the total heat transfer rate from the propagation approach are shown in the last row of Table 7-3-18. The random contribution to the total uncertainty is negligible compared to the systematic contribution. The random contribution can be computed directly when each experiment is individually simulated. The random standard uncertainty is estimated from the standard deviation in the simulated total heat transfer rate of the 10 experiments. This estimate for the random standard uncertainty is shown near the middle of Table 7-3-18. Although this estimate of the random contribution is (over a factor of 3) larger than the value from the propagation approach, the magnitude is negligible compared to the systematic uncertainty.

Table 7-3-19 Solution Verification Results for Total Heat Transfer Rate for the Model With Contact Conductance

Mesh	*h*-Tube (Relative)	*h*-Fin (Relative)	q_S, W
1	0.125	0.119	74.298318
2	0.25	0.239	74.297087
3	0.5	0.477	74.292162
4	1	1	74.272587

The standard uncertainty in the simulated total heat transfer rate due to input parameter uncertainty is approximately 6.9%. The contribution of each parameter to the uncertainty in the simulation can be identified with importance factors. Importance factors are discussed in Nonmandatory Appendix B. Importance factors indicate that the convection coefficient on the outer surface of the tube (h_2), the convection coefficient on the inner surface of the tube (h_i) and the contact conductance (h_c) account for 99% of the simulated systematic uncertainty in the total heat transfer rate; those parameters account for 66%, 24%, and 9% of the systematic uncertainty, respectively.

7-3.5.2 Evaluating the Validation Uncertainty and Interpreting the Validation Comparison

7-3.5.2.1 Evaluating the Validation Uncertainty, u_{val}. The validation uncertainty is evaluated with the propagation equation as discussed in para. 7-3.4.1. Compared to the final equation for u_{val} in para. 7-3.4.1, an additional term is included for the uncertainty in the simulation input for contact conductance. The propagation equation for u_{val} for a model with contact conductance is

$$u_{val}^2 = \left[\left(\frac{\partial q_S}{\partial \rho}\right) - \left(\frac{\partial q_D}{\partial \rho}\right)\right]^2 u_\rho^2 + \left[\left(\frac{\partial q_S}{\partial Q}\right) - \left(\frac{\partial q_D}{\partial Q}\right)\right]^2 u_Q^2 + \left[\left(\frac{\partial q_S}{\partial C_p}\right) - \left(\frac{\partial q_D}{\partial C_p}\right)\right]^2 u_{C_p}^2 + \left[\left(\frac{\partial q_S}{\partial T_i}\right) - \left(\frac{\partial q_D}{\partial T_i}\right)\right]^2 u_{T_i}^2 + \left(\frac{\partial q_S}{\partial h_c}\right)^2 u_{h_c}^2 + \left(\frac{\partial q_S}{\partial T_\infty}\right)^2 u_{T_\infty}^2 + \left(\frac{\partial q_S}{\partial_{h_1}}\right) u_{h_1}^2 + \left(\frac{\partial q_S}{\partial h_2}\right)^2 u_{h_2}^2 + \left(\frac{\partial q_S}{\partial h_f}\right)^2 u_{h_f}^2 + \left(\frac{\partial q_S}{\partial_{k_f}}\right)^2 u_{k_f}^2 + \left(\frac{\partial q_S}{\partial_{k_t}}\right)^2 u_{k_t}^2 + \left(\frac{\partial q_D}{\partial T_{o,D}}\right)^2 u_{T_{o,D}}^2 + u_{num}^2 + 2\left[\left(\frac{\partial q_S}{\partial T_i}\right) - \left(\frac{\partial q_D}{\partial T_i}\right)\right]\left[\left(\frac{\partial q_S}{\partial T_{o,D}}\right) - \left(\frac{\partial q_D}{\partial T_{o,D}}\right)\right] b_{T_i} b_{T_o} \qquad (7\text{-}3\text{-}27)$$

Table 7-3-20 Measures of the Numerical Error and Numerical Uncertainty for Total Heat Transfer Rate for the Model With Contact Conductance

Mesh Sequence	*p(observed)*	e_a^{21}, %	e_{ext}^{21}, %	GCI_{fine}^{21}, %	u_{num}, W
Mesh 2 to Mesh 4	1.99	−2.636 e-4	3.520 e-4	3.522 e-4	0.01
Mesh 1 to Mesh 3	2.00	−6.629 e-5	8.837 e-5	8.839 e-5	0.003

ASMENORMDOC.COM : Click to view the full PDF of ASME V&V 20 2009

Table 7-3-21 Partial Derivatives of the Total Heat Transfer Rate for the Simulation Model With Respect to Uncertainty Model Inputs for Model With Contact Conductance for the Average Measured Conditions

X_i	$X_i \frac{\partial q_s}{\partial X_i}$, W	Standard Uncertainty	
		Random, s_i	Systematic, b_i
k_t	0.005	...	5%
k_f	0.06	...	5%
h_1	15.64	...	10%
h_2	42.00	...	10%
h_f	1.12	...	10%
T_∞	−33.79	...	1%
T_{fl}	107.6	0.070%	0.14%
Q	2.24	0.5%	1.0%
ρ	2.24	...	0.5%
C_p	2.24	...	1%
h_c	12.81	...	20%

The additional term for the uncertainty in the contact conductance is added as the fifth term of eq. (7-3-27).

The data required to evaluate u_{val} are listed in Table 7-3-22. The uncertain parameters, standard uncertainties, and scaled sensitivity coefficients for the experimental and simulated total heat transfer rate are given in the table.

Validation results for the simulation model with contact conductance are given in Table 7-3-23. The results listed summarize the total heat transfer from the experiment and its uncertainty, the simulation result and its uncertainty from input uncertainty and numerical uncertainty, the comparison error, and the validation uncertainty u_{val} from eq. (7-3-27). The comparison error for the simulation with contact conductance is demonstrated to have a magnitude that is less than the magnitude of u_{val}. The magnitude of u_{val} computed with eq. (7-3-27) is negligibly different from the summing the squares of the individual contributions of standard uncertainty from the experimental data and simulation, assuming approximate independence between the two. This is a problem specific outcome and other cases may have a different outcome.

7-3.5.2.2 Interpreting the Validation Comparison. As discussed in para. 7-3.4.3, the validation can be interpreted in two ways. First, by comparing the magnitudes of the comparison error and the validation uncertainty, approximate inferences can be made about the presence of δ_{model}. Noting that $E \leq u_{val}$, the magnitude of δ_{model}, if it exists, is of the same order as the errors in the simulation and experimental data ($\delta_{input} - \delta_D$). Second, by making an assumption on the distribution of the parent population of the errors ($\delta_{num} + \delta_{input} - \delta_D$), an interval can be estimated within which δ_{model} falls with a specified probability. For a Gaussian distribution with $\alpha = 95\%$ confidence level, k is 2.0. The interval within which δ_{model} falls with 95% probability, $E \pm 2u_{val}$, is plotted in Fig. 7-3-8. The range characterizing δ_{model} is approximately [-12, 11] at the 95% probability level.

At this point, the validation procedure indicates the following. The model predictions are consistent with the experimental observations for the modeled uncertainty in the validation exercise. If further improvements to the simulation model are required for the engineering application (i.e., the application requires a magnitude of the average error for the heat transfer rate to be less than 11 W), the effectiveness of any model changes cannot be evaluated with the present experiments and present parametric uncertainties.

Table 7-3-22 Parameters Included in Evaluating u_{val}, Parameter Standard Uncertainty Estimates, and Parameter Sensitivity Coefficients for the Model With Contact Conductance

Parameter	Impact	Standard Uncertainty			Scaled Sensitivity Coefficients	
		Random, s_i	Systematic, b_i	Total, u_i	$X_i \frac{\partial q_D}{\partial X_i}$, W	$X_i \frac{\partial q_S}{\partial X_i}$, W
T_i (°C)	D and S	0.07%	0.14%	0.16 %	1,808	107.55
T_o (°C)	D	0.07%	0.14%	0.16%	−1,734	...
Q (m³/ sec)	D and S	0.5%	1.0%	1.12 %	74.9	2.24
ρ (kg/m³)	D and S	...	0.5%	0.5%	74.9	2.24
C_p (J/kg°C)	D and S	...	1.0%	1.0%	74.9	2.24
k_t (W/m°C)	S	...	5%	5%	...	0.005
k_f (W/m°C)	S	...	5%	5%	...	0.06
h_1 (W/m²°C)	S	...	10%	10%	...	15.64
h_2 (W/m²°C)	S	...	10%	10%	...	42.00
h_f (W/m²°C)	S	...	10%	10%	...	1.12
T_∞ (°C)	S	...	1%	1%	...	−33.79
h_c (W/m²°C)	S	...	20%	20%	...	12.81

ASMENORMDOC.COM : Click to view the full PDF of ASME V&V 20 2009

Table 7-3-23 Experimental and Simulation Values of Total Heat Transfer Rate and Associated Uncertainties

Experiment	q_D, W	u_D, W	q_S, W	u_{input}, W	u_{num}, W	E, W	u_{val}, W
1	74.0	2.65	74.3	5.19	0.01	0.27	5.58
2	75.6		73.4			−2.17	
3	75.1		73.7			−1.36	
4	71.4		73.4			2.05	
5	72.8		73.8			1.01	
6	77.0		73.5			−3.49	
7	79.3		74.1			−5.18	
8	72.1		73.7			1.61	
9	75.1		73.8			−1.29	
10	76.2		73.6			−2.43	
Average	74.9	2.17	73.8	5.18	0.01	−1.10	5.58

Fig. 7-3-8 Interval for δ_{model} ($E \pm 2u_{val}$) Assuming a Gaussian Distribution for the Errors and 95% Probability for the Model With Contact Conductance at the Fin/Tube Interface

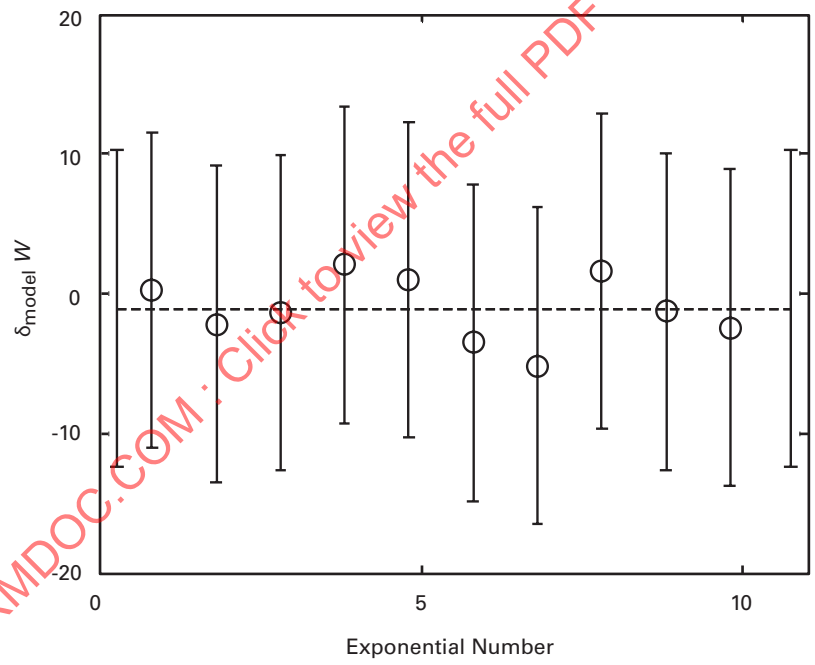

ASMENORMDOC.COM : Click to view the full PDF of ASME V V 20 2009

The evaluation of "improved" models will require that the uncertainties in the experiments and the corresponding parameters that are utilized by the simulation, be reduced through more carefully controlled or redesigned experiments.

7-4 REFERENCES

[1] Bova, S. W., Copps, K. D., and Newman, C. K., "Calore: A Computational Heat Transfer Program," Sandia National Laboratories, report SAND2006-6083P, Albuquerque, NM.

[2] Carey, G. F., Oden, J. T., "Finite Elements: Computational Aspects," Volume 03, Prentice Hall, 1984.

[3] Incropera and Dewitt, "Introduction to Heat Transfer," Wiley, New York, 1985.

Intentionally left blank

ASMENORMDOC.COM : Click to view the full PDF of ASME V V 20 2009

MANDATORY APPENDIX I
DETAILED DEVELOPMENT OF SIMULATION EQUATIONS FOR EXAMPLE PROBLEM

I-1 INTRODUCTION

The purpose of this Mandatory Appendix is to present the detailed development of the simulation equations used for the example discussed in Sections 1, 5, and 7. The physical problem is a hot fluid flowing inside a round tube with square fins on the outside of the tube. It is desired to validate a model for the bulk outlet temperature, T_o, of the fluid flowing in the tube and for the rate of heat transfer, q, from the hot fluid. A sketch of the physical problem is shown in Fig. 1-4-1 in Section 1.

I-2 DATA REDUCTION EQUATION FOR EXPERIMENTAL q

An overall energy balance on the fluid inside the tube of length, L, is

$$q_D = D = \rho Q C_p (T_i - T_o) \qquad \text{(I-2-1)}$$

where

C_p = specific heat
Q = volume flow rate
q_D = overall heat transfer rate, W
$(T_i - T_o)$ = bulk fluid temperature drop (all for the hot fluid)
ρ = density

Equation (I-2-1) is the data reduction equation for the overall heat transfer rate.

I-3 SIMULATION MODEL

A one-dimensional steady state lumped mass energy balance[1] on a differential tube length (dz) results in

$$\rho Q C_p \frac{dT}{dz} + 2\pi r_1 U_1 (T - T_\infty) = \rho Q C_p \frac{dT}{dz} + \frac{\overline{U}_1 A_1}{L}(T - T_\infty) = 0 \qquad \text{(I-3-1)}$$

where

L = tube length
$T(z)$ = position dependent bulk fluid temperature
T_∞ = (constant) ambient temperature
$\overline{U}_1$ = average overall heat transfer coefficient based on the wetted area of the tube inner surface ($A_1 = 2\pi r_1 L$)
z = distance along tube

Before integrating eq. (I-3-1) over the length of the tube, the details of how to calculate $\overline{U}_1$ will be discussed.

I-4 ASSUMED FORM FOR AXIAL VARIATION OF OVERALL HEAT TRANSFER COEFFICIENT, $\overline{U}_1$

The overall heat transfer coefficient variation is assumed in the form of a series of step functions corresponding to the finned and no-finned (bare tube) sections, as shown in Fig. I-4-1. The subscripts f and nf refer to finned and no-finned tube sections, respectively. The axially averaged overall heat transfer coefficient is given by

$$\frac{1}{L}\int_{z_i}^{z_0} U_1(z)dz = \frac{U_{f_i} w_f + U_{nf_i} w_{nf}}{w_f + w_{nf}} = \overline{U}_1 \qquad \text{(I-4-1)}$$

where the widths w_f and w_{nf} are defined in Fig. 1-4-1 in section 1 and

$$L = N(w_f + w_{nf}) \qquad \text{(I-4-2)}$$

where

N = number of fin/no-fin segments

The subscript 1 in eq. (I-4-1) is a reminder that the U's are based on area A_1. The task of getting $\overline{U}_1$ will be divided into two parts, corresponding to the no-fin and fin segments.

Fig. I-4-1 Variation of Local Value of Overall Heat Transfer Coefficient

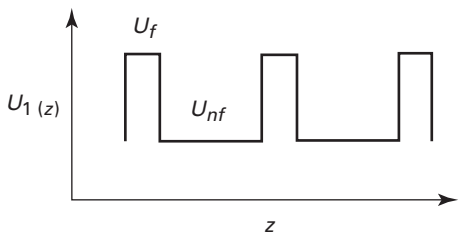

[1] Changes in potential and kinetic energy as well as axial heat conduction are ignored.

ASMENORMDOC.COM : Click to view the full PDF of ASME V&V 20 2009

I-5 OVERALL HEAT TRANSFER COEFFICIENT FOR NO-FIN SEGMENT, u_{nf_i}

The no-fin segment is treated as a bare tube with convective heat transfer on the inside and outside. From introductory heat transfer texts, the overall heat transfer coefficient for the no-fin section (for steady one-dimensional heat transfer) is given by

$$U_{nf_i} = \frac{1}{\frac{1}{h_1} + \frac{r_1 \ln(r_2/r_1)}{2\pi k_t} + \frac{r_1}{h_2 r_2}} \quad \text{(I-5-1)}$$

where

h_1 = convective heat transfer coefficients on the inside of the bare tube
h_2 = convective heat transfer coefficients on the outside of the bare tube
k_t = thermal conductivity of the tube

I-6 OVERALL HEAT TRANSFER COEFFICIENT FOR FIN SEGMENT, U_{f_i}

If the fins on the tube were circular instead of square, a one-dimensional result similar to eq. (I-5-1) could be derived analytically. However, the heat transfer in a square fin on a round tube will be addressed using a grid based computational (finite volume, finite element, etc.) model.

The three-dimensional simulation will include the circular tube and square fin attached to it and is shown schematically in Fig. I-4-1 in Section 1. A contact conductance between the tube and fin is allowed. The mathematical model is given as follows:

$$\frac{\partial}{\partial x}\left(k_t \frac{\partial T_t}{\partial x}\right) + \frac{\partial}{\partial y}\left(k_t \frac{\partial T_t}{\partial y}\right) + \frac{\partial}{\partial z}\left(k_t \frac{\partial T_t}{\partial z}\right) = 0 \text{ tube} \quad \text{(I-6-1)}$$

$$\frac{\partial}{\partial x}\left(k_f \frac{\partial T_f}{\partial x}\right) + \frac{\partial}{\partial y}\left(k_f \frac{\partial T_f}{\partial y}\right) + \frac{\partial}{\partial z}\left(k_f \frac{\partial T_f}{\partial z}\right) = 0 \text{ fin} \quad \text{(I-6-2)}$$

where the z-axis is directed along the length of the tube. While the fin and tube thermal conductivities are written inside the derivatives in eqs. (I-6-1) and (I-6-2) to directly relate the terms to the local heat flux, both conductivities are constant for this example. At the inner surface of the tube, the boundary condition is

$$-k_t \frac{\partial T_t}{\partial r}\bigg|_{r_1,\theta} = h_1 [T_{fl} - T(r_1, \theta)] \quad \text{(I-6-3)}$$

where

T_{fl} = the bulk fluid temperature
θ = traditional polar coordinate for cylindrical geometry

At the tube/fin interface where a contact conductance h_c may be present

$$-k_t \frac{\partial T_t}{\partial r}\bigg|_{r_2^-,\theta} = h_c[T_t(r_2^-,\theta) - T_f(r_2^+, \theta)] = -k_f \frac{\partial T_f}{\partial r}\bigg|_{r_2^+,\theta} \quad \text{(I-6-4)}$$

where the +/− indicates the outside/inside of the tube/fin interface. At the tip of the fin, the boundary condition is

$$-k_f \frac{\partial T_f}{\partial n}\bigg|_{x_b,y_b} = h_f [T_f(x_b,y_b) - T_\infty] \quad \text{(I-6-5)}$$

where

n = coordinate (outward) normal to the outer fin surface
(x_b, y_b) = evaluated along the outer boundary of the fin

Because of symmetry, only one-eighth of the cross section will be modeled; the symmetry boundaries are treated as adiabatic boundaries. The front and back surfaces of the fin (s_f) also have convection to the ambient air, and this boundary condition is given by

$$-k_f \frac{\partial T_f}{\partial n}\bigg|_{s_f} = h_f \left(T_f|_{s_f} - T_\infty\right) \quad \text{(I-6-6)}$$

Axial conduction in the tube is ignored.

The model presented in eqs. (I-6-1) through (I-6-6) is solved using a three-dimensional Galerkin finite element code, and the overall heat transfer coefficient for the fin section is computed by post processing the results. The overall heat transfer coefficient U_{f_i} for the fin/tube section is defined through

$$q_f = U_{f_i} \pi d_1 w_f (T_{fl} - T_\infty) = 8 w_f \int_0^{\pi/4} h_1 [T_{fl} - T_t(r_1,\theta)] r_1 d\theta \quad \text{(I-6-7)}$$

Solving eq. (I-6-7) for yields

$$U_{f_i} = \frac{4}{\pi (T_{fl} - T_\infty)} \int_0^{\pi/4} h_1 [T_{fl} - T_t(r_1,\theta)] d\theta \quad \text{(I-6-8)}$$

where $T(r_1, \theta)$ is the temperature from the simulation, eqs. (I-6-1) through (I-6-6).

A specification of the fluid temperature T_{fl} is required for the solution of the model given by eqs. (I-6-1) through (I-6-6). Note that T_{fl} varies along the length of the tube; however, for the linear constant property model considered here, it is argued that U_{f_i} computed from eq. (I-6-8) will be independent of the assumed value for T_{fl}.

I-7 INTEGRATION OF THE ENERGY BALANCE EQUATION

In eq. (I-3-1), the variables can be separated to yield

$$\int_{T_i}^{T_0} \frac{dT}{T - T_\infty} = -\frac{\overline{U}_1 A_1}{\rho Q C_p} \frac{1}{L} \int_{z_i}^{z_0} dz \quad \text{(I-7-1)}$$

Evaluating the integrals followed by algebraic manipulation yields

$$\frac{T_o - T_\infty}{T_i - T_\infty} = \exp\left(-\frac{\overline{U}_1 A_1}{\rho Q C_p}\right) \quad \text{(I-7-2)}$$

In subsection 5-2, the validation variable is T_o; solving eq. (I-7-2) for the validation variable yields

$$S = T_{o,S} = T_\infty + (T_i - T_\infty)\exp\left(-\frac{\overline{U}_1 A_1}{\rho Q C_p}\right) \quad \text{(I-7-3)}$$

The validation comparison error for this case is

$$E = S - D = T_{o,S} - T_{o,D} \quad \text{(I-7-4)}$$

In subsection 5-3, the validation variable is the heat transfer rate (q) and an expression will now be developed

ASMENORMDOC.COM : Click to view the full PDF of ASME V&V 20 2009

for it. Further algebraic manipulation of eq. (I-7-2) yields a form convenient solving for the heat flux.

$$\frac{T_i - T_o}{T_o - T_\infty} = \exp\left(\frac{\overline{U}_1 A_1}{\rho Q C_p}\right) - 1 \qquad \text{(I-7-5)}$$

Algebraic manipulation of eq. (I-7-5) yields

$$\frac{T_i - T_o}{T_o - T_\infty} = \frac{\rho Q C_p (T_i - T_o)}{\rho Q C_p (T_o - T_\infty)} = \frac{q}{\rho Q C_p (T_o - T_\infty)} = \exp\left(\frac{\overline{U}_1 A_1}{\rho Q C_p}\right) - 1 \qquad \text{(I-7-6)}$$

Solving eq. (I-7-6) for the heat transfer rate yields

$$q_S = S = \rho Q C_p (T_o - T_\infty)\left[\exp\left(\frac{\overline{U}_1 A_1}{\rho Q C_p}\right) - 1\right] \qquad \text{(I-7-7)}$$

The validation comparison error for the heat rate case is

$$E = S - D = q_S - q_D \qquad \text{(I-7-8)}$$

I-8 EXPERIMENTAL SET POINT

The set point in the experiment is the dimensionless flow rate (Re) and is given by

$$\mathrm{Re} = \frac{\rho d_1 V}{\mu} = \frac{4\rho Q}{\pi d_1 \mu} \qquad \text{(I-8-1)}$$

where

V = average velocity for the fluid inside the tube
ρ = fluid density for the fluid inside the tube
μ = dynamic viscosity for the fluid inside the tube

I-9 SUMMARY OF SIMULATION PARAMETERS

The parameters in this example can be divided into the categories of measured (in this experiment) and database (or handbook) values.

Measured:[2] $Q, T_i, T_o, T_\infty, d_1, d_2, L, a, w_f, w_{nf}$ (I-9-1)

Database: $\rho, \mu, C_p, k_f, k_t, h_1, h_2, h_c, h_f$ (I-9-2)

I-9.1 Nomenclature

A_1 = $2\pi r_1 L$, wetted tube inner area
A_2 = $2\pi r_2 L$, wetted tube outer area
a = fin width
C_P = specific heat of fluid inside tube
D = data
d_1 = inner tube diameter
d_2 = outer tube diameter
E = validation error
h = heat transfer coefficient
h_1 = heat transfer coefficient, inside of tube
h_2 = heat transfer coefficient, outside of tube
h_c = contact conductance at fin/tube interface
h_f = heat transfer coefficient, fin surface
k = thermal conductivity
k_f = fin thermal conductivity
k_t = tube thermal conductivity
L = tube length
N = number of fin/no-fin sections
Q = volumetric flow rate
q = heat transfer rate
q_D = heat transfer rate from data
q_S = heat transfer rate from simulation
Re = Reynolds number, $4\rho Q/(\pi d_1 \mu)$
r = radius
r_1 = inner tube radius
r_2 = outer tube radius
T = temperature
T_{fl} = bulk fluid temperature, see eq. (I-6-3)
T_i = inlet bulk fluid temperature
T_o = outlet bulk fluid temperature
T_∞ = ambient temperature
$\overline{U}_1$ = overall heat transfer coefficient based on A_1
U_{f_1} = overall heat transfer coefficient for fin, based on A_1
U_{nf} = overall heat transfer coefficient for no-fin, based on A_1
V = average fluid velocity in tube
w_f = width of fin sections
w_{nf} = width of no-fin sections
x_b, y_b = coordinates on outer boundary of fin
z = axial coordinate
θ = angular position
ρ = fluid density
μ = fluid dynamic viscosity

[2] It is easier to measure a diameter, d, than a radius, r, so diameter will be treated as the measured value.

ASMENORMDOC.COM : Click to view the full PDF of ASME V V 20 2009